CAPACI OCCASIO
FOUNDED 1894

SAIMM

THE SOUTHERN AFRICAN INSTITUTE OF MINING AND METALLURGY

VOLUME 120 NO. 12 DECEMBER 2020

SAFETY - FIRST, LAST AND ALWAYS.

REDPATH

Mining Contractors
and Engineers

Postal Address:
P.O. Box 296, Isando,1600, Gauteng, South Africa
Physical Address: 18 Industry Road, Isando,
Kempton Park, Gauteng, South Africa

Telephone: +27 (0) 11 570-4300
Facsimile: +27 (0) 11 974-2075
Email: info.africa@redpathmining.com

redpathmining.com

ISOQAR REGISTERED
UKAS MANAGEMENT SYSTEMS 0026
Certificate Number : 7910
ISO 9001, ISO 14001, ISO 45001

PROVIDING FULL SERVICE MINING SOLUTIONS AND INNOVATION AROUND THE WORLD SINCE 1962.

Redpath's multidisciplinary engineering and technical services team offers practical, innovative and reliable designs, with the ability to provide a total mine package.

- Underground Construction
- Shaft Sinking
- Raiseboring
- Contract Mining
- Raise Mining
- Mine Development
- Engineering & Technical Services

Africa | Asia | Australia | Europe | North America

Consider it done - safely.

OFFICE BEARERS AND COUNCIL FOR THE 2020/2021 SESSION

Honorary President

Mxolisi Mgojo
President, Minerals Council South Africa

Honorary Vice Presidents

Gwede Mantashe
Minister of Mineral Resources, South Africa

Ebrahim Patel
Minister of Trade, Industry and Competition, South Africa

Blade Nzimande
Minister of Higher Education, Science and Technology, South Africa

President

V.G. Duke

President Elect

I.J. Geldenhuys

Senior Vice President

Z. Botha

Junior Vice President

W.C. Joughin

Incoming Junior Vice President

E Matinde

Immediate Past President

M.I. Mthenjane

Co-opted to Office Bearers

S. Ndlovu
G.R. Lane

Honorary Treasurer

W.C. Joughin

Ordinary Members on Council

B. Genc
G.R. Lane
K.M. Letsoalo
T.M. Mmola
G. Njowa
S.J. Ntsoelengoe
S.M Rupprecht
N. Singh
A.G. Smith
M.H. Solomon
A.J.S. Spearing
S.J. Tose
M.I. van der Bank
A.T. van Zyl
E.J. Walls

Co-opted Members

Z. Fakhraei

Past Presidents Serving on Council

N.A. Barcza
R.D. Beck
J.R. Dixon
H.E. James
R.T. Jones
A.S. Macfarlane
C. Musingwini
S. Ndlovu
J.L. Porter
S.J. Ramokgopa
M.H. Rogers
D.A.J. Ross-Watt
G.L. Smith
W.H. van Niekerk

G.R. Lane–TPC Mining Chairperson
Z. Botha–TPC Metallurgy Chairperson

S.F. Manjengwa–YPC Chairperson
A.T. Chinhava–YPC Vice Chairperson

Branch Chairpersons

Johannesburg	D.F. Jensen
Namibia	N.M. Namate
Northern Cape	I. Lute
Pretoria	S. Uludag
Western Cape	A.B. Nesbitt
Zambia	D. Muma
Zimbabwe	C.P. Sadomba
Zululand	C.W. Mienie

PAST PRESIDENTS

*Deceased

* W. Bettel (1894–1895)
* A.F. Crosse (1895–1896)
* W.R. Feldtmann (1896–1897)
* C. Butters (1897–1898)
* J. Loevy (1898–1899)
* J.R. Williams (1899–1903)
* S.H. Pearce (1903–1904)
* W.A. Caldecott (1904–1905)
* W. Cullen (1905–1906)
* E.H. Johnson (1906–1907)
* J. Yates (1907–1908)
* R.G. Bevington (1908–1909)
* A. McA. Johnston (1909–1910)
* J. Moir (1910–1911)
* C.B. Saner (1911–1912)
* W.R. Dowling (1912–1913)
* A. Richardson (1913–1914)
* G.H. Stanley (1914–1915)
* J.E. Thomas (1915–1916)
* J.A. Wilkinson (1916–1917)
* G. Hildick-Smith (1917–1918)
* H.S. Meyer (1918–1919)
* J. Gray (1919–1920)
* J. Chilton (1920–1921)
* F. Wartenweiler (1921–1922)
* G.A. Watermeyer (1922–1923)
* F.W. Watson (1923–1924)
* C.J. Gray (1924–1925)
* H.A. White (1925–1926)
* H.R. Adam (1926–1927)
* Sir Robert Kotze (1927–1928)
* J.A. Woodburn (1928–1929)
* H. Pirow (1929–1930)
* J. Henderson (1930–1931)
* A. King (1931–1932)
* V. Nimmo-Dewar (1932–1933)
* P.N. Lategan (1933–1934)
* E.C. Ranson (1934–1935)
* R.A. Flugge-De-Smidt (1935–1936)
* T.K. Prentice (1936–1937)
* R.S.G. Stokes (1937–1938)
* P.E. Hall (1938–1939)
* E.H.A. Joseph (1939–1940)
* J.H. Dobson (1940–1941)
* Theo Meyer (1941–1942)
* John V. Muller (1942–1943)
* C. Biccard Jeppe (1943–1944)
* P.J. Louis Bok (1944–1945)
* J.T. McIntyre (1945–1946)
* M. Falcon (1946–1947)
* A. Clemens (1947–1948)
* F.G. Hill (1948–1949)
* O.A.E. Jackson (1949–1950)
* W.E. Gooday (1950–1951)
* C.J. Irving (1951–1952)
* D.D. Stitt (1952–1953)
* M.C.G. Meyer (1953–1954)
* L.A. Bushell (1954–1955)
* H. Britten (1955–1956)
* Wm. Bleloch (1956–1957)
* H. Simon (1957–1958)
* M. Barcza (1958–1959)
* R.J. Adamson (1959–1960)
* W.S. Findlay (1960–1961)
* D.G. Maxwell (1961–1962)
* J. de V. Lambrechts (1962–1963)
* J.F. Reid (1963–1964)
* D.M. Jamieson (1964–1965)
* H.E. Cross (1965–1966)
* D. Gordon Jones (1966–1967)
* P. Lambooy (1967–1968)
* R.C.J. Goode (1968–1969)
* J.K.E. Douglas (1969–1970)
* V.C. Robinson (1970–1971)
* D.D. Howat (1971–1972)
* J.P. Hugo (1972–1973)
* P.W.J. van Rensburg (1973–1974)
* R.P. Plewman (1974–1975)
* R.E. Robinson (1975–1976)
* M.D.G. Salamon (1976–1977)
* P.A. Von Wielligh (1977–1978)
* M.G. Atmore (1978–1979)
* D.A. Viljoen (1979–1980)
* P.R. Jochens (1980–1981)
G.Y. Nisbet (1981–1982)
A.N. Brown (1982–1983)
* R.P. King (1983–1984)
J.D. Austin (1984–1985)
H.E. James (1985–1986)
H. Wagner (1986–1987)
* B.C. Alberts (1987–1988)
* C.E. Fivaz (1988–1989)
* O.K.H. Steffen (1989–1990)
* H.G. Mosenthal (1990–1991)
R.D. Beck (1991–1992)
* J.P. Hoffman (1992–1993)
* H. Scott-Russell (1993–1994)
J.A. Cruise (1994–1995)
D.A.J. Ross-Watt (1995–1996)
N.A. Barcza (1996–1997)
* R.P. Mohring (1997–1998)
J.R. Dixon (1998–1999)
M.H. Rogers (1999–2000)
L.A. Cramer (2000–2001)
* A.A.B. Douglas (2001–2002)
S.J. Ramokgopa (2002-2003)
T.R. Stacey (2003–2004)
F.M.G. Egerton (2004–2005)
W.H. van Niekerk (2005–2006)
R.P.H. Willis (2006–2007)
R.G.B. Pickering (2007–2008)
A.M. Garbers-Craig (2008–2009)
J.C. Ngoma (2009–2010)
G.V.R. Landman (2010–2011)
J.N. van der Merwe (2011–2012)
G.L. Smith (2012–2013)
M. Dworzanowski (2013–2014)
J.L. Porter (2014–2015)
R.T. Jones (2015–2016)
C. Musingwini (2016–2017)
S. Ndlovu (2017–2018)
A.S. Macfarlane (2018–2019)
M.I. Mthenjane (2019–2020)

Honorary Legal Advisers
MH Attorneys

Auditors
Genesis Chartered Accountants

Secretaries
The Southern African Institute of Mining and Metallurgy
Fifth Floor, Minerals Council South Africa
5 Hollard Street, Johannesburg 2001 • P.O. Box 61127, Marshalltown 2107
Telephone (011) 834-1273/7 • Fax (011) 838-5923 or (011) 833-8156
E-mail: journal@saimm.co.za

Typeset and Published by

The Southern African Institute of Mining and Metallurgy
P.O. Box 61127
Marshalltown 2107
Telephone (011) 834-1273/7
Fax (011) 838-5923
E-mail: journal@saimm.co.za

Printed by

Camera Press, Johannesburg

Advertising Representative

Barbara Spence
Avenue Advertising
Telephone (011) 463-7940
E-mail: barbara@avenue.co.za

ISSN 2225-6253 (print)
ISSN 2411-9717 (online)

SAIMM
JOURNAL OF THE SOUTHERN AFRICAN INSTITUTE OF MINING AND METALLURGY
VOLUME 120 NO. 12 DECEMBER 2020

Contents

Welcome to another edition containing papers of general interest. In this issue, you will find a total of six papers, four of them are mining-related and the rest metallurgy.

This is a typical example of how the *Journal* intends to maintain a 50/50 split of papers between mining and metallurgy. The topics related to mining include practical modelling of long-term production scheduling, future trends in the international reporting codes, evaluation of mineral resources carrying capacity, and the prediction of flyrock and flyrock-related fields.

Metallurgical papers include a nonlinear prediction model with mass transfer theory and expert rules for refining low-carbon ferrochrome, shock heating of quartz used in silicon and ferrosilicon production, and optimization of chlorite and talc flotation using the experimental design methodology.

It is important to note that the *Journal* continues to receive papers from the international community, as only two out of the six papers in this edition are from South Africa. This is in line with *Journal* editor Professor Rosemary Falcon's observation in May 2020, that approximately 70% of the papers submitted for publication are from international sources. With the Journal's latest improved impact factor, this trend is expected to continue.

Enjoy the December edition of the *Journal*!

B. Genc

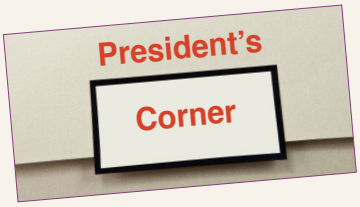

I was recently reminded that it is customary to reflect on the past 12 months in the December Journal.

We live in a beautiful country with a wonderful climate and amongst South Africans who are usually able to laugh at themselves and handle life's challenges. One just needs to tap into social media to see evidence of this. This collective ability to deal with stress was tested to the limit when, early in the year, Covid-19 brought on a level of uncertainty that many of us had not experienced before. It has been a tumultuous year and one that I am sure none of us will ever forget. Ongoing media reports highlighted some of the good, the bad, and the ugly of 2020.

The Good

For the first time in a long while, we saw signs of courageous leadership in South Africa. Despite knowing that our country would have to take a huge economic hit, brave unpopular decisions were taken to make it possible for us to assist those impacted by the virus.

Covid-19 forced us to stress-test our current technologies and the way we structure our businesses. People had to adapt, innovate, and make decisions around change. They quickly realized how easily it is to work differently. Our industry seemed to take Covid-19 in its stride and just carry on, while its employees learned how to operate outside of the office. Many of our members found that they were busier, more productive, and generally very comfortable using the various digital platforms available to them for communicating or holding virtual meetings.

The SAIMM successfully held its first digital Annual General Meeting after having had to rapidly adjust to a new way of operating at the onset of Covid-19. I was impressed at how quickly our staff and members working on the Technical Programmes Committee embraced the challenge and just did what needed to be done to carry on delivering to our membership base.

In fact, this was also true for our country as a whole, where we witnessed how South Africans from all walks of life rallied to keep the wheels turning at our schools, universities, hospitals, and many other institutions. In many ways, the pandemic brought people together, with some like myself spending more time with family as we worked on our homes and exercised together in the garden.

The Bad

The world was not prepared, especially some of the 'first world' countries. At home, the initial five weeks of complete isolation came quickly and unexpectedly. It brought with it both economic and social stress. Routines were disrupted and for many, social isolation was emotionally draining.

We witnessed people having to take salary cuts, suffer job losses, and take on debt just to survive, and for most, it will take a long time to recover. Members also found themselves working longer hours at home while having to look after children, spouses, and the elderly. Overall screen time increased and I expect that the gaming and streaming industries did very well.

Covid-19 exposed the true depth of divisions in South African society as the 'haves' seemed to fare better than the 'have-nots'. The less fortunate appeared to be more exposed to the consequences.

The Ugly

When considering the ugly, three things stood out – American politics, local corruption, and domestic violence. It was unfortunate to see how easily prejudice, uncertainty, and fear were able to polarize society as a consequence of American politics.

Pools of anger, resentment, and desperation during the lockdown revealed the raw wound of domestic violence that exists in our own society. This also highlighted how fragile we are when it comes to managing corruption. I found it difficult to comprehend how easily and quickly corrupt opportunists were able to pounce and take advantage of Covid-19 funding.

President's Corner *(continued)*

Looking forward

We need to remember, though, that we hear only what the media tells us, and should be more discerning in what we choose to believe. While it is good that we are informed by the media, we should regularly ask ourselves what did we not hear? 2020 was hard and we now need to move into 2021. I believe that a positive atmosphere is emerging, with people more optimistic about a brighter future, and a hopefully a vaccine for Covid-19.

We are seeing improvements in the markets, a resurgence in commodity demand, and an uplift in our industry. There is a general increase in interest in projects previously placed on ice.

Persistent guidance by President Ramaphosa is resulting in visible signs of authorities acting against corruption, and positive efforts at Eskom and SARS.

There is general recognition by everyone that things are not going to be the same and that we need to change the way they think about business. The world is now seeing things differently, and this provides a good space for people who want to change. The industry has got off to a good start and our leaders, many of whom are associated with the SAIMM, can accelerate these efforts.

Our members don't need to be holding on to the norms of the past. The fourth industrial revolution, or 4IR, has brought on significant technological progress. Systems have improved, efficiencies are up, and we now need to work harder on developing the human capacity needed for us to simply stay abreast. Let's meet the challenge and continue to innovate. Look at your own individual sphere of influence and consider how you can contribute to the collective efforts of everyone else.

All in all, it has been a difficult and eventful year, and now it is time to recharge. The SAIMM is looking forward to 2021, and I would like to thank all Fellows, Members, the Secretariat, and our Company Affiliates for their continued support of the Institute and its activities. I wish all our members, colleagues, and loved ones a peaceful holiday and trust that you will all have a blessed festive season.

V.G. Duke
President, SAIMM

Future trends in the international Reporting Codes based on SEC's Regulations SK-1300

S.M. Rupprecht[1]

Affiliation:
[1] University of Johannesburg, Johannesburg, South Africa.

Correspondence to:
S.M. Rupprecht

Email:
rupprecht.steven@gmail.com

Dates:
Received: 28 Jul. 2020
Revised: 8 Nov. 2020
Accepted: 23 Nov. 2020
Published: December 2020

How to cite:
Rupprecht, S.M. 2020
Future trends in the international Reporting Codes based on SEC's Regulations SK-1300.
Journal of the Southern African Institute of Mining and Metallurgy, vol. 120, no. 12, pp. 659–664.

DOI ID:
http://dx.doi.org/10.17159/2411-9717/1300/2020

ORCID
S.M. Rupprecht
https://orcid.org/0000-0003-2462-2819

This paper will be presented at the *SAMCODES Conference 2021*, 26–27 October 2021, Mandela Mining Precinct, Auckland Park, Johannesburg, South Africa.

Synopsis

In June 2016, the US Securities and Exchange Commission (SEC) 'proposed a revision to its disclosure requirements-related guidance under the Securities Act and Exchange Act for properties owned or operated by mining companies'. On 31 October 2018, the SEC released its adopted final rules for property disclosures for mining registrants – '*Modernization of Property Disclosures for Mining Registrants*'. The amendments are aimed at providing investors with a more comprehensive understanding of a registrant's mining properties, which should help them make more informed investment decisions. The new rules replace the SEC's Industry Guide 7 as of January 1, 2021. This paper investigates how the new subpart 1300 of Regulation S-K may affect future updates to the Committee for Mineral Reserves International Reporting Standards (CRIRSCO) International Reporting Template, as well as international Reporting Codes. Critical changes such as the reporting of Mineral Resources exclusive of Mineral Reserves are discussed, the impact of third-party reporting regarding reducing Section 11 liability is considered, as is the trend of utilizing multiple qualified persons for technical reports. This paper highlights areas in the CRIRSCO and international Reporting Codes that may require consideration by Qualified and Competent Persons providing technical report summaries and Competent Persons Reports (CPRs).

Keywords
SEC, 1300 of Regulation S-K, international Reporting Codes, CRIRSCO, Qualified/Competent Person, mineral reporting.

Introduction

On 16 June 2016, the US Securities and Exchange Commission (SEC) announced and published proposed changes to the reporting requirements for mining and mineral exploration companies. The final document, Release No. 33-10570, was published on 31 October 2018 and replaces Industry Guide 7 in subpart 229.1300 of Regulation S-K (SK-1300). Reporting under the new rules is required by the first fiscal year beginning on or after 1 January 2021. The replacement of Industry Guide 7 was brought about as it was found to be outdated; it only recognized Mineral Reserves based on a Feasibility Study, failed to acknowledge the full mining value chain of Exploration Results or Mineral Resources, and did not require Competent Persons to sign off on Company Technical Disclosures (Parsons *et al.*, 2019).

For this paper, the author has chosen to use the term 'Competent Person' rather than the SEC's and Canadian term of 'Qualified Person' as this is more familiar to the intended audience. For the purposes of this paper one should take the terms 'Competent Person' and 'Qualified Person' as synonymous.

Alignment with other international Reporting Codes

The proposed changes are intended to bring the US reporting requirements in line with other international Reporting Code requirements and are based on the Committee for Mineral Reserves International Reporting Standards (CRIRSCO) documents. The revised SK-1300 makes requirements for reporting of Exploration Results, Mineral Resources, and Mineral Reserves in the USA similar to those in other major mining jurisdictions such as Canada, Australia, South Africa, and Chile. The format for reporting is now similar to South Africa's SAMREC Code, Australasia's JORC Code, and Canada's National Instrument (NI) 43-101. It is also in line with the European PERC and the codes of Chile, Peru, and the Philippines, in which several US companies have operations.

The justification for the change from the SEC Industry Guide 7 to the revised SEC SK-1300 is to remove previous requirements that may have placed US mining registrants at a competitive disadvantage with non-US companies listed on the same exchanges. Also, the revised SK-1300 is intended to aid investors or potential investors (the public) 'by providing them with a more

comprehensive understanding of a registrant's mining properties' so that the public can make more informed investment decisions (SEC, 2018, p. 6).

Type of study required to support a Mineral Resource or Mineral Reserve declaration

International Reporting Code requirements and SK-1300 revisions

Technical report summaries are required to support the disclosure of Mineral Resources and Mineral Reserves, with the option for disclosure of Exploration Results. CRIRSCO, as well as other international Reporting Codes, provide definitions for the various types of studies, *i.e.* Scoping, Pre-Feasibility, and Feasibility. These definitions are essential as they provide the level of confidence associated with the study and, as per reporting requirements for a Pre-Feasibility or a Feasibility Study, allow the disclosure of a Mineral Reserve.

The SEC has aligned itself with the same requirements as CRIRSCO and other international Reporting Codes in that either a Pre-Feasibility Study or a Feasibility Study is required for the declaration of a Mineral Reserve. The SK-1300 requirements for declaring a Mineral Reserve have been reduced from the Industry Guide 7 approach, which previously required a Mineral Reserve declaration to be based on a Feasibility Study – a Preliminary Feasibility Study was not sufficient to declare a Mineral Reserve.

The basis of the new rules requires three types of technical report summary:

- A technical report summary for the disclosure of Exploration Results (optional unless material to investors)
- An initial (qualitative) assessment on the reasonable prospects for economic extraction is required for the declaration of Mineral Resources, must be prepared by a Competent Person
- A Preliminary Feasibility Study or Feasibility Study, which is the minimum study level required to establish a Mineral Reserve.

The option of reporting Exploration Results is slightly different from CRIRSCO and other international Reporting Codes, which require public reports for all material information relating to Exploration Targets, Exploration Results, Mineral Resources, and Mineral Reserves (CRIRSCO, 2019).

Study types and definitions

Similar to other international Reporting Codes, SK-1300 provides definitions of the various technical studies, as well as the level of accuracy and level of contingency required for each study. The provision of definitions is important – the author has observed that some Competent Persons are declaring Mineral Reserves based on Scoping Studies (initial assessments). Future trends will see more scrutiny of the actual work conducted in technical reports or CPRs to support the declaration of Mineral Reserves.

The SEC's SK-1300 states that 'factors to be considered in a Pre-Feasibility Study are typically the same as those required for a Feasibility Study, but considered at a lower level of detail or an earlier stage of development' (SEC, 2018, p. 205). Also, SK-1300 requires the Pre-Feasibility Study to identify sources of uncertainty that require further refinement in a final Feasibility Study, noting that it is the Competent Person's responsibility to assess risk in a Pre-Feasibility Study. Further, the Competent Person must make a reasonable effort to identify any obstacles to obtaining permits and entering into the necessary sales contracts, and reasonably believe that the chances of obtaining such approvals and contracts in a timely manner are highly likely. It may be appropriate for international Reporting Codes to provide further guidance around the current terminology, that 'there is a reasonable basis to believe all permits required will be obtained', especially as environmental, social, and governance issues are becoming more relevant to these Codes.

The SK-1300 regulation observes that a preliminary market study may be required where a mine's product cannot be traded on an exchange, there is no other established market for the product, and no sales contract exists (SEC, 2018, p. 209). Further guidance regarding the reporting of the marketing aspects of a mineral project may be necessary, as this aspect of technical reports often falls short of what the international Reporting Codes require

Minimum level of study requirements

It is noteworthy that the SEC has reduced the minimum requirement for the declaration of a Mineral Reserve from a Feasibility Study (Industry Guide 7) to a Pre-Feasibility Study (SK-1300, p. 406). Previously, the SEC was of the opinion that a 'comprehensive technical and economic study', which includes detailed assessments of all relevant modifying factors together with any relevant operational factors (SEC, 2018, p. 406) was the cut-off point. The SEC implied that Pre-Feasibility Studies still contain some uncertainties related to shortcomings that would be investigated in the Feasibility Study. International Reporting Codes such as the JORC Code 2012 and SAMREC Code 2016 (Table 2) have incorporated guidelines to technical studies.

CRIRSCO and the international Reporting Codes should require improved disclosure regarding the level and accuracy of the technical study used to support the declaration of a Mineral Reserve. Inclusion of the executive summary of the technical study should be considered as a minimum requirement, and it may be prudent for the authors of the said study to also 'sign off' on the level of study. The above, although more prescriptive, will ensure that Competent Persons are not mistakenly using a study at a level lower than that of a Pre-Feasibility Study.

It remains a concern to the author that the definitions of a Scoping Study and Pre-Feasibility Study are being abused by some Competent Persons and registrants who use studies at less than a Pre-Feasibility level to support the declaration of a Mineral Reserve.

As a final comment, the SK-1300 regulation requires the registrant to compare Mineral Resources and Mineral Reserves as of the end of the last fiscal year with the Mineral Resources and Mineral Reserves of the end of preceding fiscal rear (SEC, 2018, p. 244). Notably, the net difference between the last two fiscal years should be disclosed as a percentage and an explanation provided regarding the difference and the cause of any discrepancy between the two reporting periods. Although the above is in line with other international Reporting Codes, providing the net change as a percentage should be considered for inclusion of the reporting template by CRIRSCO and further guidance provided on how to improve the explanation as to the causes of discrepancies. Currently, far too many Competent Persons fail to address these differences in a transparent or material manner, often failing to provide meaningful commentary or information on how future risk can be mitigated when the differences are material and not associated with mining depletion.

Geotechnical and hydrogeology

The SEC, through the SK-1300, specifically requires geotechnical and hydrogeology aspects to be discussed when considering the Modifying Factors to convert Mineral Resources to Mineral Reserves. The SEC views the reporting of the geotechnical and hydrogeology aspects as providing insight into the adequacy and appropriateness of the mine design. For the international Codes, mining factors are highlighted. Geotechnical and hydrogeology are not explicitly highlighted, and although most technical studies typically cover these aspects, some Mineral Reserve declarations are void of geotechnical and hydrogeology aspects. In the opinion of the author, this requirement will strengthen the quality of reporting and therefore should be considered by CRIRSCO and international Reporting Codes when updating the individual Codes. In addition, the aspects of ventilation should also be considered as a reporting requirement for underground mining projects declaring a Mineral Reserve.

Cut-off grade

The final rules require that a Competent Person includes in the initial assessment a cut-off grade estimation based on assumed unit costs for surface or underground operations and estimated mineral prices. The SEC is of the opinion that a discussion of cut-off grade is an appropriate requirement for a technical study that supports a Mineral Resource estimate because, by definition, a Mineral Resource estimate is not just an inventory of all mineralization. It is an estimate of that part of the deposit that has reasonable prospects of economic extraction.

The discussion of cut-off grade in technical reports or ongoing reporting is often overlooked by the Competent Person. The SEC provides further guidance to ensure appropriate disclosure, especially in the area of price information, which is material to an investor's understanding of the Mineral Resource and Mineral Reserve estimate.

New technologies

Where new technologies are to be used in extraction or mineral processing and are still in a testing (beta) stage, Mineral Reserves will not be allowed to be declared if viability depends on these technologies. It is not uncommon for mineral projects to encounter cash flow constraints due to mine plans that were reliant on new technology but were unable to meet planned productivity. In South Africa, the Burnstone gold mine provides an example of a project that failed due to the unsuccessful implementation of narrow reef longhole stoping. Based on the SEC's reluctance to allow Mineral Reserves to be declared based on new technology, it may prove prudent for international Reporting Codes to provide guidance as to how new technology is used to justify Reasonable Prospects for Eventual Economic Extraction for Mineral Resources and the declaration of Mineral Reserves. There is some uncertainty as to how the SEC will treat new technologies that have been tested and proven to work, but are not yet implemented commercially. This question regarding new technologies is also relevant to international Reporting Codes and should be included in the risk section.

Reporting Mineral Resources and Mineral Reserves

Threshold materiality standard

SK-1300 requires a registrant to 'provide additional disclosure about individual mining properties when those individual properties themselves are material to the company's business or financial condition' (Hogan Lovells, 2019). The Hogan Lovells (2019) communiqué stresses that a mining operation will be considered material if there is 'a substantial likelihood that a reasonable investor would attach importance to the information about the mining operations when deciding whether to buy, hold, or sell the company's securities'. Although this disclosure alone will not provide all relevant information about the property, its assets, or revenues, detailed disclosure regarding material properties is necessary to provide investors with a comprehensive understanding of a mining company's operations (Body and Rupprecht, 2019). Body and Rupprecht (2019) further comment that the SK-1300 'final rules include a provision that establishes guidelines for classifying the current stage of a property as exploration, development, or production'.

For listed companies, the relevant stock exchange will provide disclosure requirements highlighting the reporting requirements for non-mineral companies with mineral assets, exploration companies, and mineral companies. In the case of South African companies listed on the JSE, Section 12.11 of the JSE Listing Requirements guides the ongoing reporting requirements. However, for non-listed companies using an international Reporting Code, the definition of materiality may not be sufficient. In terms of materiality and the international Reporting Codes, it may be time that further guidance is provided to Competent Persons on what information should be provided to the public to enhance understanding. For example, if the registrant's Mineral Resources have been reduced due to unexpected geological losses, the public would anticipate transparent and material commentary regarding geological setting and why and how the geology has impacted on the mineral asset. There are still too many examples in the public domain where the Competent Person has failed to report on activities that have had a material impact on the mineral asset or where quantitative and qualitative information is lacking.

Future addenda to international Reporting Codes must provide further guidance around technical reports that 'help to educate the investor as to the likely range of outcomes for a project' (Fairfield, 2016).

Level of detail in the summary technical report

Technical reports are increasing in size and technical detail, as Competent Persons feel the need to protect themselves from compliance and associated personal and reputational risk (Fairfield, 2016).

Technical reporting is further complicated, as highlighted by Fairfield (2016), by many investors viewing compliance with an international Reporting Code as implying precision and accuracy, with investors often only interested in chasing returns. Although this latter provision is consistent with the transparency principle under the CRIRSCO standards and will help investors better understand a registrant's mining operations, there are still too many technical reports that fail to report material information in a transparent manner.

Often the information provided is not in plain English, as called for by SK-1300 ('plain English principles'). In addition, reporting requires registrants to include only geological information that is brief and relevant to property disclosure rather than an extensive description of regional geology. Body and Rupprecht, 2019)

Classification of Mineral Resources and Mineral Reserves

The new regulations have brought the SEC in line with the other international classification systems in that the SK-1300 classifications are now the same as for SAMREC, JORC, (NI 43-101 and similar international Reporting Codes.

Inclusive and exclusive Mineral Reserves

The debate regarding whether Mineral Resources should be reported inclusive or exclusive of Mineral Reserves has been ongoing for years, and circa 2012 it was classified as a 'parked issue' by the SAMREC Working Group as no consensus was reached. Thus, the SAMREC Code 2016 (Clause 42) continued to comment that 'in some situations, there are reasons for reporting Mineral Resources inclusive of Mineral Reserves. In other situations, there are reasons for reporting Mineral Resources additional to Mineral Reserves. It should be made clear which form of reporting has been adopted.'

The SEC has indirectly resolved the debate in that SK-1300 requires that Mineral Resources to be reported exclusive of Mineral Reserves as the SEC believes that disclosure of Mineral Resources exclusive of Mineral Reserves reduces the risk of investor confusion. SK-1300 further allows a Competent Person to disclose Mineral Resources inclusive of Mineral Reserves, however, the Competent Person must also report the Mineral Resources exclusive of Mineral Reserves.

Admittedly, the reporting of Mineral Resources exclusive of Mineral Reserves will make it easier for the public to value mineral assets provided one fully understands the excluded Mineral Resources and their reasonable potential for eventual economic extraction. One must note that the Mineral Resources outside (excluded from) the Mineral Resources that are converted to a Mineral Reserve by adding a mine plan and extraction schedule will have a different value to those converted to a Mineral Reserve.

In terms of the SK-1300 requirements, many companies that have traditionally reported Mineral Resources on an inclusive basis will now be required to report on an exclusive basis. The author proposes that international Reporting Codes consider preparing guidelines for the estimating of the Mineral Resources exclusive of Mineral Reserves, as there will be several nuances the Competent Person must consider for this declaration, and not simply a subtraction of the Mineral Resources used in the estimation of the Mineral Reserve.

Inferred Mineral Resources

Inferred Mineral Resources remain an enigma in that the JORC 2012 and NI 43-101 Codes do not allow Inferred Mineral Resources to be included in Pre-Feasibility and Feasibility Studies. For example, the JORC Code 2012 states in its guidelines of Clause 21 that 'Confidence in the estimate of Inferred Mineral Resources is not sufficient to allow the results of the application of technical and economic parameters to be used for detailed planning in Pre-Feasibility or Feasibility Studies' (JORC, 2012, p. 13). The NI 43-101 instrument prohibits the disclosure of an economic analysis that includes Inferred Mineral Resource except in the case of Preliminary Economic Assessments. At the same time, the 2019 CRIRSCO template warns that 'Caution should be exercised if this category [*i.e.* Inferred Mineral Resources] is considered in technical and economic studies' (CRIRSCO, 2019). While the SAMREC Code (2016) accepts that 'mine design and planning may include a portion of Inferred Mineral Resources', the Code does add that if a material amount of Inferred Mineral Resources is used in the mine plan the technical study should compare the results obtained with and without the Inferred Mineral Resources.

The SK-1300 regulation states 'The level of uncertainty associated with an Inferred Mineral Resource is too high to apply relevant technical and economic factors likely to influence economic extraction in a manner useful for the evaluation of viability' (SEC, 2018, p. 136). This statement is provided with a footnote that further clarifies that 'an Inferred Mineral Resource may not be considered when assessing the economic viability of a mineral project' (SEC, 2018, p. 136).

It is time for CRIRSCO and the international Reporting Codes to address the issues of Inferred Mineral Resources and their use in mine planning. Some Inferred Mineral Resources have 'Reasonable Prospects for Eventual Economic Extraction' (RPEEE) and are important to an investor's understanding, as they may be converted to Indicated or Measured Mineral Resources with further exploration (SEC, 2019).

Perhaps it is time for CRIRSCO to provide further guidance around the use of Inferred Mineral Resources in mine planning. In cases where only Inferred Mineral Resources exist, then one may agree that there is insufficient geological verification to support the use of an Inferred Mineral Resource on its own for mine planning purposes. However, it may be appropriate to include Inferred Mineral Resources in mine plans in conjunction with Indicated and Measured Mineral Resources. Further conditions could be considered, such as inferred Mineral Resources should not be used before the payback period is ended, or similar to the SAMREC Code, where the financial analysis should be reported based on a mine plan with and without Inferred Mineral Resource so that the public can see the impact that Inferred Mineral Resources have on the economic viability of the mining project. There may be several potential solutions to the inconsistency of how Inferred Mineral Resources are used in mine planning, but for certain, it is time for clarity on the matter.

Liability and professional responsibility

Continuing professional development and RPOs

The SEC's definition of a Competent Person is in alignment with the CRIRSCO definitions. SK-1300 stresses that Competent Persons should have 'sufficient experience', which means that a Competent Person should have adequate experience to be able to 'identify with substantial confidence, problems that could affect the reliability of data and issues associated with processing' (SEC, 2018, p. 84). Furthermore, the Competent Person must 'have both sufficient knowledge and experience in the application of [the modifying factors] to the mineral deposits under consideration, as well as experience with geology, geostatistics, mining, extraction, and processing that is applicable to the type of mineral and mining under consideration' (SEC, 2018, p. 88).

The above discussion around a Competent Person's experience is more detailed than what is typically portrayed. In the author's opinion, the above suggests the use of specialists in several technical areas, since finding a single or even two Competent Persons with such a vast range of knowledge will be extremely difficult. Thus one or two Competent Persons authoring a technical report is no longer acceptable. SK-1300 indicates that technical reports need to draw upon expertise in a number

of areas so that sufficient expertise is used to ensure reliable reporting. CRIRSCO and international Reporting Codes should provide guidance on the use of technical experts in technical reports and who should be responsible for the respective sections of the report. Areas such as exploration geology and sampling, geological modelling, Mineral Resource estimation, geotechnical, ventilation, engineering, processing, cost estimation, financial analysis, risk, and environmental, social, governmental, and other areas should be supported by technical specialists identified in the technical report. This increase in the number of technical specialists will increase human resource requirements for the technical report but will also ensure that the process is multidisciplinary, with specialists reporting on material issues in a competent and transparent manner.

The new SK-1300 regulation also discusses continuing professional development. The SEC encourages professional development as one of the defining criteria of a recognized professional organization (RPO). In South Africa, this would include the Engineering Council of South Africa (ECSA), SACNASP, and the Geological Society of South Africa (GSSA) but would exclude the Southern African Institute of Mining and Metallurgy (SAIMM). Based on the SEC's interpretation, it is the author's opinion that continuing professional development will need to be inclusive of learned societies and not just professional bodies.

The SEC does not support the publishing of a list of RPOs as it is of the opinion that the list would become outdated as circumstances change, which could adversely affect the quality of disclosure (SEC, 2018, p. 90). The SEC does specify the minimum competencies and requires professional registration of all Competent Persons. 'In practice, the designation of Competent Persons does not change for most foreign companies operating in countries which require reporting to CRIRSCO standards. In the USA, as well as South Africa, environmental practitioners, geologists, engineers, and financial, legal, and other experts are generally required to hold professional registration in the jurisdiction in which they operate and would automatically qualify in terms of the new regulations' (Body and Rupprecht, 2018).

Third-party reporting and Section 11 liability

The final rules of the SK-1300 regulation allows for 'third-party firms comprising of mining experts, such as professional geologists or mining engineers, to sign off on the technical summary report instead of, and without naming, its employee, member, or other affiliated persons who prepared the summary' (SEC, 2018, p. 71). The SEC states that the third-party signatures and written consent provision will reduce some of the concerns in connection with Section 11 liability of Competent Persons. As the firm is not required to name individual employees, members, or other affiliated persons 'thus, the third-party firm will incur potential liability under Section 11 rather than the unnamed individual' (SEC, 2018, p. 72).

However, it should be noted that Competent Persons who are employed by third-party firms are not entirely exempt from expert liability under Section 11 of the Securities Act as 'not imposing Section 11 liability would be a departure from the current requirement that imposes such liability on the named person that prepares the reserve estimate' (SEC. 2018, p. 72). The SK-1300 regulation further explains that providing total exemption to the Competent Person(s) 'would be at odds with the express design of the statute, which specifically suggests engineers or any person whose profession gives authority to a statement made by him [or her] as potentially subject to Section 11 liability, and would greatly diminish the protection afforded investors under the Securities Act' (SEC, 2018, p. 73).

Regarding modifying factors, the S'EC enables the Competent Person to indicate in the technical report summary that he/she has 'relied on information provided by the registrant in preparing their findings and conclusions regarding the modifying factors' (SEC, 2018, 74).

The final SK-1300 rules also provide that, in a separately captioned section of the technical report entitled 'Reliance on Information Provided by the Registrant', the [Competent Person] must:

- Identify the categories of information provided by the registrant
- Identify the particular portions of the technical report summary that were prepared relying on information provided by the registrant
- State the extent of that reliance
- Disclose why the Competent Person considers it reasonable to rely upon the registrant for any of the information.

The SEC states that 'this disclosure will help investors and other interested persons understand the source and reliability of the information pertaining to those factors. [The SEC] also notes that this disclosure is consistent with the disclosure recommended when a qualified or competent person relies on information provided by the registrant under the CRIRSCO standards' (SEC, 2018, pp. 74–75).

Furthermore, the SEC states that 'where the registrant has provided the information relied upon by the [Competent Person] when addressing these modifying factors, we believe that it would be appropriate for the registrant, rather than the Qualified Person, to be subject to potential Section 11 liability. The registrant remains liable for the contents of the registration statement and consequently will be incentivized to exercise due care in the preparation of information' (SEC, 2018, p. 75).

Finally, regarding reliance on other 'third-party specialists who are not a [Competent Person], such as an attorney, appraiser, and economic or environmental consultant, upon which the [Competent Person] has relied in preparing the technical report summary', 'the final rules provide that the Competent Person 'may not disclaim responsibility for any information and documentation prepared by a third-party specialist upon which the [Competent Person] has relied, or any part of the technical report summary based upon or related to that information and documentation' (SEC, 2018, p. 76). 'Doing so could undermine the quality of the technical report summary, as neither the [Competent Person] nor the third-party specialist would be accountable for material misstatements or omissions in such information and documentation' (SEC, 2018, p. 76). Interesting to note, a Competent Person working for the registrant must provide written consent on an individual basis. The author is already aware of employees of companies who have indicated their reluctance to sign off as a qualified person due to concerns of potential Section 11 liabilities.

The SK-1300 regulation raises a number of points. The use of one or two qualified persons may no longer be the norm, with more reliance being applied to technical experts to sign off under their areas of speciality. The requirement for additional

technical specialists to support Competent Persons Reports may result in larger professional organizations being used to produce technical reports. Future reporting codes may require a more formal approach of technical specialists being used to sign off on technical reports. Environmental, social, and governmental (ESG) reporting is already covered as a guide, but may transform into a reporting code in itself. South Africa has published a guide for reporting ESG issues – the SAMESG Guideline 2017. Other technical areas, such tailings storage facilities may follow suit in the future.

The author welcomes the idea of the Competent Person reporting on the 'Reliance on Information Provided by the Registrant' as this places the onus on the registrant to provide all material information in a transparent manner. Furthermore, the registrant is also subject to potential Section 11 liability for information provided by the registrant. The author would like to see the reporting of information supplied by the registrant to the Competent Person become a standard requirement for CPRs, thus promoting due care in the preparation of information by registrants.

The introduction of third-party sign-off in order to limit the risk of Section 11 liability may impact on the international Reporting Codes. The use of third-party sign-off may provide some comfort to individual Qualified Persons and may also increase the costs of producing Competent Persons Reports for companies listed in the USA. From an international perspective, third-party sign-off moves away from the concept that Competent Persons need to 'face their peers and demonstrate competence in the commodity, type of deposit and situation under consideration' (SAMREC, 2016). It is the author's position that professional bodies and learned societies can take disciplinary measures in cases of non-compliance. It is preferred that professional organizations generally handle the cases of non-deliberate material misstatements and omissions, and only deliberate misrepresentation or fraud would be covered by other regulations, laws, and litigation.

The appetite for risk of individuals or owners of small consulting companies is still to be determined. Risk-averse persons will most likely move away from signing off on technical reports for companies listed in the USA. How companies handle this issue is yet to be determined. Will this result in only high-level executives signing off or a move to third-party reporting to limit individual liability? Most likely a consultant will need to increase charge-out fees to cover liability insurance.

Conclusion

SK-1300 provides insight into how the USA perceives Property Disclosure for Mining Registrants. Although the new rules are mainly aligned with CRIRSCO, the SK-1300 regulations highlight some of the future trends that may affect CRIRSCO and other international Reporting Codes, such as the SAMREC Code.

Some of the SK-1300 regulations that CRIRSCO and the international Reporting Codes should consider are as follows.

- The reporting of Mineral Resources exclusive of Mineral Reserves as required, and preparing guidelines for the estimating of the Mineral Resources exclusive to Mineral Reserves, as there will several nuances that the Competent Person must consider for this declaration.
- Technical Reports require Competent Persons with sufficient knowledge and experience, alluding to the use of technical specialists to ensure that the full mining process or value chain is adequately reported. Guidance for the formal use of technical experts should be provided in updated international Reporting Codes.
- Based on the SEC's reluctance to allow Mineral Reserves to declared on the basis of new technology, it may prove prudent for international Reporting Codes to provide guidance on how new technology may be used to justify Reasonable Prospects for Eventual Economic Extraction for Mineral Resources and the declaration of Mineral Reserves.
- The SK-1300 regulation requires Competent Persons to include geotechnical and geohydrological aspects in technical reports. This requirement, as well as ventilation aspects for underground operations, should be investigated as a reporting requirement.
- Continuous professional development is a requirement for a certain recognized professional organization. Hence, continuing professional development will need to be inclusive of learned societies, *e.g.* the SAIMM, and not just professional bodies.
- Allowing third-party firms to sign off technical reports to reduce the risk of Section. 11 liability. Third-party sign-off will be of particular interest, and if adopted by other international Reporting Codes may prevent complaints from being lodged against individual Competent Persons.

The author has provided a number of suggestions to be considered when updating CRIRSCO and international Reporting Codes. In many situations, the author suggests best-practice commentary or guidance notes as the overall goal of the Reporting Codes is to provide guidance towards the minimum reporting standards rather than becoming prescriptive. In the end, the Competent Persons must use their professional judgement in providing adequate disclosure of all material aspects, bearing in mind that the 'Competent Person must be clearly satisfied in their own minds that they are able to face their peers and demonstrate competence' (SAMREC, 2016).

References

Body, K. and Ruppprecht, S.M. 2019. Annual Review of Mineral Resources and Mineral Reserves. Red Bush Geoservices (Pty) Ltd, Johannesburg.

CRIRSCO. 2019. International Reporting Template for the public reporting of Exploration Results, Mineral Resources and Mineral Reserves. Committee for Mineral Reserves International Reporting Standards, Council of Mining and Metallurgical Institutions.

Fairfield, P.J. 2016. Managing expectations – From buyer beware to buyer be aware. *Proceedings of Evaluation 2016 – Good Practice and Communication*. Adelaide, South Australia, 8-9 March 2016. Australasian Institute of Mining and Metallurgy, Melbourne.

Hogan Lovells. 2019. SEC overhauls mining property disclosure regime. 16 January 2019. https://www.hoganlovells.com/~/media/hogan-lovells/pdf/2019/2019_01_23_sec_overhauls_mining_property_disclosure_regime.pdf

Parsons, B., Lehner, J., McCombie, D., and Sullivan, M. 2019. Investment Implication of U.S. SEC's Rule S-K 1300. *Proceedings of the 7th Annual Current Trend in Mining Finance Conference*, 29 April – 1 May 2019. Society for Mining, Metallurgy and Exploration, Littleton, CO.

SAMREC. 2016. South African Mineral Resource Committee. The South African Code for the Reporting of Exploration Results, Minerals Resources and Mineral Reserves (the SAMREC Code) 2016 Edition. http://www.samcode.co.za/downloads/SAMREC2016.pdf

SEC. 2018. Modernization of Property Disclosure for Mining Registrants. https://www.sec.gov/corpfin/secg-modernization-property-disclosures-mining-registrants. ◆

A practical, long-term production scheduling model in open pit mines using integer linear programming

J. Gholamnejad[1], R. Lotfian[1], and S. Kasmaeeyazdi[2]

Affiliation:
[1] Department of Mining and Metallurgical Engineering, Yazd University, Yazd, Iran.
[2] Department of Civil, Chemical, Environmental and Material Engineering, University of Bologna, Bologna, Italy.

Correspondence to:
J. Gholamnejad

Email:
j.gholamnejad@yazd.ac.ir

Dates:
Received: 1 Jun. 2019
Revised: 20 Oct. 2020
Accepted: 3 Nov. 2020
Published: December 2020

How to cite:
Gholamnejad, J., Lotfian, R., and Kasmaeeyazdi, S. 2020
A practical, long-term production scheduling model in open pit mines using integer linear programming.
Journal of the Southern African Institute of Mining and Metallurgy, vol. 120, no. 12, pp. 665–670.

DOI ID:
http://dx.doi.org/10.17159/2411-9717/769/2020

ORCID
J. Gholamnejad
https://orcid.org/0000-0003-3480-9644

S. Kasmaeeyazdi
https://orcid.org/0000-0003-2438-8743

Synopsis

Long-term production scheduling is a major step in open pit mine planning and design. It aims to maximize the net present value (NPV) of the cash flows from a mining project while satisfying all the operational constraints, such as grade blending, ore production, mining capacity, and pit slope during each scheduling period. Long-term plans not only determine the cash flow generated over the mine life, but are also the basis for medium- and short-term production scheduling. Mathematical programming methods, such as linear programming, mixed integer linear programming, dynamic programming, and graph theory, have shown to be well suited for optimization of mine production scheduling. However, the long-term plans generated by the mathematical formulations mostly create a scattered block extraction order on several benches that cannot be implemented in practice. The reason is the excessive movement of mining equipment between benches in a single scheduling period. In this paper, an alternative integer linear programming (ILP) formulation is presented for long-term production scheduling that reduced the number of active benches in any scheduling period. Numerical results of the proposed model on a small-scale open pit gold mine show a 34% reduction in the average number of working benches in a given scheduling period.

Keywords
long-term production scheduling, mathematical programming, practical plans, equipment movements.

Introduction

One of the significant stages in open pit mine planning and designing is the optimization of long-term production scheduling. The objective is to determine the extraction sequence of ore and waste blocks in order to maximize the NPV of the mining operation within the existing economic, technical, and environmental constraints. The applied constraints are the mining extraction sequences; mining, milling and refining capacities; mill head grades; and various operational requirements such as minimum pit bottom width.

Mathematical programming has been effectively used by various researchers to tackle long-term open pit scheduling problems. Linear programming (LP) was first applied by Johnson (1969), and led to the mixed integer linear programming (MILP) formulations by Gershon (1983) for the production scheduling problem. Many researchers subsequently used mathematical programming models to solve the long-term production scheduling problems (Dagdelen and Johnson, 1986; Ramazan and Dimitrakopoulos, 2003; Dimitrakopoulos and Ramazan, 2009; Goodfellow and Dimitrakopoulos, 2015, 2017). A complete bibliography of the mathematical programming models that were used in mine production scheduling is provided by Osanloo, Gholamnejad, and Karimi (2008) for open pit optimization, and by Newman *et al.* (2010) for optimization in underground mine planning.

One of the most important problems in a production schedule from the mathematical models is excessive movement of loading and hauling equipment between benches in a given period of scheduling. This increases both the mining costs and the complexity of the excavation operations. For technical and economic reasons, mining operations will not be performed on a large number of widely spread levels in any given scheduling period (Djilani and Dowd 1994).

Caccetta and Hill (2003) restricted the maximum vertical depth, D, that can be mined in each scheduling period. They added some constraints to ensure that blocks separated by vertical distances greater than D are mined in different time periods.

Dimitrakopoulos and Ramazan (2004) proposed an alternative MILP model in which access to equipment and mobility constraints are taken into account. They considered two concentric inner and outer windows around each block (i). The optimization model attempted to mine each block (i) together with the adjacent blocks within the inner (smaller) window. If the blocks within the inner and outer

windows could not be mined out, their tonnage was considered as 'deviations', which were then minimized in the objective function along with their deviation costs. The resulting schedule decreases the movement of equipment on each bench.

Pourrahimian, Askari Nasab, and Tannant (2009) presented two MILP formulations to prevent scattering of the excavation sequence in a given scheduling period. Their first model, which is a block-based model, was a modification of the approach by Ramazan and Dimitrakopoulos (2004). They introduced constraints into the optimization model that enforced extraction of a working block with at least 40% of its surrounding blocks in the same period. The second model was developed based on a combination of concepts from Caccetta and Hill (2003) and Boland *et al.* (2009). In the second model, the blocks were aggregated prior to the schedule optimization based on their attributes such as the spatial location, rock type, and grade distribution. The authors termed these block clusters 'mining-cuts' and the scheduling model was then applied on the generated mining cuts instead of mining blocks. They showed that the schedule generated by the second model (mining-cut based model) is more feasible in practice.

Askari-Nasab, Awuah-Offei, and Eivazy (2010) presented a mixed integer nonlinear programming (MINLP) model for long-term production scheduling. To reduce the number of continuous and binary variables in the model, they aggregated blocks into larger units, referred to as mining cuts, using clustering algorithms. Then, they defined a binary integer decision variable, equal to unity if a mining-cut is scheduled to be extracted in period *t*, and zero otherwise. Finally, they added a set of constraints to control the maximum number of fractions that mining cuts are allowed to be extracted over. For large-scale models with many scheduling periods, this value was set equal to two or three fractions. Due to the difficulties in solving nonlinear models, the nonlinear equation was linearized by introducing a new continuous variable. The model ensured that the generated schedule is practical in terms of equipment movement (Askari-Nasab, Awuah-Offei, and Eivazy, 2010).

Past efforts to deal with production of practical plans attempted to reduce the movement of equipment on a particular bench, (not between the benches), with the exception of Caccetta and Hill (2003). In this paper, a new ILP model is presented for the open pit mine sequencing and scheduling problem. Traditionally, in ILP models, some physical and technical constraints are used such as grade blending, processing and mining capacity, pit slope, and reserve constraints. The novelty of this work lies in the definition and incorporation of additional constraints in the ILP model, in order to reduce the number of active benches in each scheduling period.

The remainder of the paper is organized as follows. The section on materials and methods presents the problem definition, with the notations of variables and the ILP formulations of the problem. Moreover, addition of the novel constraints (equipment movement constraints) to the traditional model for each scheduling period is investigated. This is followed by a comparison of the results from the suggested model with those from the traditional one, using a mining case study, and finally, a discussion and conclusion.

Materials and methods

Mathematical optimization techniques use a linear or nonlinear model to represent the mining operation and find an optimal schedule, taking into account the physical constraints imposed by the mining system. The general criterion of optimization can be maximizing the NPV, minimizing mining costs, or minimizing the variance of the grade, *etc.*

LP is the most widely used technique for decision-making in business and industry, and also in open pit mine scheduling optimization. Usually in a LP decision, variables are allowed to be fractional. In ILP, all decision variables are integer, and in MILP, some, but not all, variables are restricted to being integer.

The mathematical programming model presented here is based on ILP and can be extended easily to a MILP model simply by defining the variables as linear instead of integer. The model for long-term production scheduling contains an objective function and a set of constraints.

Objective function

In long-term production scheduling for open pit mines, the objective function is usually constructed to maximize the overall NPV of the project over the model's scheduling horizon. The scheduling horizon is divided into a finite number of time intervals with predefined durations. Even though this objective is the most commonly used criterion in long-term scheduling optimization (Chanda and Ricciardone 2002), other objectives such as cost minimization, reserve maximization (Askari-Nasab, Awuah-Offei, and Eivazy, 2010), and risk minimization (Montiel and Dimitrakopoulos, 2015) can also be applied. The objective function can be identified as follows:

$$Max\ Z = \sum_{i=1}^{I}\sum_{j=1}^{J}\sum_{k=1}^{K}\sum_{t=1}^{T} c_{ijkt} \cdot x_{ijkt} \quad [1]$$

where

- ijk Indices correspond to the row, column, and level of blocks in the model, $i = 1,2,...I, j = 1,2,...,J$ and $k = 1,2,...,K$. These are block counters in the x, y, and z directions respectively with k decreasing with depth. I, J, and k are, respectively, the number of blocks in the block model in the x, y, and z directions.
- I Long-term schedule time period, $t = 1,2,...,T$
- T The number of periods over which blocks are being scheduled
- c_{ijkt} The NPV obtained from mining, processing, and selling of block ijk in period t
- x_{ijkt} A binary variable which is equal to 1 if block (i,j,k) is mined in period t, and zero otherwise.

c_{ijkt} can be calculated easily based on the weight and type of the block; grade(s) within block; mining, processing. and smelting recovery percentages; costs of mining, processing, and smelting; selling price of final product(s); and discount rate. A key assumption in the calculation of block values is that the block cost of mining does not depend on the mining sequence.

Constraints

Grade blending constraints

The grade blending constraints adjust the feed quality to the mill. These constraints guarantee that the average grade of the feed to the mill is less than or equal to an upper bound value, , and more than or equal to a lower bound value, , for each scheduling period (t):

$$\sum_{i=1}^{I}\sum_{j=1}^{J}\sum_{k=1}^{K}(g_{ijk} - AG^{t}_{\max}) \times OT_{ijk} \times x_{ijkt} \leq 0 \quad \forall t \quad [2]$$

$$\sum_{i=1}^{I}\sum_{j=1}^{J}\sum_{k=1}^{K}(g_{ijk}-AG^{t}_{\min})\times OT_{ijk}\times x_{ijkt}\geq 0 \quad \forall t \quad [3]$$

where

g_{ijk} Average grade of block *ijk*

$AG^{t}_{\max}$ Maximum average grade of ore sent to the mill in period *t*

$AG^{t}_{\min}$ Minimum average grade of ore sent to the mill in period *t*

OT_{ijk} Ore tonnage in block *ijk*.

If necessary, these constraints can also be written for other by-products (such as gold in copper deposits) and deleterious elements (such as phosphorus in an iron ore deposit) that may have an impact on the efficiency and costs of the metallurgical process.

Processing capacity constraints

The processing capacity constraints ensure that the total tonnage of ore processed by the mill does not exceed the mill capacity (PU_t) and is less than a predefined amount (PL_t) in any scheduling period (t):

$$\sum_{i=1}^{I}\sum_{j=1}^{J}\sum_{k=1}^{K}(OT_{ijk}\times x_{ijkt})\leq PU_t \quad \forall t \quad [4]$$

$$\sum_{i=1}^{I}\sum_{j=1}^{J}\sum_{k=1}^{K}(OT_{ijk}\times x_{ijkt})\geq PL_t \quad \forall t \quad [5]$$

where

PU_t Maximum processing capacity in any period, *t*

PL_t Minimum amount of ore that should be processed in period *t*.

In practice, in order to provide a uniform feed to the mill, the processing capacity constraints should be set within limited upper and lower bounds (Askari-Nasab, Awuah-Offei, and Eivazy, 2010).

Mining capacity constraints

The mining capacity constraints guarantee that the maximum mining capacity of equipment, MU_t, is respected. Moreover, the stripping ratio can be controlled by the lower bound mining capacity (MU_l) as follows:

$$\sum_{i=1}^{I}\sum_{j=1}^{J}\sum_{k=1}^{K}\left(OT_{ijk}+WT_{ijk}\right)\times x_{ijkt}\leq MU_t \quad \forall t \quad [6]$$

$$\sum_{i=1}^{I}\sum_{j=1}^{J}\sum_{k=1}^{K}\left(OT_{ijk}+WT_{ijk}\right)\times x_{ijkt}\geq ML_t \quad \forall t \quad [7]$$

where

MU_t Maximum available equipment capacity for each period *t*

ML_t Minimum amount of material (waste and ore) that should be removed in each scheduling period *t*

WT_{ijk} Tonnage of waste material within block *ijk*.

Equation [7] is useful to balance waste production over the mine life. When the stripping ratio is more or less constant throughout the life of the mine, equipment fleet size and labour requirements are also relatively constant.

Local block precedence constraints

A block can be mined in a given scheduling period only if the directly overlying blocks have already been mined. The overlying blocks can be determined by applying the precedence constraints. There are several slope patterns that are used to identify precedence relationships, such as the 1:5 pattern, 1:9 pattern, and 1:5:9 pattern (Mousavi. Kozan, and Liu, 2014). The precedence constraints for a 1:9 pattern (Figure 1) can be written as follows:

$$\begin{aligned}&9x_{ijkt}-\sum_{r=1}^{t}(x_{i-1,j-1,k+1,r}+x_{i-1,j,k+1,r}+\\&x_{i-1,j+1,k+1,r}+x_{i,j-1,k+1,r}+x_{i,j,k+1,r}+\\&x_{i,j+1,k+1,r}+x_{i+1,j-1,k+1,r}+\\&x_{i+1,j,k+1,r}+x_{i+1,j+1,k+1,r})\leq 0\end{aligned} \quad \forall\, t,i,j,k \quad [8]$$

where

r Time period index, r = 1,2, …,*t*.

Reserve constraints

The reserve constraints signify that each block cannot be mined more than once, and can be formulated as follows:

$$\sum_{t=1}^{T}x_{ijkt}\leq 1 \quad \forall\, i,j,k \quad [9]$$

Equipment movement constraints

These constraints guarantee that the average number of working benches over each scheduling period will not exceed an integer number (η), which is specified by the designer. These constrains minimize the movement of equipment between working benches in a given scheduling period. The related constraints can be written as:

$$\frac{\sum_{i=1}^{I}\sum_{j=1}^{J}x_{ijkt}}{I\times J}\leq y_{kt}\leq\sum_{i=1}^{I}\sum_{j=1}^{J}x_{ijkt} \quad \forall\, k,t \quad [10]$$

$$\frac{\sum_{t=1}^{T}\sum_{k=1}^{K}y_{kt}}{T}\leq\eta \quad [11]$$

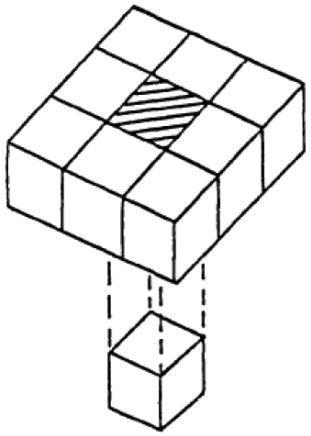

Figure 1—Slope constraints for a 1:9 pattern

where

η An integer number representing the maximum average number of benches that are allowed to be mined in each period

y_{kt} A binary variable which is equal to 1 if at least one block within the kth bench is mined in period t, and 0 otherwise.

In fact $\sum_{k} y_{kt}$, represents the number of mined benches in a scheduling period (t). If only one block of a bench is extracted in a particular scheduling period, that bench is considered to be active at that time; therefore, the left-hand side of constraint [11] represents the average number of mined benches in a given scheduling period.

As shown in constraints [10] and [11], the number of binary variables and constraints added to the problem (due to the consideration of the new constraints) are KT and 2TK+1, respectively.

Application to a gold mine

The implementation of the ILP model for long-term production scheduling is demonstrated for an open pit gold mine in Iran. The mine is a conventional truck-and-loader operation. The final pit contains 1 273 446 t of rock containing 714 834 t of ore with an average grade of 1.62 g/t Au (at a 0.6 g/t cut-off grade). It will take about 10 years to exploit the final pit, considering the capacity constraints of the operation. The final pit contains 2690 blocks (1510 ore blocks and 1180 waste blocks) of 6 × 6 × 5 m with the information containing block coordinates (x, y, and z), rock type, rock density. and gold grade in grams per ton. The total number of benches in this model is 16.

In order to reduce the number of decision variables and consequently reduce the solution time, the long-term production scheduling model is run over five scheduling periods (each period is 2 years long). In this study, it is assumed that the ore materials that are destined for the processing plant are limited to between 100 000 and 200 000 t and the total mined material is between 140 000 and 300 000 t during each production period. According to the processing plant layout, the average grade of the feed to the mill must be more than 1.5 g/t. To have a benchmark in the proposed model, two schedules were produced; one using the new model (NM) proposed in this paper and another, referred to as the traditional model (TM), which ignores constraints [10] and [11]. Based on the number of loading and hauling machines and authors' experiences at this mine, the value of η is assumed to be 5 in NM.

Results

These two models were solved on a PC with an Intel(R) Xeon(R) CPU E5-2699 v4 at 2.2 GHz and 16 GB RAM using the CPLEX solver in GAMS version 24.7.4. As Table I shows, it took 108 seconds for the TM to be solved, while running the NM took about 2627 seconds.

Figure 2 shows cross-sectional views of the two schedules for the gold deposit: one obtained using the TM and the other generated by the NM. It can be seen that the NM scheduling pattern appears more practical and needs less equipment movement between benches within each scheduling period.

Table II summarizes the results of the schedules obtained using these two models. The average number of active benches in the schedules was 7.6 for the TM and 5 for the NM, which represents a 34% reduction. This means that mining equipment would need less relocation between benches in a given scheduling period using the NM, and all activities would be concentrated on a smaller number of benches. Table II shows that in the schedule by the NM, the amount of ore extracted in the first period decreases by 10%, while the amount of waste mined in this period increases by 8.5%. However, the processing and mining capacity constraints were satisfied. The total generated

Table I

Information of TM of NM runs for gold deposit in case study

Description	TM	NM
Total number of blocks	2.690	2.690
Total number of periods	5	5
Annual discount rate	10%	10%
Number of constraints	16.165	16.326
Total 0-1 variables	13.450	13.530
Solution time (seconds)	108	2627

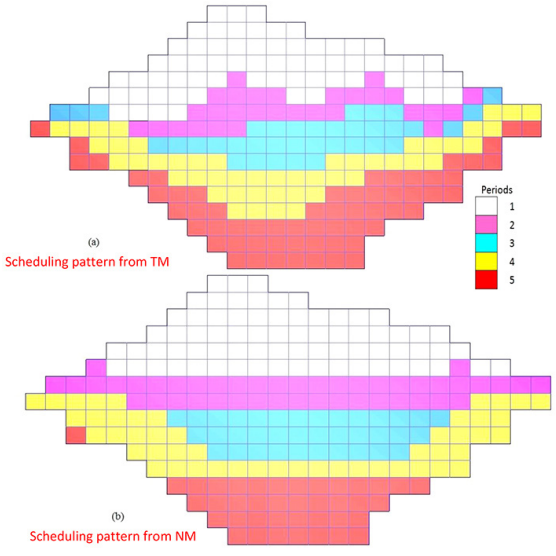

Figure 2—Cross-sectional views of production scheduling pattern from the traditional (a) and new (b) approaches

Table II

Summary of results for production scheduling using the TM and NM

Period	Ore production		Waste production		Au average grade		No. of active benches	
	TM	NM	TM	NM	TM	NM	TM	NM
1	199.775	181.786	56.335	61.542	1.77	1.94	9	6
2	123.557	161.429	59.648	138.233	1.50	1.50	5	3
3	115.036	159.062	134.919	27.931	1.59	1.52	6	3
4	127.818	103.675	164.743	180.365	1.53	1.51	8	5
5	148.648	108.882	142.967	150.541	1.61	1.50	10	8
Average	142.967	142.967	111.722	111.722	1.62	1.62	7.6	5
Total	714.834	714.834	558.612	558.612	–	–	–	–

NPVs from the TM and NM models are about $21.57 million and $20.77 million, respectively, which shows a 3.7% reduction of NPV in the NM. One of the main reasons for this is that the objective function in the NM cannot extract more ore from more benches to satisfy the ore tonnage requirements, which stems from constraints [10] and [11]. Instead, in order to satisfying the grade blending constraints, the model extracts high-grade materials in the first scheduling period.

In order to investigate the horizontal scheduling pattern, the number of time periods for the extraction of each bench was calculated (Table III). Remarkably, the average number of time periods required to extract a bench is reduced from 2.4 in the TM to 1.6 in the NM (a 37.5% reduction).

As an example, the plan views of the scheduling patterns generated from the NM and TM for the 8th bench of the open pit mine are illustrated in Figure 3. As illustrated, bench 8 is mined in five scheduling periods (1, 2 ,3, 4, and 5) with the schedules produced by the TM, while by employing the NM, this is reduced to two scheduling periods (2 and 4). Therefore, mining a single bench requires less movement of equipment compared with the schedules obtained from the NM.

Discussion

Open pit mine scheduling can be divided into three phases, *i.e.* long-, medium-, and short-term production scheduling. Long-term production scheduling usually aims to maximize the NPV, and defines the yearly production schedules. In short-term production scheduling, the micro-level operational constraints such as mining and mill capacity, grade requirements, equipment constraints, stockpile constraints, availability of consumable additives, and block accessibility are taken into account to minimize deviations from production targets. Short-term plans, which define monthly, weekly, or even daily production schedules, are based on medium- and long-term plans. The optimality and practicality of the short-term plans depend strongly on the optimality and practicality of long-term plans; therefore, in order to have a practical short-term schedule, the long-term plans should be practical to the greatest possible extent. On the other hand, if planners can reach the optimal production target through short-term scheduling, then the main objective of the mining operation, which is maximizing NPV, is secured in the long term. One of the operational aspects of short-term scheduling is that the total number of active benches in each scheduling period should be kept as low as possible. This reduces the movement of equipment between benches, which in turn can reduce the total mining costs (Bai *et al.*, 2018). In the authors' experience, if the number of benches that are active simultaneously during a long-term planning horizon is high, the number of active benches in each short-term scheduling horizon will be high as well. This point, as a significant consideration, persuaded the authors to add linear constraints (equipment movement) to the traditional long-term production scheduling models in order to decrease the number of active benches in each scheduling period.

Comparison of the scheduling patterns of the TM and NM (Figure 2) showed that the schedule obtained by the TM was further developed vertically while that obtained by NM was developed horizontally without violating the constraints. The spread of sequencing patterns obtained from TM (Figure 2a) shows that in a given scheduling period, mining equipment would need to be moved frequently between active benches. Hence, the resultant TM plans require more complex short-term scheduling compared to those obtained from the NM.

Basically, by adding constraints to the optimization problems, the objective function either remains unchanged or becomes worse (it decreases in maximization problems and increases in minimization problems). In the presented case study, although adding mobility constraints leads to a 3.7% reduction in the

Table III

The scheduling periods for each bench extraction

Bench No.	Period	
	TM	NM
1	1	1
2	1	1
3	1	1
4	1	1
5	2	1
6	4	2
7	5	1
8	5	2
9	5	3
10	3	3
11	3	3
12	2	2
13	2	1
14	1	1
15	1	1
16	1	1
Ave.	2.4	1.6

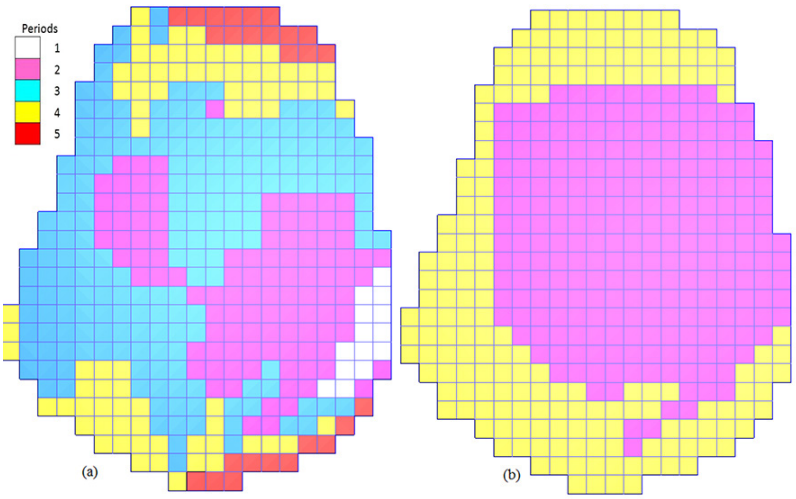

Figure 3—Plan views of the production scheduling patterns from the traditional (a) and new (b) approaches

theoretical NPV, the materialized NPV may be increased because of the reduction in mining equipment movement. This, in turn, will increase the efficiencies in the utilization of loading and hauling equipment. This is very important since the haulage costs in open pit mines can be 60% or more of the mine's operating cost (Ribeiro, 2013). Also, compared with the length of the planning horizon in long-term production scheduling, there was no noticeable increase in the computation time of the NM relative to the TM.

Conclusion

In this paper, a new optimization formulation is presented for long-term production scheduling in open pit mines that reduces the movement of mining equipment between the excavated benches by restricting the number of working benches in each scheduling period. This can increase the productivity and efficiency of mining equipment. Although the proposed approach needs more computation time, and may reduce the theoretical NPV of a project, it generates a more realistic NPV by reducing the costs of equipment movements. The average number of active benches within each scheduling period was decreased by about 34% in the presented ILP model, with less scattered block sequencing within each bench.

Acknowledgements

This work was supported by Yazd University under Grant 539-P-97.

References

Askari-Nasab. H., Awuah-Offei, K., and Eivazy, H. 2010. Large-scale open pit production scheduling using Mixed Integer Linear Programming. *International Journal of Mining and Mineral Engineering*, vol. 2, no. 3. pp. 185–214.

Bai, X., Marcotte, D., Gamache, M., Gregory, D., and Lapworth, A. 2018. Automatic generation of feasible mining pushbacks for open pit strategic planning. *Journal of the Southern African Institute of Mining and Metallurgy*, vol. 118, no. 6. pp. 515–530.

Boland, N., Dumitrescu, I., Froyland, G, and Gleixner, A,M. 2009. LP-based disaggregation approaches to solving the open pit mining production scheduling problem with block processing selectivity. *Computers and Operations Research*, vo. 36, no. 4. pp. 1064–1089.

Caccetta, L. and Hill, S.P. 2003. An application of branch and cut to open pit mine scheduling. *Journal of Global Optimization*, vol. 27. pp. 349–365. doi: 10.1023/A:1024835022186

Chanda, E.K. and Ricciardone, J. 2002. Long term production scheduling optimization for a surface mining operation: an application of Minemax2 scheduling software. *International Journal of Surface Mining, Reclamation and Environment*, vol. 16, no. 2. pp. 144–158.

Dagdelen, K. and Johnson, T.B. 1986. Optimum open pit mine production scheduling by Lagrangian parameterization. *Proceedings of the 19th International Symposium on Application of Computers and Operations Research in the Mineral Industry*. Ramani, R.V. (ed.). Society of Mining Engineers, Littleton, CO. pp. 127–142.

Dimitrakopoulos, R. and Ramazan, S. 2004. Uncertainty based production scheduling in open pit mining. *SME Transactions*, vol. 316. pp. 106–116.

Djilani, M.C. and Dowd, P.A. 1994. Optimal production scheduling in open pit mines. *Leeds University Mining Association Journal (LUMA)*, vol. 12. pp. 133–140.

Gershon, M.E. 1983. Mine scheduling optimization with mixed integer programming. *Journal of Mining Engineering*, vol. 35, no. 4. pp. 351–354.

Goodfellow, R.C. and Dimitrakopoulos, R. 2015. Global optimization of open pit mining complexes with uncertainty. *Journal of Applied Soft Computing*, vol. 40. pp. 292–304. doi: 10.1016/j.asoc. 2015.11.038

Goodfellow, R.C. and Dimitrakopoulos, R. 2017. Simultaneous stochastic optimization of mining complexes and mineral value chains. *Mathematical Geosciences*, vol. 49. pp. 341–360.

Johnson, T.B. 1969. Optimum open-pit mine production scheduling. *Proceedings of the 8th International Symposium on Computers and Operations Research*, Salt Lake City, UT. pp. 539–562.

Montiel, L. and Dimitrakopoulos, R. 2015. Optimizing mining complexes with multiple processing and transportation alternatives: An uncertainty-based approach. *European Journal of Operational Researc*h, vol. 247, no. 1. pp. 166-178. doi: 10.1016/j.ejor.2015.05.002

Mousavi, A., Kozan, E., and Liu, S.Q. 2014. An integrated approach to optimize open-pit mine block sequencing. *Industrial Engineering Non-Traditional Applications in International Settings*. Bidanda, B., Sabuncuoglu, I., and Kara, B.Y. (eds). CRC Press. pp. 83–98.

Newman, A.M., Rubio, E., Caro, R., Weintraub, A., and Eurek, K. 2010 A review of operations research in mine planning. *Interfaces*, vol. 40, no. 3. pp. 222–245.

Osanloo, M, Gholamnejad, J., and Karimi, B. 2008. Long-term open pit mine production planning: a review of models and algorithms. *International Journal of Mining, Reclamation and Environment*, vol. 22, no. 1. pp. 3–35.

Pourrahimian, Y., Askari Nasab, H., and Tannant, D. 2009. Production scheduling with minimum mining width constraints using mathematical programming. *Proceedings of the 18th International Symposium on Mine Planning and Equipment Selection (MPES 2009)*, Banff, Canada. Singhal, R., Mehrotra, A., Fytas, K., and Ge, H. (eds). Reading Matrix, Inc., Calgary. pp. 646–653.

Ramazan, S. and Dimitrakopoulos, R. 2003. Production scheduling optimization in a nickel laterite deposit: MIP and LP application and in the presence of orebody variability mine. *Proceedings of the Twelfth International Symposium on Mine Planning and Equipment Selection (MPES 2003)*, Kalgoorlie, WA. Australasian Institute of Mining and Metallurgy, Melbourne. pp. 1–5.

Ramazan, S. and Dimitrakopoulos, R. 2004. Recent applications of operations research and efficient MIP formulation in open pit mining. *Transactions of the Society for Mining, Metallurgy and Exploration*, vol. 316. pp. 73–78.

Ramazan, S. and Dimitrakopoulos, R. 2004. Traditional and new MIP models for production scheduling with in-situ grade variability. *International Journal of Surface Mining, Reclamation and Environment*, vol. 18, no. 2. pp. 85–98.

Ribeiro, B. 2013. Estudo de viabilidade econômica para a implantação de correias transportadoras de rom de minério de ferro. Estudo de Caso da Mina Fábrica em Congonhas, Estado de Minas Gerais. Master's thesis Federal University of Ouro Preto, Brazil. 81 pp. [in Portuguese] ◆

A nonlinear prediction model, incorporating mass transfer theory and expert rules, for refining low-carbon ferrochrome

C -J. Guan[2] and W. You[1,2]

Affiliation:
[1] School of Electrical and Electronic Engineering, Changchun University of Technology, Changchun, 130012, China.
[2] School of Mechatronic Engineering, Changchun University of Technology, Changchun, 130012, China.

Correspondence to:
W. You

Email:
youwen@ccut.edu.cn.

Dates:
Received: 11 Feb. 2020
Revised: 8 Nov. 2020
Accepted: 10 Nov. 2020
Published: December 2020

How to cite:
Guan, C -J., and You, W. 2020 A nonlinear prediction model, incorporating mass transfer theory and expert rules, for refining low-carbon ferrochrome. Journal of the Southern African Institute of Mining and Metallurgy, vol. 120, no. 12, pp. 671–680.

DOI ID:
http://dx.doi.org/10.17159/2411-9717/1119/2020

ORCID
C -J. Guan
https://orcid.org/0000-0002-7606-6546
W. You
https://orcid.org/0000-0003-3800-3963

Synopsis

We present an optimal oxygen-blowing system with expert rules to improve the efficiency of refining low-carbon ferrochrome. A nonlinear model based on mass transfer theory, the principles of heat transfer, and the principles of high-temperature chemical reactions for refining low-carbon ferrochrome are established. The model is mainly used to control the oxygen supply rate during argon-oxygen top-bottom double-blown refining, thereby controlling the refining temperature and reducing the carbon content. Twenty production tests using a 5 t argon-oxygen refining furnace demonstrate the effectiveness of the system and reliability of the nonlinear model. A comparison of the model data with the experimental data shows that although the model fails to predict the silicon content in the final refined product, it can predict the contents of the main components at the refining end-point and the refining temperature accurately.

Keywords
prediction model, end-point control, mass transfer theory, expert rules.

Introduction

Low-carbon ferrochrome (LCFeCr) is used for trimming additions in stainless steel production as well as other specialist applications. LCFeCr can be produced by various processes, such as the low-basicity furnace process, Perrin process, electric-silicothermic process, bottom-blown converter process, argon-oxygen decarburization (AOD) process, and vacuum furnace reactor process. (Weitz and Garbers-Craig, 2016; Heikkinen and Fabritius, 2012; Booysen *et al.*, 1998; Bhonde, Ghodgaonkar, and Angal, 2007).

The AOD process has been extensively researched and numerous models have been developed. Noting the change in the partial pressure of carbon monoxide with the bath height, Roy and Robertson (1978a, 1978b) introduced the heat balance to take into account the non-isothermal nature of the bath and proposed a mathematical model for stainless steelmaking. On the basis of the mass and heat balances, Reichel and Szekely (1995) developed a mathematical model of the AOD process for stainless steel. Görnerup and Sjöberg (1999) mathematically modelled the AOD/Creusot-Loire Uddeholm process. Wei and Zhu (2002a, 2002b) modelled the whole AOD process, including the top, side, and combined blowing operations in the decarburization phase and the reduction practice.

In these models, the main product is generally stainless steel. In recent years, many experts have studied the production of LCFeCr by the AOD process (Ville-Valtteri *et al.*, 2013a, 2013b; Qiu *et al.*, 2013; Deo and Srivastava, 2003). In the refining process, the oxygen supply rate, refining duration, refining temperature, and other factors will have a great impact on the composition of the products.

The existing models for stainless steel are not suitable for LCFeCr refining of due to the differences in composition and technology (Heikkinen and Fabritius, 2012). Industry experts and researchers have attached importance to the establishment of mathematical models of LCFeCr production technology, and have conducted research on various aspects of the process. Some scholars have established corresponding mathematical models. Booysen *et al.* (1998) developed a bottom-blown AOD model based on phenomenological heat and kinetic mass transfer. Bhonde, Ghodgaonkar, and Angal (2007) developed a mathematical model according to the metallothermic reduction, triplex process, and vacuum technique. Akimov *et al.* (2013) developed a mathematical model based on the results of industrial smelts and thermodynamic analysis. Although some models describing ferrochrome production have been developed, most of the models focus on individual phenomena rather than the total process. Some important parameters, such as refining temperature, carbon oxidation rate, and mass transfer

rate (Wei and Zhu, 2002a; Ville-Valtteri *et al.*, 2017), have not been reliably determined to date. There is still no accurate mathematical model for LCFeCr production by the top-bottom double-blown AOD process. Many producers still rely on the experience of workers in the refining of LCFeCr. There is therefore an urgent need to establish an accurate model to describe this process.

Mathematical model for low-carbon ferrochrome

Modelling conditions

An AOD furnace with a capacity of 5 t was selected for the experimental work. Oxygen is blown into the furnace through a top lance, and is mixed with the ferrochrome melt. The main lance and the secondary lance are installed at the bottom of the furnace. The main lance blows oxygen and argon. The secondary lance blows argon only.

The solid raw materials are melted in the electric arc furnace, then the molten ferrochrome is poured into the argon-oxygen top-bottom double-blown refining furnace for refining. The initial temperature in the refining furnace is about 1600K. The electric arc furnace provides feed material of fixed composition for the refining furnace. The carbon content is 6.5–8.5%, the silicon content 1.5–2.0%, the chromium content 57–65%, the iron content 25–35%, and the other elements are less than 0.1%.

The following assumptions are made in order to simplify the modeling of the refining process with a small refining capacity:

(1) During the refining process, elements such as Fe, Cr, C, and Si in the high-temperature melt are oxidized. The oxidation reactions and the reduction reactions take place continuously.
(2) It is assumed that the redox reaction in the furnace is uniform during the refining process.
(3) Others trace elements in the melt are ignored.
(4) The refining temperature is controlled between 1800 and 2100K. The temperature inside the furnace is assumed to be uniform.

Chemical reactions in the refining process

The reactions during argon-oxygen refining of LCFeCr occur at normal pressure, in the presence of sufficient oxygen, and at high temperature. The chemical reactions are complex. The main chemical reactions that occur during the stabilization period can be described by Equations [1]–[8] (Bi, 1975; Cai, 1995; Wei *et al.*, 2011).

$$2Fe_{(l)} + O_{2(g)} \rightarrow 2FeO_{(l)} \quad [1]$$

$$C_{(l)} + FeO_{(l)} \rightarrow CO_{(g)} + Fe_{(l)} \quad [2]$$

$$2C_{(l)} + O_{2(g)} \rightarrow 2CO_{(g)} \quad [3]$$

$$C_{(l)} + O_{2(g)} \rightarrow CO_{2(g)} \quad [4]$$

$$2Si_{(l)} + O_{2(g)} \rightarrow 2SiO_{2(s)} \quad [5]$$

$$C_{(l)} + 2FeO_{(l)} \rightarrow CO_{2(g)} + 2Fe_{(l)} \quad [6]$$

$$4Cr_{(l)} + 3O_{2(g)} \rightarrow 2Cr_2O_{3(s)} \quad [7]$$

$$3C_{(l)} + Cr_2O_{3(s)} \rightarrow 2Cr_{(l)} + 3CO_{(g)} \quad [8]$$

where (l) indicates a component of the melt, (s) a component of the slag, and (g) a component of the gaseous phase.

The refining process entails the dynamic equilibrium of high-temperature chemical reactions. The gas produced by the chemical reaction is discharged as flue gas. The molten oxide matter produce by the chemical reactions become the slag. Based on the above reactions, a mathematical model is established to predict the melt content during the refining process and the reaction rates, which can be used to guide production.

Mathematical model of the refining process

Mathematical model based on heat balance

The ultimate goal of refining LCFeCr is to remove carbon and other impurities. Elemental oxidation occurs at the gas-liquid interface (Manuela, Sergey, and Masamichi, 1997), and the elements at the interface are transported by mass transfer (Olga, Genii, and Pavel, 2014). Therefore, the oxidation rate of an element can be calculated from its mass transfer rate (Ville-Valtteri *et al.*, 2017). In this way, the elemental composition of the ferrochrome melt can be predicted.

Heat balance calculation

The heat generated and heat lost during the refining process, are made up of several components (Table I).

According to the law of energy conservation and heat analysis, the heat balance equation is obtained as:

$$\begin{aligned} &W_m c_{p,m} T_0 + W_s c_{p,s} T_0 + \\ &\left(\frac{dO_2}{dt}\rho_{O_2} c_{pO_2} + \frac{dAr}{dt}\rho_{Ar} c_{pAr}\right) T_c + \\ &\frac{W_m}{100}\left(\frac{dW[C]\%}{dt}\Delta H_C + \frac{dW[Cr]\%}{dt}\Delta H_{Cr} + \right. \\ &\left.\frac{dW[Si]\%}{dt}\Delta H_{Si}\right) dt = W_m c_{p,m} T \\ &\left[1 + \frac{dt}{100}\left(\frac{dW[C]\%}{dt} + \frac{dW[Cr]\%}{dt} + \frac{dW[Si]\%}{dt}\right)\right] \\ &+ c_y \frac{2p_y V_y M_y}{RT} T + Q_t + Q_d \end{aligned} \quad [9]$$

Table I

Heat input items and output items

Heat input	Heat output
Enthalpy of molten ferrochrome fed into the furnace	Enthalpy of ferrochrome melt at the end of refining
Enthalpy released by the oxidation reactions	Enthalpy of slag
Heat of the gas	Heat loss due to flue gas
Heat of additives	The loss heat by the furnace body

A nonlinear prediction model, incorporating mass transfer theory and expert rules

The symbols used in this and subsequent equations are defined at the end of the paper.

The heating rate of the furnace is given by Equation [10]. It can be seen that the rate of temperature increase is mainly affected by the oxidation reactions and the heat loss.

$$\frac{dT}{dt} = \left[\left(\frac{dW[C\%]}{dt}\Delta H_C + \frac{dW[Cr\%]}{dt}\Delta H_{Cr} + \frac{dW[Si\%]}{dt}\Delta H_{Si}\right) - c_{p,m}T\frac{dW[C]\%}{dt} + \frac{dW[Cr]\%}{dt} + \frac{dW[Si]\%}{dt}\right]\frac{W_m + W_s}{100c_mW_m + 100c_sW_s} - c_y\frac{2p_yq_yM_y}{RT}T - \left(q_t + q_d\right) \quad [10]$$

Oxidation rate calculation

Diffusion of carbon through the gas-liquid boundary layer has been shown to be the rate-controlling mechanism (He *et al.*, 1994). According to mass transfer theory, the mass transfer rate of carbon across the gas-liquid interface can be calculated as (Guo, 2006):

$$\frac{dn_C}{dt} = Ak_d\left(c_{[C]} - c_{[C],s}\right) \quad [11]$$

where $A = 4\varpi r^2$ is the bubble surface area; k_d is mass transfer coefficient of oxygen; $c_{[C]}$ is the concentration of carbon in molten ferrochrome, and $c_{[C]s}$ is the concentration of carbon at the bubble interface of molten ferrochrome.

$$c_{[C]} - c_{[C]s} = c_{[O]} - c_{[O]s} = \Delta c_{[O]} \quad [12]$$

where $c_{[O]}$ is the concentration of oxygen in molten ferrochrome in mol/m^3; $c_{[O]s}$ is the concentration of oxygen at the bubble interface in mol/m^3; and $\Delta c_{[O]}$ is the equilibrium concentration of oxygen (Guo, 2006).

$$\Delta c_{[O]} = \frac{\rho}{Ar_0}\Delta\omega_{[O]} \quad [13]$$

where r_0 is the initial radius of the bubble (6×10^{-3} m) (Guo, (2006), and $\Delta\omega_{[O]}$ is the degree of supersaturation. The reported values for the parameter $\Delta\omega_{[O]}$ range from 0.015% to 0.025% (Guo, 2006). In this work, $\Delta\omega_{[O]} = 0.02\%$.

$$k_d = 2\sqrt{\frac{D_C}{\pi t_e}} = 4\left(\frac{gD_C}{9\pi^2 r}\right)^{\frac{1}{4}} \quad [14]$$

where D_C is the diffusion coefficient of carbon in molten ferrochrome (5×10^{-9} m^2/s) (Li, 2004); t_e is element contact time; g is acceleration due to gravity (9.81 m/s^2); and r is the bubble radius.

$$r = \left\{\frac{14RT}{\sqrt[4]{g}}\left(\frac{3D}{\pi}\right)^{\frac{1}{2}}\left(\frac{\Delta c_{[O]}}{\rho g}\right)\left[\ln\left(h + \frac{p_g}{\rho g}\right) - \ln\frac{p_g}{\rho g}\right]\right\}^{\frac{4}{7}} \quad [15]$$

where R is the gas constant (–8.314 J/(mol·K)); ρ is the density of molten ferrochrome (7×10^3 kg/m^3), p_g is standard atmosphere, and h is the depth of the furnace.

Substituting R, ρ, p_g, h and Equation [13], the bubble radius is calculated as follows:

$$r = 0.5 \times 10^{-5}T \quad [16]$$

Substituting Equations [13], [14], and [16] into Equation [11] yields:

$$\frac{dn_C}{dt} = 1.13 \times 10^{-8}T^{\frac{7}{4}} \quad [17]$$

$dW[C]\%$ is the rate of decline in carbon content in the molten ferrochrome, which is a function of the rate of ascent of bubbles through the melt. The relationship between dn_C and $dW[C]\%$ is as follows (Guo, (2006):

$$dW[C]\% = \frac{M_C dn_C}{1000W} \times 100 = \frac{12\times10^{-4}dn_C}{W} \quad [18]$$

The rate of change in carbon content in molten ferrochrome can be expressed as follows:

$$\frac{dW[C]\%}{dt} = \frac{M_C dn_C}{1000Wdt} \times 100 = \frac{12 \times 10^{-4}dn_C}{Wdt} = \frac{1.36 \times 10^{-11}T^{\frac{7}{4}}}{W} \quad [19]$$

From the temperature, refining time, and the weight of molten ferrochrome, the oxidation rate of carbon in the furnace can be predicted. Thereby the carbon content in the melt can be also calculated.

The oxidation rate of chromium at the gas-liquid interface is positively correlated with the mass transfer rate of chromium while the temperature is higher than 1873K. The mass transfer rate can be described as follows:

$$\frac{dn_{Cr}}{dt} = Ak_{Cr}\left(c_{[Cr]} - c_{[Cr]s}\right) = 0.41 \times 10^{-8}T^{\frac{7}{4}} \quad [20]$$

where $k_{Cr} = 4\left(\frac{gD_{Cr}}{9\pi^2 r}\right)^{\frac{1}{4}}$ is the mass transfer coefficient of chromium, and $D_{Cr} = 1.8 \times 10^{-9}$ m^2/s is the diffusion coefficient of chromium in molten ferrochrome.

The oxidation rate of chromium, which can be used to predict the chromium content in the alloy, is given as follows:

$$\frac{dW[Cr]\%}{dt} = \frac{M_{Cr}dn_{Cr}}{1000Wdt} \times 100 = \frac{2.13\times10^{-11}T^{\frac{7}{4}}}{W} \quad [21]$$

From the temperature, refining time, and the weight of molten ferrochrome, the oxidation rate of chromium in the furnace can be predicted. Thereby the chromium content in the melt can be also calculated.

The oxidation of silicon is similar to that of carbon. The mass transfer rate of silicon can be described as follows:

$$\frac{dn_{Si}}{dt} = Ak_{Si}\left(c_{[Si]} - c_{[Si]s}\right) = 0.1 \times 10^{-8}T^{\frac{7}{4}} \quad [22]$$

where $k_{Si} = 4\left(\frac{gD_{Si}}{9\pi^2 r}\right)^{\frac{1}{4}}$ is the mass transfer coefficient of silicon, and D_{Cr} is the diffusion coefficient of silicon in molten ferrochrome (0.44×10^{-9}) m^2/s).

The oxidation rate of silicon is given by Equation [23].

$$\frac{dW[Si]\%}{dt} = \frac{M_{Si}dn_{Si}}{1000Wdt} \times 100 = \frac{1.23\times10^{-11}T^{\frac{7}{4}}}{W} \quad [23]$$

The oxidation rate of silicon in the furnace can be predicted from the temperature, refining time, and the weight of molten ferrochrome. Thereby the silicon content in the bath can be calculated.

The standard enthalpies of formation of the respective oxides (at 298K) involved in the following equations and the relevant heat capacities at constant pressure with the enthalpies of solution formation were all taken from Wei and Zhu (2002a) and Turkdogan (1980).

$$\Delta H_C = \Delta H_{CO} - \Delta H_C - \frac{\Delta H_{O_2}}{2}\ \Delta H_C = 11852 - \left(2.367T_g + 1.708 \times 10^{-4}T_g^2 + 3.853 \times 10^3/T_g\right) \quad [24]$$

$$\Delta H_{Cr} = \Delta H_{Cr_2O_3} - 2\Delta H_{Cr} - 3\frac{\Delta H_{O_2}}{2}\ \Delta H_{Cr} = 11519 - \left(1.148T + 4.4 \times 10^{-5}T^2 + 1.5 \times 10^4/T\right) \quad [25]$$

$$\Delta H_{Si} = \Delta H_{SiO_2} - \Delta H_{Si} - \Delta H_{O_2}\ \Delta H_{Si} = 30658 - \left(2.15T + 1.45 \times 10^{-4}T^2\right) \quad [26]$$

Heat dissipation

Heat dissipation calculation for furnace body

An elevation diagram of the argon-oxygen refining furnace is shown in Figure 1. The furnace is composed of two parts: a furnace body and a furnace cap. The middle part of the furnace body is cylindrical; the upper and lower parts are truncated cones. The ratio between the depth of the molten bath and the height of the furnace chamber is 1:3. The ratio between the molten bath depth and the diameter of the molten pool surface is 1:2. The furnace body is regarded as a cylinder for convenience of calculation. The refractory lining of the shaft has two layers. The inner (working) layer consists of chrome-magnesia refractory brick with a thickness of 350 mm. The outer layer is insulated and reinforced with refractory clay bricks. Its thickness is 115 mm.

In the LCFeCr production process in an AOD furnace, the temperature in the furnace is about 1873–2073K, the outer wall temperature is about 623K, and the ambient temperature is 293–303K. In the refining process, the heat losses consist of the conduction heat and radiant heat from the furnace body, the conduction heat and radiant heat at the bottom of the furnace, and the heat loss in the flue gas (Farrera-Buenrostro *et al.*, 2019). According to the equation for the heat transfer rate, the heat loss from the furnace body can be calculated.

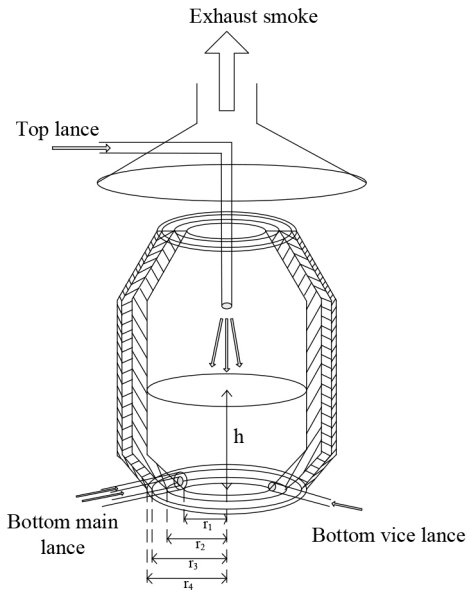

Figure 1—Schematic diagram of an AOD furnace

The exothermic reactions occur within a few minutes, and no heat is transferred to the lining during this time. It is assumed that each part of the furnace lining has the same heat transfer characteristics, which is convenient for theoretical analysis and modelling. Therefore, the heat transfer state is assumed to be stable. The heat transfer rate of a three-layer lining furnace body (Liao, *et al.* 2017) can be described as follows:

$$q_t = \frac{2\pi L(T_1 - T_4)}{\frac{1}{\lambda_1}\ln\frac{r_2}{r_1} + \frac{1}{\lambda_2}\ln\frac{r_3}{r_2} + \frac{1}{\lambda_3}\ln\frac{r_4}{r_3}} \quad [27]$$

where T_1 is the temperature in the furnace, T_4 is the outer wall temperature, λ_1 is the thermal conductivity of magnesia brick, λ_2 is the thermal conductivity of magnesia-chrome brick, λ_3 is the thermal conductivity of the shell, and r_i is the radius. In this work, $\lambda_1 = 3.49$, $\lambda_2 = 1.42$, $\lambda_3 = 60$, $r_1 = 0.7$ m, $r_2 = 1.0$ m, $r_3 = 1.06$ m, and $r_4 = 1.15$ m. Therefore, the heat loss from the body of the furnace, q_t, is $41.87\Delta T$.

The heat transfer rate at the bottom of the furnace (Liao, *et al.* 2017) can be described as follows:

$$q_d = \lambda A\frac{dT}{dn} = \frac{A(T_1 - T_4)}{\frac{\delta_1}{\lambda_1} + \frac{\delta_2}{\lambda_2} + \frac{\delta_3}{\lambda_3}} \quad [28]$$

where $\delta_1 = 0.6$ m is the thickness of the magnesia brick, $\delta_2 = 0.12$ m is the thickness of magnesia-chrome brick, and $\delta_3 = 0.1$ m is the thickness of shell. Therefore, the heat loss from the bottom of the furnace, q_d, is $3.12\Delta T$.

Flue gas heat loss calculation with expert rules

The flue gas is composed mainly of carbon monoxide, oxygen, argon, and some dust. Dust, which consists of solid particles, can be collected by the dust collector and the heat loss calculated together with that of the slag. Therefore, the flue gas is considered to be composed of carbon monoxide, carbon dioxide, oxygen, and argon only.

The flue gas heat can be calculated as follows:

$$Q_y = CmT_g \quad [29]$$

where C_y is the specific heat capacity, m is the material quality, and T_g is the temperature of the flue gas.

The gas quality can be calculated as follows, assuming it follows the Ideal Gas Law:

$$m = pVM/RT_g \quad [30]$$

where p is the gas pressure, V is the volume of gas, M is the molar mass of gas, and T_g is the gas temperature.

If the flue gas flow is substituted for the gas volume, the heat loss rates via the flue gas can be obtained as follows:

$$q_y = C_y\frac{2P_y\frac{dQ_y}{dt}M_y}{RT_g}T_g \quad [31]$$

where C_y is the specific heat capacity of the flue gas, P_y is the flue gas pressure, $\frac{dQ_y}{dt}$ is the flue gas flow, M_y is the molar mass of flue gas, and R is the gas constant. From the oxygen utilization efficiency, the oxygen partial ratio, and the specific heat capacity of the gas, the specific heat capacity of the flue gas can be calculated. The pressure of the flue gas is equal to atmospheric pressure. From the oxygen utilization efficiency, the oxygen

Table II

Flue gas me parameters

P_y = 1.01325 × 10^5Pa	CO_2 = 0.9184
C_{Ar} = 0.5238	C_{CO} = 1.0447
η = 0.8	MO_2 = 32 × 10^{-3}kg/mol
M_{Ar} = 40 × 10^{-3}kg/mol	M_{CO} = 28 × 10^{-3}kg/mol

partial ratio, and the molar mass of the gas, the molar mass of the flue gas can be calculated. The flue gas temperature is about half of the furnace temperature (He, 2016). The values of some flue gas parameters (Chen, 1984; Gorges, Pulvemacher, and Rubens, 1978) are shown in Table II:

In order to lessen the oxidation of chromium and avoid excessive temperatures, the ratio of oxygen to argon needs to be adjusted with the carbon content and refining temperature of the furnace (Andersson *et al.*, 2012). The physical and chemical reactions in the high-temperature refining process are very complex. The rate of reaction will be affected by factors such as the flow rate of oxygen, the amount of feed, and the rate of diffusion of elements in the bath (Odenthal, 2010). Therefore, the amounts of argon and oxygen should be adjusted according to expert rules. In the early stage of refining, slag-forming agent should be added to prevent chromium volatilization. In the later stage of refining, deoxidizer should be added to remove oxygen in the bath. Chromium ore should be added to increase the chromium content of the end product. Figure 2 shows the flow chart of the model strategy. The whole process is divided into three stages based on expert rules. The corresponding information is listed in Table III.

From the ratio of the gases and the oxygen utilization efficiency, the flow rate of flue gas for the three stages can be calculated separately.

For the first stage:

$$\frac{dQ_y}{dt} = (1-85\%)\frac{dO_2}{dt} + \frac{1}{6}\frac{dO_2}{dt} + 30\% \times 85\%\frac{dO_2}{dt} = 0.58\frac{dO_2}{dt} \quad [32]$$

For the second stage:

$$\frac{dQ_y}{dt} = (1-65\%)\frac{dO_2}{dt} + \frac{3}{7}\frac{\mathrm{d}O_2}{\mathrm{d}t} + 80\% \times 65\%\frac{dO_2}{dt} = 1.3\frac{dO_2}{dt} \quad [33]$$

For the third stage:

$$\frac{dQ_y}{dt} = (1-35\%)\frac{dO_2}{dt} + \frac{4}{5}\frac{dO_2}{dt} + 35\%\frac{dO_2}{dt} = 1.8\frac{dO_2}{dt} \quad [34]$$

The specific heat capacity of the flue gas can be calculated based on the ratio of carbon monoxide, oxygen, and argon as follows:

For the first stage:

$$C_y = \frac{(1-85\%)}{(1-85\%)+1/6+30\%\times85\%}c_{O_2} + \frac{1/6}{(1-85\%)+1/6+30\%\times85\%}c_{Ar} + \frac{30\%\times85\%}{(1-85\%)+1/6+30\%\times85\%}c_{CO} = 0.26c_{O_2} + 0.29c_{Ar} + 0.45c_{CO} = 0.86 \quad [35]$$

For the second stage:

$$C_y = \frac{(1-65\%)}{(1-65\%)+3/7+80\%\times65\%}c_{O_2} + \frac{3/7}{(1-65\%)+3/7+80\%\times65\%}c_{Ar} + \frac{80\%\times65\%}{(1-65\%)+3/7+80\%\times65\%}c_{CO} = 0.27c_{O_2} + 0.33c_{Ar} + 0.40c_{CO} = 0.84 \quad [36]$$

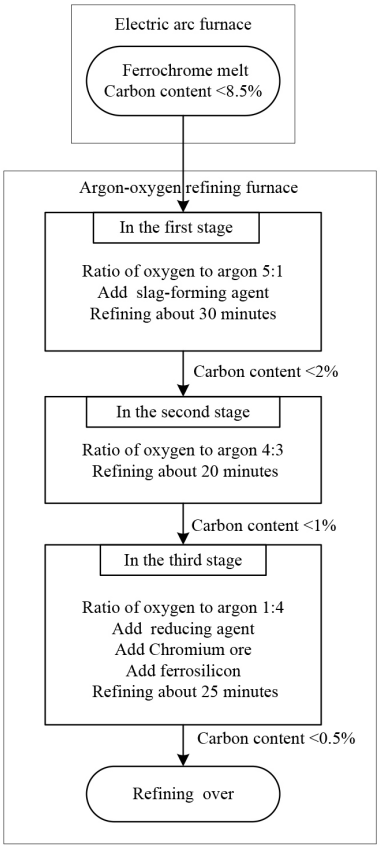

Figure 2—Flow chart of model strategy

Table III

The data of three stages

	The volume ratio of oxygen to argon	Oxygen utilization efficiency(%)	The oxygen partial ratio
The first stage	5:1	80–90	C ≤ 30%, Si ≤ 30%
The second stage	4:3	60–70	C ≤ 80% Si ≤ 10%
The third stage	1:4	30–40	C ≤ 90% Si ≤ 0%

For the third stage:

$$C_y = \frac{(1-35\%)}{(1-35\%)+4/5+35\%} c_{O_2} + \frac{4/5}{(1-35\%)+4/5+35\%} c_{Ar} + \frac{35\%}{(1-35\%)+4/5+35\%} c_{CO} = 0.33c_{O_2} + 0.24c_{Ar} + 0.20c_{CO} = 0.77 \quad [37]$$

The molar mass of the flue gas can be calculated based on the carbon monoxide, oxygen, and argon contents as follows:

For the first stage:

$$M_y = \frac{(1-85\%)}{(1-85\%)+1/6+30\%\times85\%} M_{O_2} + \frac{1/6}{(1-85\%)+1/6+30\%\times85\%} M_{Ar} + \frac{85\%}{(1-85\%)+1/6+30\%\times85\%} M_{CO} = 0.26M_{O_2} + 0.29M_{Ar} + 0.45M_{CO} = 32.52\times10^{-3}\text{kg mol}^{-1} \quad [38]$$

For the second stage:

$$M_y = \frac{(1-65\%)}{(1-65\%)+3/7+80\%\times65\%} M_{O_2} + \frac{3/7}{(1-65\%)+3/7+80\%\times65\%} M_{Ar} + \frac{65\%}{(1-65\%)+3/7+80\%\times65\%} M_{CO} = 0.27M_{O_2} + 0.33M_{Ar} + 0.40M_{CO} = 33.04\times10^{-3}\text{kg mol}^{-1} \quad [39]$$

For the third stage:

$$M_y = \frac{(1-35\%)}{(1-35\%)+4/5+35\%} M_{O_2} + \frac{4/5}{(1-35\%)+4/5+35\%} M_{Ar} + \frac{35\%}{(1-35\%)+4/5+35\%} M_{CO} = 0.36M_{O_2} + 0.45M_{Ar} + 0.19M_{CO} = 34.84\times10^{-3}\text{kg mol}^{-1} \quad [40]$$

The heat loss rates *via* flue gas in the three stages are calculated as follows:

For the first stage:

$$q_y = C_y \frac{2P_y \frac{dQ_y}{dt} M_y}{RT} T = 3.99\times10^3 \frac{dO_2}{dt} \quad [41]$$

For the second stage:

$$q_y = C_y \frac{2P_y \frac{dQ_y}{dt} M_y}{\text{RT}} T = 8.99\times10^3 \frac{dO_2}{dt} \quad [42]$$

For the third stage:

$$q_y = C_y \frac{2P_y \frac{dQ_y}{dt} M_y}{RT} T = 12.04\times10^3 \frac{dO_2}{dt} \quad [43]$$

It can be shown from the model that the bath temperature is related to the oxygen blowing rate, the oxygen blowing time, and the weight of the ferrochrome. Hence the bath temperature can be predicted as follows.

For the first stage:

$$\frac{dO_2}{dt} = \frac{1\times10^{-14}T^{\frac{7}{4}}}{W}\left(1.96\times10^4 - 1.69\text{T} - 0.83\times10^{-4}T^2 - \frac{1.07\times10^4}{T}\right) -1.13\times10^{-2}T + 7.02 - 0.25\times10^{-3}\frac{dT}{dt} \quad [44]$$

For the second stage:

$$\frac{dO_2}{dt} = \frac{1\times10^{-14}T^{\frac{7}{4}}}{W}\left(0.87\times10^4 - 0.75T - 0.37\times10^{-4}T^2 - \frac{0.47\times10^4}{T}\right) -0.5\times10^{-2}T + 3.11 - 0.11\times10^{-3}\frac{dT}{dt} \quad [45]$$

For the third stage:

$$\frac{dO_2}{dt} = \frac{1\times10^{-14}T^{\frac{7}{4}}}{W}\left(0.65\times10^4 - 0.56\text{T} - 0.27\times10^{-4}T^2 - \frac{0.35\times10^4}{T}\right) -0.37\times10^{-2}T + 2.33 - 0.08\times10^{-3}\frac{dT}{dt} \quad [46]$$

Experimental results and analysis

Twenty production tests were carried out in a 5 t argon-oxygen refining furnace, and the results compared with the predicted values. As shown in Figures 3–6, the changes in carbon, silicon, and chromium content and temperature during the refining process can be clearly seen.

The reducing agent is fed into the refining process in the third stage and affects the contents of C and Si in the reaction. Therefore, the actual contents of C and Si in the third stage show a large deviation from the predicted values.

Temperature is the most important parameter in the whole argon-oxygen refining process. The control of C, Si, and Cr contents and temperature are closely related. The changes in C, Si, and Cr content are shown in Figures 3–5, and the corresponding temperature change trend is shown in Figure 6.

In the first reaction stage, the top lance supplies oxygen from the top of the furnace, the main lance supplies the oxygen- argon mixture from the bottom of the furnace, and the secondary lance supplies argon from the bottom of the furnace. The ratio of oxygen to argon is 5:1. Elements such as carbon, chromium, and silicon in the ferrochrome melt are oxidized rapidly, and the refining temperature increases rapidly due to the exothermic oxidation reactions. In order to reduce the volatilization of chromium, 150 kg of slag-forming agent is added, and the refining temperature drops slightly.

At the end of the first reaction stage, the temperature reaches 2047K, the carbon content falls to 1.24%, and the silicon content is 0.49%. This takes about 30 minutes, and the total amount of oxygen blown is about 105 Nm³. The oxidation rate of chromium slows down. In the second reaction stage, the top lance stops supplying oxygen, the main lance supplies the oxygen- argon mixture, and the secondary lance supplies argon. The ratio of oxygen to argon is 4:3. The total supply of oxygen is reduced, the supply of argon is increased, and the temperature of the molten pool is allowed to rise in a controlled fashion. The oxidation of

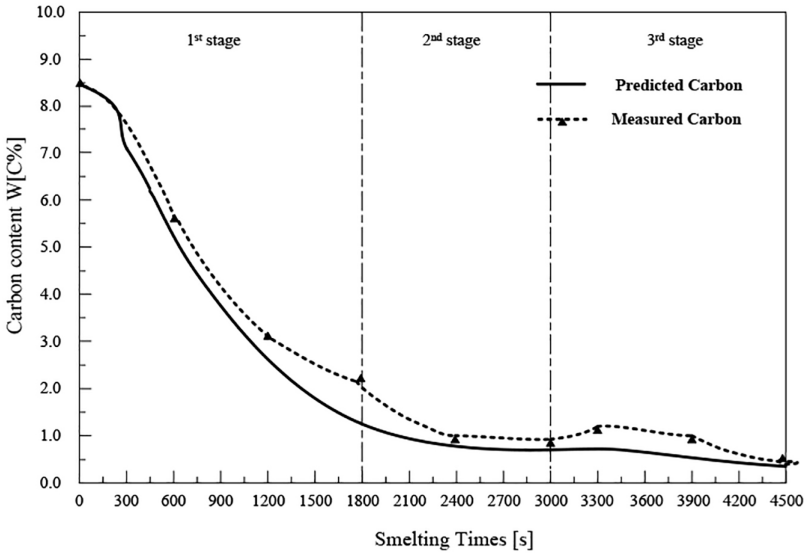

Figure 3—Change in carbon content during the refining process

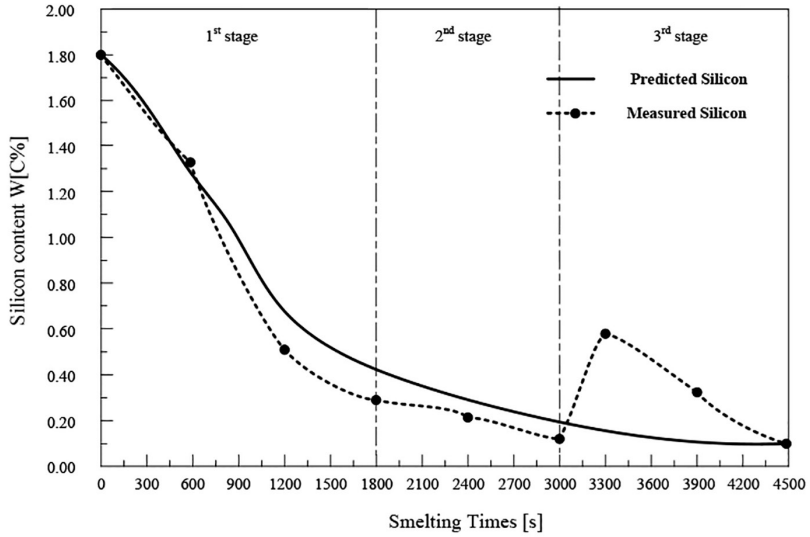

Figure 4—Change in silicon content during the refining process

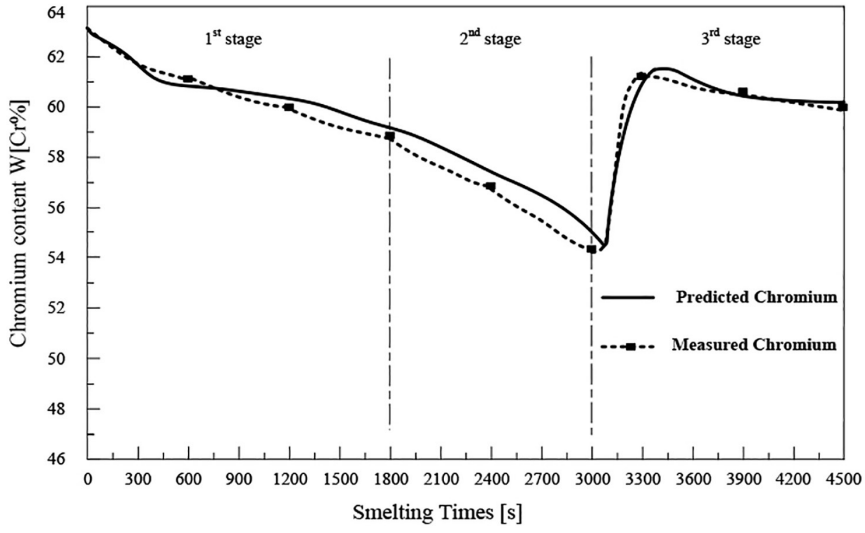

Figure 5—Change in chromium content during the refining process

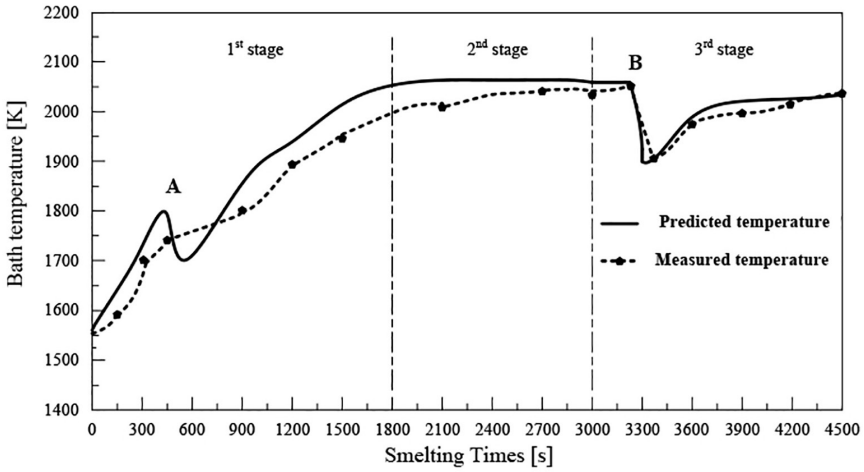

Figure 6—Temperature change during the refining process

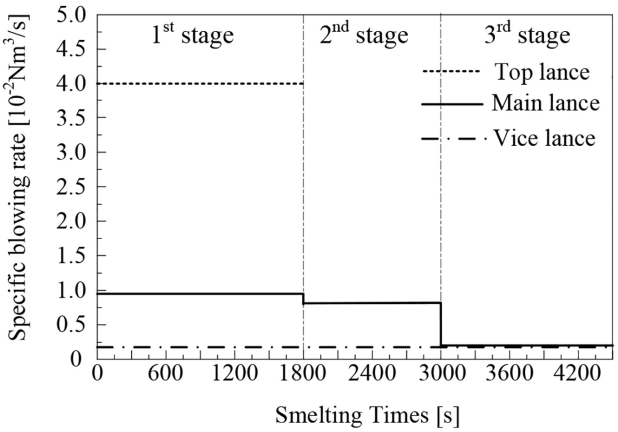

Figure 7—Specific blowing rate

carbon and oxygen takes place mainly in the molten pool, the carbon content is further reduced, the oxidative heat release and heat dissipation are balanced, and the temperature of the bath tends to be stable. After 20 minutes of refining, the total amount of oxygen blown is about 55 m³, the carbon content is 0.96%, and the temperature is 2053K. Entering the third reaction stage, the ratio of oxygen to argon blown is 1:4. 100 kg of reducing agent is added to reduce the chromium from the slag. In order to increase the chromium content at the end of the refining process, 200 kg of chromium ore is added, and 150 kg of ferrosilicon is added to remove oxygen. After 25 minutes, refining is stopped. The total oxygen supply is about 30 m³, the final carbon content is 0.43%, the chromium content is 60.1%, and the temperature is 2036K.

The specific blowing rate is shown in Figure 7.

The test data is shown in Table IV, which lists the liquid phase mass, initial temperature, composition, and refining time.

The predicted and experiments data for the 20 production tests are listed in Table V. The maximum absolute errors between the model predictions and the measured values of carbon content, chromium content, and temperature are 0.07 mass%, 2.92 mass%, and 6K, respectively. The average relative errors between the predicted and the measured values of carbon content, chromium content, and temperature are 5.49%, 1.79%, and 0.21%, respectively. The results show that the model can accurately predict the contents of the main components at the refining end point and the refining temperature, which proves that the model is reliable. However, the predicted value of the silicon content deviates considerably from the measured value. The reason for this is that deoxidizers were been added in the later stages of refining.

Conclusion

A mathematical model has been established for refining low-carbon ferrochrome based on high-temperature oxidation reactions, mass transfer theory, and expert rules. The effectiveness of the model was verified by comparing the predicted compositions of the metal phase with the measured values from 20 test runs in a 5 t argon-oxygen refining furnace. Statistical analysis of the results showed that the prediction accuracy is high in terms of final carbon content, chromium content, and metal bath temperature. The model can accurately estimate the refining end point composition and the temperature, and can be used to guide the production of low-carbon ferrochrome by the AOD process. The experimental data, such as furnace capacity, geometry, and additives, can be adjusted to the actual production requirements.

List of symbols

W_m	Mass of liquid ferrochrome (kg)
W_s	Mass of slag (kg)
T_g	Temperature of flue gas (K)

Table IV

Test data from the 5 t argon-oxygen refining furnace

Refining No.	Initial mass (t)	Initial temperature (K)	Initial composition of molten ferrochrome (mass%)			Refining time (min)
			C	Si	Cr	
1#	5.13	1535	8.45	1.80	62.87	75
2#	5.24	1575	8.40	1.82	61.58	77
3#	4.75	1543	8.31	1.79	60.72	74
4#	5.00	1554	8.56	1.89	62.52	60
5#	4.55	1563	8.35	1.85	61.97	64
6#	5.28	1568	8.57	1.96	62.03	75
7#	3.54	1574	7.98	1.81	61.88	62
8#	5.30	1558	8.04	1.99	61.48	68w
9#	3.18	1578	7.81	1.85	63.36	52
10#	4.98	1566	8.14	2.01	60.59	63
11#	5.04	1568	8.34	1.86	61.33	65w
12#	5.34	1547	8.20	2.03	61.5	80
13#	4.63	1561	8.06	1.88	62.05	68
14#	4.13	1569	7.86	1.94	60.84	57
15#	3.89	1578	8.42	2.01	61.10	62
16#	5.21	1584	7.48	1.79	58.7	74
17#	4.37	1560	8.11	1.82	61.87	63
18#	4.62	1571	8.20	1.89	61.59	67
19#	4.81	1562	8.33	1.85	60.93	w65
20#	4.46	1577	7.88	1.96	61.47	60

Table V

Predicted data, experiments data and relative error

Refining No.	Composition of molten ferrochrome at endpoint of refining period											
	C(mass%)			Cr(mass%)			Si(mass%)			Temperature (K)		
	Pred	Mea	RE	Pred	Mea	RE	Pred	Mea	RE	Pred	Mea	RE
1#	0.50	0.45	11.1%	61.53	58.61	5.0%	0.10	0.28	64.3%	2033	2038	0.2%
2#	0.50	0.48	4.2%	60.52	60.18	0.6%	0.13	0.26	50.0%	2033	2039w	0.3%
3#	0.50	0.45	11.1%	58.24	58.03	0.4%	0.15	0.28	46.4%	2033	2029	0.2%
4#	0.50	0.43	16.3%	61.28	60.09	2.0%	0.13	0.21	38.1%	2033	2036w	0.1%
5#	0.50	0.51	2.0%	61.09	60.62	0.8%	0.13	0.32	59.4%	2033	2035	0.1%
6#	0.50	0.48	4.2%	60.31	59.71	1.0%	0.12	0.22	45.5%	2033	2038	0.2%
7#	0.50	0.49	2.0%	60.85	60.26	1.0%	0.14	0.25	44.0%	2033	2029	0.2%
8#	0.50	0.47	6.4%	59.76	57.87	3.3%	0.12	0.24	50.0%	2033	2034	0.3%
9#	0.50	0.51	2.0%	59.02	60.90	3.1%	0.11	0.35	68.6%	2033	2029	0.2%
10#	0.50	0.49	2.0%	58.81	58.43	0.7%	0.15	0.31	51.6%	2033	2037	0.2%
11#	0.50	0.52	3.8%	60.13	58.86	2.2%	0.16	0.30	46.7%	2033	2039	0.3%
12#	0.50	0.55	9.1%	58.19	57.81	0.7%	0.18	0.37	51.4%	2033	2037	0.2%
13#	0.50	0.51	2.0%	60.84	59.53	2.2%	0.14	0.34	58.8%	2033	2040	0.3%
14#	0.50	0.47	6.4%	57.37	56.90	0.8%	0.11	0.20	45.0%	2033	2038	0.2%
15#	0.50	0.52	3.8%	58.68	57.04	2.9%	0.15	0.36	58.3%	2033	2040	0.3%
16#	0.50	0.46	8.7%	56.83	56.63	0.4%	0.09	0.26	58.6%	2033	2036	0.1%
17#	0.50	0.49	2.0%	60.42	58.77	2.8%	0.12	0.24	50.0%	2033	2028	0.2%
18#	0.50	0.51	2.0%	60.61	59.25	2.3%	0.16	0.28	42.9%	2033	2037	0.2%
19#	0.50	0.48	4.2%	58.88	57.52	2.4%	0.13	0.29	55.2%	2033	2038	0.2%
20#	0.50	0.47	6.4%	58.44	57.81	1.1%	0.13	0.25	48.0%	2033	2029	0.2%

Pred: predicted; Mea: measured; RE: relative error .

T_0 Initial temperature (K)
T_c Room temperature (K)
$dW[i]\%/dt$ Change rate of element i in metal bath (mol/(kg·s))
dO_2/dt Oxygen blowing rate (Nm^3/s)
dAr/dt Argon blowing rate (Nm^3/s)
ΔH_i Reaction enthalpy of element i (J/mol)
M_i Molar mass of element i (kg/mol)
Q_t Heat transfer through furnace body (J)
I Heat transfer through the bottom of the furnace (J)
C_m Specific heat capacity of the ferrochrome melt at constant pressure (J/(kg·K))
C_i Specific heat capacity of element i at constant pressure (J/(kg·K))
C_s Specific heat capacity at constant pressure of the slag (J/(kg·K))
A Surface area (m^2)
R Gas constant (J/(mol·K))
m Mass (kg)
dn_i/dt Mass transfer rate of element i (V/s)
$\Delta C_{[O]}$ Equilibrium concentration of oxygen (mol/m^3)
Ip_g Ambient pressure (Pa)

t_e	Contact time (s)
g	Standard gravity (m/s²)
$\Delta\omega_{[i]}$	Degree of supersaturation (mol/m³)
C_y	Specific heat capacity of the flue gas at constant pressure (J/(kg·K))
V_y	Flue gas volume (m³)
p_y	Flue gas pressure (Pa)
q_y	Heat loss rate via flue gas (J/s)
k_i	Mass transfer coefficient of element i (m/s)
D_i	Diffusion coefficient (m²/s)
r^i	Radius (m)
h	Depth of the furnace (m)
q_t	Heat transfer rate through furnace body (J/s)
q_d	Heat transfer rate through the bottom of the furnace (J/s)
λ_i	Heat conductivity (W/(m·K))
δi	Thickness of the diffusion boundary layer (m)
ρ_i	Density of element i (kg/m³)
π	Mathematical constant (m)

Acknowledgement

The authors gratefully acknowledge the support of the National Natural Science Foundation of China (51374040).

References

Akimov, E.N., Voronov, Y.I., Senin, A.V., and Roshchin, V.E. 2013. Production low-carbon ferrochrome with low content of phosphorus using the complex reducer. *INFACON XIII. Proceedings of the Thirteenth International Ferroalloys Congress: Efficient Technologies in Ferroalloy Industry,* Almaty, Kazakhstan. pp. 49-56. https://www.pyrometallurgy.co.za/InfaconXIII/0049-Akimov.pdf

Andersson, J-A. 1988. A thermodynamic evaluation of the Fe-Cr-C system. **Metallurgical Transactions A**, vol. 19A. pp. 627-636.

Andersson, N.Å.I., Anders, T., Jonsson, L.T.I., and Jönsson. PG. 2012. An in-depth model-based analysis of decarburization in the AOD process. *Steel Research International*, vol. 83, no. 11. pp. 1039–1052.

Bhonde, P.J., Ghodgaonkar, A.M., and Angal, R.D. 2007. Various techniques to produce low carbon ferrochrome. *INFACON XI: Proceedings of the 11th International Conference on Innovations in the Ferro Alloy Industry*. Indian Ferro Alloy Producers Association, New Delhi. pp. 85-90. https://www.pyrometallurgy.co.za/InfaconXI/085-Bhonde.pdf

Bi, M. 1975. Equilibrium relationship of oxygen decarburization for ferrochrome. *Iron and Steel*, no. 2. pp. 86–88.

Booysen, L.M., Nelson, L.R., Narayana, S.K., and Visser, M. 1998. Development of an operator guidance system for intermediate carbon charge chromium production. *Proceedings of INFACON 8*, Beijing, China, 7–10 June 1998. pp. 343–349. https://www.pyrometallurgy.co.za/InfaconVIII/343-Booysen.pdf

Cai, H.D. 1995. Thermodynamics and kinetics of stainless steel refining. *Metallurgy of Sichuan*, no. 3. pp. 19, 25–29.

Chen, J. 1984. Handbook of Common Using, Graphs and Tables in Steelmaking. Metallurgical Industry Press. Beijing.

Debroy, T. and Robertson, D.G.C. 1978a. A mathematical model for stainless steelmaking. Part I. Argon oxygen steam mixtures. *Ironmaking and Steelmaking*, vol. 5. pp. 198–206.

Debroy, T. and Robertson, D.G.C. 1978b. A mathematical model for stainless steelmaking. Part II. Application to AOD heats. *Ironmaking and Steelmaking*, vol. 5. pp. 206–210.

Deo. B. and Srivastava, V. 2003. Process control and optimization of the AOD process using genetic algorithm. *Materials and Manufacturing Processes*, vol. 18. pp. 401–408.

Farrera-Buenrostro, J.E., Hernández-Bocanegra, C.A., Ramos-Banderas, J.A., Torres-Alonso, E., López-Granados, N.M., and Ramírez-Argáez M.A. 2019. Analysis of temperature losses of the liquid steel in a ladle furnace during desulfurization stage. *Transactions of the Indian Institute of Metals*, vol. 72, no. 4. pp. 899–909.

Gorges. H., Pulvemacher. W., and Rubens. W. 1978. Development and advantages of top blowing in combination with the AOD process at Fried. *Iron & Steelmaker*, vol. 5, no. 7. pp. 40–33.

Görnerup, M. and Sjöberg, P. 1999. AOD/CLU process modelling: optimum mixed reductants addition. *Ironmaking and Steelmaking*, vol. 26, no. 1. pp. 58–63.

Guo. H. 2006. Physical and Chemical Principles of Metallurgical Industry. Metallurgical Industry Press. Beijing.

He, G. 2016. Temperature control of the evaporative cooler outlet at converter steelmaking. *Metallurgical Industry Automation*, vol. 40, no. 5. pp. 26–30.

He, P., Xing, K.W., and Zhang R.S. 1994. Study on mass transfer behaviour of refining reduction of prereduced pellets in Fe-C melt. *Engineering Chemistry & Metallurgy*, vol. 15, no. 1. pp. 15–22.

Heikkinen, E-P. and Fabritius, T. 2012. Modelling of the refining processes in the production of ferrochrome and stainless steel. *Recent Researches in Metallurgical Engineering - From Extraction to Forming*. IntechOpen, London. https://cdn.intechopen.com/pdfs/32751/InTech-Modelling_of_the_refining_processes_in_the_production_of_ferrochrome_and_stainless_steel.pdf

Hockaday, S.A.C. and Bisaka, K. 2010. Some aspects of the production of ferrochrome alloys in pilot DC arc furnaces at Mintek. *Proceedings of the Twelfth International Ferroalloys Congress: Sustainable Future*, Helsinki, Finland. Outotec Oyj, Helsinki. pp. 367–376. http://www.mintek.co.za/Pyromet/Files/2010Hockaday.pdf

Li, W. 2001. Physical Chemistry of Metallurgy and Materials. *Metallurgical Industry Publishing*, Beijing. pp. 535.

Liao, C., Li, H., and You, J. 2017. Heat transfer technology, equipment and industrial applications. *Chemical Industry Publishing*, Beijing. pp. 14–17.

Manuela, C.D., Komarov, S., and Sano, M. 1997. Bubble behaviour and absorption rate in gas injection through rotary lances. *ISIJ International*, vol. 37, no. 1. pp. 1–8.

Odenthal, H-J. 2010. Simulation of fluid flow and oscillation of the argon oxygen decarburization (AOD) process. *Metallurgical and Materials Transactions B*, vol. 41B. pp. 396–413.

Qiu, D., Fu, Y-Y, Zhang, N., and Zhao, C.-X. 2013. Research on relationship model of dephosphorization efficiency and slag basicity based on support vector machine. *Proceedings of the International Conference on Mechanical and Automation Engineering*, Jiujang, China, 21–23 July 2013. pp. 184–187. https://www.computer.org/csdl/proceedings-article/maee/2013/4975a184/12OmNBPtJCi

Reichel, J. and Szekely, J. 1995. Mathematical models and experimental verification in the decarburization of industrial scale stainless steel melts. *Iron and Steelmaker*, vol. 5. pp. 41–48.

Turkdogan, E.T. 1980. Physical Chemistry of High Temperature Technology. Academic Publishing. New York. pp. 112–114.

Visuri, V-V., Järvinen, M., Sulasalmi, P., Heikkinen, E-P., Savolainen, J., and Fabritius, T. 2017. A mathematical model for reactions during top-blowing in the AOD process: Validation and results. *Metallurgical and Materials Transactions B*, vol. 48B. pp. 1868–1884.

Visuri, V-V., Järvinen, M., Sulasalmi, P., Heikkinen, E-P., Savolainen, J., and Fabritius. T. 2013a. A mathematical model for the reduction stage of the AOD process. Part I: Derivation of the model. *ISIJ International*, vol. 53, no. 4. pp. 603–612.

Visuri, V-V., Järvinen, M., Sulasalmi, P., Heikkinen, E-P., Savolainen, J., and Fabritius. T. 2013b. A mathematical model for the reduction stage of the AOD process. Part II: Model validation and results. *ISIJ International*, vol. 53, no. 4. pp. 613–621.

Vysokomornaya, O.V., Kuznetsov, G.V., and Strizhak, P.A. 2014. Mathematical simulation of heat and mass transfer processes at the ignition of liquid fuel by concentrated flux of radiation. *Mathematical Problems in Engineering*, vol. 2014. pp. 1–7.

Wei, J-H., Cao, Y., Zhu, H-L., and Chi, H-B. 2011. Mathematical modeling study on combined side and top blowing AOD refining process of stainless steel. *ISIJ International*, vol. 51, no. 3. pp. 365–374.

Wei, J-H. and Zhu, D-P. 2002a. Mathematical modeling of the argon-oxygen decarburization refining process of stainless steel: Part I. Mathematical model of the process. *Metallurgical and Materials Transactions B*, vol. 33B. pp. 111–119.

Wei, J-H. and Zhu, D-P. 2002b. Mathematical modeling of the argon-oxygen decarburization refining process of stainless steel: Part II. application of the model to industrial practice. *Metallurgical and Materials Transactions B*, vol. 33B. pp. 121–127.

Weitz, H. and Garbers-Craig A.M. 2016. Evaluation of the furnace method for the production of low carbon ferrochrome. *Mineral Processing nd Extractive Metallurgy Review*, vol. 37, no. 3, pp. 168–178. ◆

Evaluation of mineral resources carrying capacity based on the particle swarm optimization clustering algorithm

S. He[1,2], D. Luo[1], and K. Guo[1]

Affiliation:
[1] College of Management Science, Geomathematics Key Laboratory of Sichuan Province, Chengdu University of Technology, China.
[2] Department of Computer Science and Information Engineering, Yibin University, China.

Correspondence to:
luodejiang06@cdut.cn

Email:
D. Luo

Dates:
Received: 21 Feb. 2020
Revised: 7 Oct. 2020
Accepted: 24 Nov. 2020
Published: December 2020

How to cite:
He, S., Luo, D., and Guo, K. 2020 Evaluation of mineral resources carrying capacity based on the particle swarm optimization clustering algorithm. Journal of the Southern African Institute of Mining and Metallurgy, vol. 120, no. 12, pp. 681–692.

DOI ID:
http://dx.doi.org/10.17159/2411-9717/1139/2020

ORCID
S. He
https://orcid.org/0000-0002-0650-458x
D. Luo
https://orcid.org/0000-0002-0374-5855

Synopsis

As minerals are a non-renewable resource, sustainability must be considered in their development and utilization. Evaluation of the mineral resources carrying capacity is necessary for the sustainable development of mineral resource-based regions. Following the construction of a comprehensive evaluation index system from four aspects, namely resource endowment, socio-economic status, environmental pollution, and ecological restoration, a method combining particle swarm optimization (PSO) and the K-means algorithm (PSO-Kmeans) was used to evaluate the mineral resources carrying capacity of the Panxi region southwest Sichuan Province, China. The evaluation method is data-driven and does not consider the classification standards of different carrying capacity levels. At the same time, it avoids the problems of local optimization and sensitivity to initial points of the K-means algorithm, thereby providing more objective evaluation results and solving the problem of subjective division of each grade volume capacity in carrying capacity evaluation. The algorithm was verified through UCI data-sets and virtual samples. By superimposing a single index on the carrying capacity map for analysis, the rationality of the evaluation results was validated.

Keywords
particle swarm optimization, K-means algorithm , mineral resources, carrying capacity, sustainability.

Introduction

The sustainable use of resources is an issue that any country should pay attention to and monitor over the long term. In China, the world's largest energy producer, the rational exploitation and utilization of mineral resources is the key to the healthy development of energy production, the economy, and society. Xie, Zhou, and Lin (2005) pointed out that the population and economic development of China have not exceeded the natural resources carrying capacity, but some areas and natural resources are seriously overloaded. The mineral resources carrying capacity is the capacity of mineral resources to support human social and economic activities in a foreseeable period under certain resource and environmental constraints. Monitoring the mineral resources carrying capacity in natural resource exploitation must be conducted over the long term.

An objective evaluation of the carrying capacity of regional mineral resources will enable rational development and utilization. However, at present there are few studies on the evaluation of the mineral resources carrying capacity, and mathematical statistical models or related integration methods have been adopted using indexes constructed from the aspects of economy, society, and environment. Li and Lyu (2018) used the set pair analysis and entropy value methods to evaluate mineral resources carrying capacity. Wang *et al.* (2016) used the entropy method. Wei (2006) used the fuzzy comprehensive evaluation method. Wanga, Shi, and Wan (2020) proposed the RCA-TOPSIS-RSR method to comprehensively evaluate the carrying capacity of mineral resource-based cities. In the process of classification, the RCA-TOPSIS-RSR method was used to classify the cities into high, medium, and low carrying capacity levels by evaluating the range of the rank-sum ratio (RSR). Bakhtavar and Yousefi (2019) used TOPSIS to rank 14 candidate well-sites and choose the best.

In these studies, the determination of classification standards for different carrying capacity grades is generally subjective, done mainly by setting thresholds or demarcating ranges. At present, there is also a lack of common methods for classifying the carrying capacity. The clustering algorithm, a common method in data mining technology, is a data-driven method, without considering classification standards of different grades, to solve the problem of the subjective classification of carrying capacity grades, which makes the evaluation results more objective and reasonable.

In recent years, an increasing number of clustering algorithms have been applied to ecological environment evaluation, functional region division, and other problems. The K-means clustering algorithm is the most commonly used. Celestino and Cruz (2018) proposed using the PCA method

to reduce the data dimensionality and the K-means clustering algorithm to evaluate groundwater quality. Xua *et al.* (2018) proposed an improved entropy-weighted method and K-means clustering algorithm for an urban flood risk assessment model. Compared with the traditional clustering and TOPSIS methods, the improved algorithm achieved better results. Salehnia, Ansari, and Kolsoumi (2019) described the common characteristics of low-, medium- and high- yield wheat years by clustering climate data. In addition, the fitness function was used to evaluate the climate data clustering results with the AI, AOC, GA, and K-means algorithms. Wang, Wang, and Niu (2017) proposed an effective mapping framework for landslide susceptibility by combining information theory, K-means clustering analysis, and a statistical model. Liu, Peng, and Wu (2018) proposed a method to identify urban expansion, using K-means clustering of the gridded population density and local spatial entropy to cluster four geographical units through two indicators. Javadi *et al.* (2017) used K-means clustering to evaluate the vulnerability of groundwater, but pointed out that the limitations in the application of the K-means clustering algorithm still need to be considered.

The K-means clustering algorithm is one of the most widely used clustering algorithms. The algorithm is simple and easy to use and is suitable for processing large-scale data. It is suitable for the clustering of numerical attributes and provides good clustering results for superspherical and convex data (Wei, 2013), and it converges to a local optimum (Lei *et al.*, 2008). The shortcomings of the K-means clustering algorithm are also clear, as it is very sensitive to initial point selection. Improper initial point selection can easily cause the clustering result to converge to a local optimum or even provide an incorrect clustering result (Ismkhan 2018; Xiong, Peng, and Yagb, 2017; Ia and Li *et al.*, 2016; Ye *et al.*, 2015; Lei *et al.*, 2008; Sun, Li, and He *et al.*, 2008). At the same time, the K-means clustering algorithm is based on the gradient descent solution, which easily determines a local optimum but does not necessarily determine a global one (Xu, Xu, and Zhang , 2018; Ye *et al.*, 2015). The simplicity and ease of use of the K-means clustering algorithm are also subject to its shortcomings. Optimizing the initial cluster centre and determining the appropriate number of clusters have therefore been the focus of research on K-means clustering.

Although the K-means clustering algorithm has been widely used in ecological environment assessment, its clustering results may be only local optimal results instead of strictly global ones. At the same time, the clustering results may suffer instability problems. In this paper we propose an optimized K-means algorithm and apply it to the assessment of mineral resources carrying capacity.

Recently, there have been an increasing number of studies on improving the K-means algorithm, mainly combining an optimization algorithm with the K-means clustering algorithm. Niknam and Amiri (2010) proposed a hybrid algorithm based on particle swarm optimization (PSO), ant colony optimization (ACO), and the K-means algorithm to optimize clustering. Xu and Li (2011) and Xie and Li (2014) proposed a K-means optimized clustering algorithm based on the improved PSO algorithm. The powerful global search ability of the PSO algorithm was used to optimize the selection of the initial clustering centre. The clustering accuracy rate was higher than 80% through UCI data-set verification. Because of the PSO algorithm, it could maintain its random behaviour better than the artificial bee colony (ABC) algorithm in determining the global optimum, and the result was superior to that of the ABC algorithm (Niknam and Amiri, 2010).

In this paper, the proposed method combines the PSO and K-means algorithms to conduct a global search for particles in the solution space after initial random classification, thereby classifying the shortest distance of the K-means as its principle, and adopts the fitness function of K-means as the standard for detecting updated particles. A sufficient number of iterations is carried out to make the final clustering result both globally optimal and locally optimal, so that the fitness function value converges. This method entails carrying out a local search and a global search simultaneously, which is also different from other PSO-Kmeans algorithms, which first carry out a global search to find the optimal initial point, followed by a local search from the initial point. When this model is applied to the evaluation of mineral resources carrying capacity, the evaluation unit can be placed into different classes by global and local optimization based on the value of the multi-attribute index, and the number of each class also depends on the index data itself. This model also avoids the traditional evaluation methods (such as the traditional entropy method) to get the order of evaluation units after the comprehensive evaluation, and how to divide the grades and how many evaluation units of each grade to use can only be done using subjective experience.

Study area and data-set

Study area

The Panxi region is located in the southwest of Sichuan Province, and comprises Panzhihua City and the Liangshan Yi Autonomous Prefecture. The region borders Ya'an City in the north, Leshan City and Yibin City in the northeast, the Ganzi Tibetan Autonomous Prefecture in the northwest, and Yunnan Province in the east, south, and southwest. The Panxi region is one of the most resource-rich areas in western China and is characterized by large reserves of vanadium-titanium magnetite, which are excellent rare earth resources, and suitable resource development conditions. Abundant vanadium-titanium magnetite ore reserves have been identified, accounting for more than 15% of the total iron ore reserves in China. Therefore, this paper mainly considers vanadium-titanium magnetite as a single mineral in its evaluation. The evaluation area consists of the districts and counties in Panxi with iron ore mining, production, and reclamation activities in 2017, including Dongqu, Yanbian County, and Miyi County of Panzhihua City, Xichang City, Dechang County, Huili County, Huidong County, Ningnan County, Yuexi County, Xide County, Mianning County, and Yanyuan County of the Liangshan Yi Autonomous Prefecture. There are 12 counties (cities) in total, as shown in Figure. 1.

Data

To evaluate the mineral resources carrying capacity in the 12 counties (cities) of Panxi, data was collected on social, economic, and environmental aspects, including the following.

- The population and area data are from the Panzhihua 2018 Statistical Yearbook and the Liangshan Yi Autonomous Prefecture 2018 Statistical Yearbook
- The data on the remaining recoverable mineral reserves, employment in the mining industry, annual taxes, sales revenue from mineral products, actual production amounts, and treated areas are from the Department of Natural Resources of Sichuan Province.

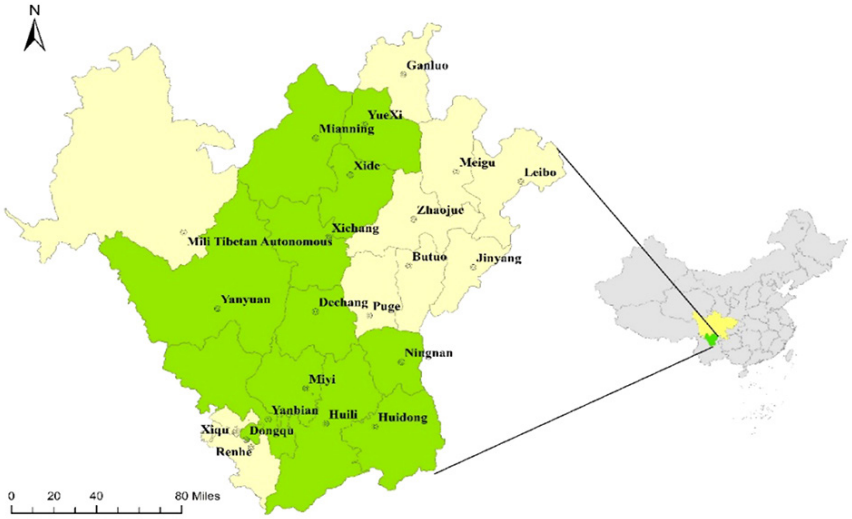

Figure 1—Schematic diagram of the Panxi area (counties/cities)

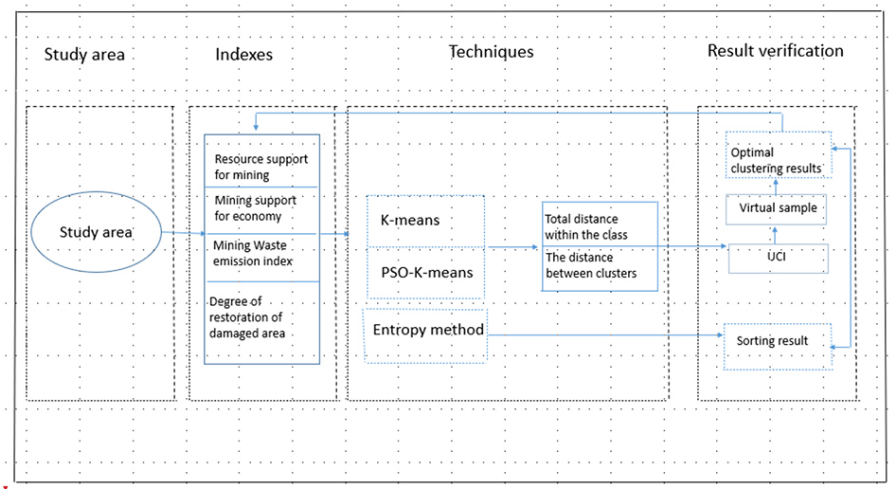

Figure 2—Methodology developed for the study

- The waste emission coefficient data from iron ore mining came from the Manual of the First National Pollution Source Survey of Emission Coefficient of Industrial Pollution Sources (revised in 2010).

Methodology

Overall framework of the study

The overall framework of the research method in this paper is shown in Figure. 2. It mainly consists of the following three parts.

- On the basis of establishing an index system, the K-means clustering and PSO-Kmeans algorithms are used to cluster the evaluation units according to the attribute value of the index. The total distance of the class centre and the total distance within the class are used as criteria for evaluating the validity of the clustering results. The robustness of the algorithm is verified with UCI data-sets and virtual samples.
- Under the same index system, the entropy method is used to determine the weight, calculate the comprehensive evaluation value of the evaluation unit, and rank the carrying capacity of the evaluation unit. The ranking result is then compared with the optimal clustering result.
- A single indicator is superimposed on the carrying capacity map, and the results are analysed in combination with the carrying capacity evaluation level to verify the results.

Indicator system

The selection of mineral resources carrying capacity evaluation indicators is considered mainly from the economic, social, and environmental aspects (Li and Lyu, 2018; Wei, 2006). Clearly, the population carrying capacity (Wang,1998) and economic carrying capacity (Hou, 2007) are also evaluated. This paper will start from the four aspects of resource endowment, social economy, environmental pollution, and ecological restoration to reflect the mineral resources carrying capacity of human social and economic activities. At the same time, reference is made to the technical requirements for regional geological resources and environmental carrying capacity evaluation in accordance with the mineral industry standards of China. An index system is established consisting of resource support for mining, mining support for the economy, mining waste emission index, and degree of restoration of damaged areas.

Resource support for mining

The number of years that the resource endowment of each region can actually support the regional mining production is also the

sustainable period of its resources. The remaining recoverable reserves of the region divided by the actual annual mining rate were used to measure the degree of support of the resource endowment of the region to the mining industry, represented by R in Equation [1], which is a positive indicator.

$$R = \frac{S}{P_a} \quad [1]$$

where S is remaining recoverable reserves, and P_a is the actual annual mining rate.

Mining support for the economy

The social and economic benefits generated by the mining industry in each region are reflected by the proportion that mining contributes to the economy, the tax rate paid by the mining industry, and the proportion of employment in the mining industry, and is represented by E in Equation [2], which is a positive indicator.

$$E = \alpha * \frac{A}{G} + \beta * \frac{T}{C} + \gamma * \frac{Q}{D} \quad [2]$$

where A is the added value of the industry, G is the GDP of the city/district, T is the annual tax, C is the sales revenue of mining products, Q is the mining employment, D is the total population of the city/district, and α,β,and γ are proportion indexes. These factors are determined by experts according to the general trend of national industrial added value, employment rate, and taxation growth trends. Take 2017 as an example. According to data from the Ministry of Industry and Information Technology, the country's industrial added value in 2017 was the best in the past three years, indicating that industrial added value has an increasing impact on social and economic support, therefore experts assign a larger value to α. For 2017, α,β and γ are 0.45, 0.30, and 0.25 respectively.

Mining waste emission index

To reflect the environmental pollution caused by waste discharge during the mining and production processes, according to the Manual of the First National Pollution Source Survey of Emission Coefficient of Industrial Pollution Sources (revised in 2010), the various waste emission coefficients generated during the mining and production of iron ore are determined, including industrial wastewater, chemical oxygen demand, petroleum, industrial waste gas, industrial dust, sulphur dioxide, and nitrogen oxides. Based on the above coefficients, the pollution emission index per square kilometre of ore production is calculated as a measure of the environmental pollution caused by mining, and is represented by P, which is a negative indicator.

$$P = F_i \times \frac{H}{V} \sum W_i N_i \quad [3]$$

where H is the output of mineral products, V is the total area of the city/district, W_i is the weight of class i waste in the total discharge, which is calculated by analytic hierarchy process. N_i is the discharge coefficient of class i waste, and F_i is the normalization coefficient of class i waste. The value of F_i is 100 times the reciprocal of the maximum value of waste emission.

Degree of restoration of damaged areas

To reflect the ecological restoration of damaged areas during mining in each region, the damaged area that has been treated is divided by the damaged area that should be restored; that is, the treatment rate; and O is the restoration degree index of damaged areas in mining development, which is a positive indicator.

$$O = \frac{V_a}{V_b} \quad [4]$$

where V_a is he damaged area that has been treated, and V_b is the damaged area that should be restored.

Evaluation method of the mineral resources carrying capacity based on the PSO-Kmeans algorithm

Cluster analysis is data-driven. Based on the establishment of the index system, clustering is performed by evaluating the similarity between the unit index attribute values. The most commonly used and simplest clustering algorithm is the K-means clusteriwng algorithm.

K-means clustering

K-means clustering is a classification approach based on partitioning. After the initial clustering centre has been randomly selected according to the number of clusters, the classification is redistributed by calculating the distances between other points and the clustering centre, and the clustering centre is iterated continuously using Equation [6] until the objective function J obtains the optimal solution *via* Equation [5].

$$J = \sum_{j=1}^{k} \sum_{i \in j} ||x_i - c_j||^2 \quad [5]$$

$$c_j = \frac{\sum_{i \in j} x_i}{n_j} \quad [6]$$

where x_i is the ith data object in the X data-set, c_j is the jth clustering centre, and n_j is the number of data objects in the jth clustering centre.

PSO-Kmeans clustering

The PSO algorithm is a group of behaviour algorithms simulating the foraging activities of birds. According to the optimal position of individuals relative to food and the optimal position shared by the group, the flight direction is changed, and the optimal position relative to food is reached after constantly updating the position and speed. Assuming that the particle flight space is an m-dimensional space, at the t iteration, the position and velocity vectors of the j-th particle are expressed as $X_j^t = (x_{j1}^t, x_{j2}^t, x_{j3}^t, \ldots\ldots, x_{jm}^t)$ and $V_j^t = (v_{j1}^t, v_{j2}^t, v_{j3}^t, \ldots\ldots, v_{jm}^t)$, respectively. The individual optimal position is found in each iteration, $Pbest_j = (p_{j1}, p_{j2}, \ldots\ldots p_{jm})$, and the global optimal position is $G_{best} = (g_1, g_2, \ldots\ldots g_m)$. At each iteration, the particles update their speed and position with Equations [7] and [8], respectively (Shi and Eberhart, 1998).

$$V_j^{t+1} = \omega V_j^t + c_1 r_1 \left(Pbest_j - X_j^t\right) + c_2 r_2 (Gbest - X_j^t) \quad [7]$$

$$X_j^{t+1} = X_j^t + V_j^{t+1} \quad [8]$$

where c_1 and c_2 are learning factors controlling the maximum duration of the iteration, with a value of generally 2, r_1 and r_2 are random numbers between 0 and 1, and ω is the inertial weight (Equation [9]), which has the ability to balance local and global optima. Generally, the initial value of ω decreases rapidly

as the number of iterations increases. When the particle swarm converges to the optimal solution, the value of ω decreases slowly.

$$\omega(t) = \omega_{max} - t * (\omega_{max} - \omega_{min})/t_{max} \quad [9]$$

where ω_{max} and ω_{min} are the maximum and minimum inertia weights, t_{max} is maximum number of iterations, and t is current iteration number.

Therefore, PSO-Kmeans combines the two algorithms to conduct a global search for particles in the solution space after initial random classification, thereby classifying the shortest distance of the K-means as its principle, and adopts the fitness function of K-means as the standard for detecting updated particles. The steps of the mineral resources carrying capacity evaluation model proposed in this paper are as follows:

Input: Number of particles *N*, number of iterations *M*, number of clusters *K*, data-set data, learning factor c_1, c_2, maximum and minimum weights ω_{max}, ω_{min}, maximum and minimum speeds v_{max}, v_{min}, maximum and minimum positions x_{max}, x_{min}.

Output: fitness function value *J*, *K* clustering centres, data data-set classification, data data-set evaluation level.

Model steps:

Step 1: Initialization and random classification

① Initializes each set value of particle velocity and input.

② The data-set is randomly divided into *K* classes, and the category centre of each class is calculated by Equation [6]. The category centre is the position of the particle. If the data-set has *m* dimension, the position of the *i*th particle is $x_i = (x_0^i, x_1^i \ldots\ldots x_k^i)$, $x_k^i = (Y_{k1}^i, Y_{k2}^i \ldots\ldots, Y_{km}^i)$ Y_{km}^i, is the *m*-dimensional data of the *K*th clustering center of the *i*th particle.

③ Equation [5] is used to calculate the fitness function value of the particle, which is taken as the initial value of the optimal fitness of the particle.

④ Repeat ②–③ to generate the positions of *N* particles and take them as the best positions for individual particles. The minimum value of the individual optimal fitness of *N* particles is taken as the group optimal fitness, and the particle position under the fitness is taken as the group optimal position, *Gbest*.

Step 2: Construct a new generation of particles

The particle speed is updated in Equation [7] and controlled within [v_{max} v_{min}], while the particle position is updated in Equation [8] and controlled within [x_{max} x_{min}]. Update the individual optimal and group optimal positions of particles.

Step 3: Generate new cluster centres.

Step 4: Generate the optimal fitness and optimal position of individual particles.

Step 5: Generate the optimal fitness and optimal position of group.

Step 6: Reduce the inertia weight value.

Step 7: Divide *Gbest* into *K* clustering centres.

Step 8: Reclassify the data-set according to the principle of the shortest distance between *K* clustering centres.

Step 9: Calculate the fitness function value by Equation [5].

Step 10: Repeat step 2 – step 9 until reach the set number of iterations, then go to step 12.

Step 11: Output fitness function value *J*, *K* clustering centres, data data-set classification.

Step 12: Calculate the data mean value of each category of *K* categories, and assign each class an ordered label according to the mean value (Xu *et al.*, 2018).

The process of mineral resource carrying capacity evaluation based on the PSO-Kmeans algorithm is shown in Figure 3.

Virtual sample

Faced with the problem of small samples in actual engineering practice, one solution is to generate virtual samples in order to expand the number of samples and enrich the limited information content of small samples (Zhu, Chen, and Yu, 2016). Yang *et al.* (2011), according to smoothness, proposed a novel VSG method based on Gaussian distribution (VSGGD). The basic concept is to generate several Gaussian random numbers around a certain original sample, and keep the label unchanged. Based on the methods of Yang *et al.* (2011) and Ding (2013), the original data is transformed to a Gaussian distribution to generate virtual samples. There are many methods for Gaussian distribution transformation, such as square root transformation, logarithmic transformation, and BOX-COX transformation. We use the logarithmic transformation to construct a Gaussian distribution $N(\mu,\sigma^2)$, where μ is the mean and σ^2 the standard deviation, as in Equation [10]. The number of ore-producing areas is inherently small, so there is small sample problem. It is proposed to use the method of putting the virtual samples into the model together with the original samples, and then removing the virtual samples after classification. In this way, the consistency of the evaluation results obtained with the original samples and after adding the virtual samples is tested.

$$x' = \log_{10} x \quad [10]$$

When x is 0 or a small number, Equations [11] and [12] are used to avoid negative numbers and wrong values.

$$x' = \log_{10}(x+1) \quad [11]$$

$$x' = \log_{10}(n * x) \quad [12]$$

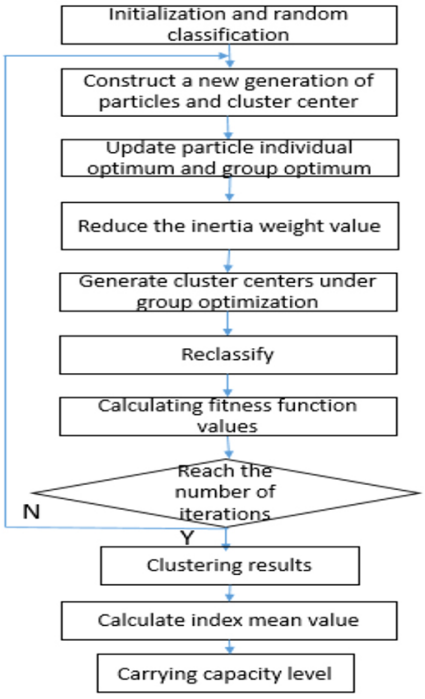

Figure 3—Flow chart of the PSO-Kmeans clustering method

Results and discussion

According to the previous modeling steps, use MATLAB software for modeling. The evaluation index data and weights are shown in Table I for data normalization and input as data-set. Input particle number $N = 50$, number of iterations $M = 50$, number of clusters $K = 4$, learning factor $c_1 = c_2 = 2$, maximum and minimum weights $\omega_{max} = 0.9$, $\omega_{min} = 0.4$, maximum and minimum speeds $v_{max} = 1$, $v_{min} = -$, maximum and minimum positions $x_{max} = 1$, $x_{min} = 0$. Number of clusters $K = 4$, namely, the rating grade of data-set can be divided into four categories: high, medium-high, medium, and low.

By using the K-means and PSO-Kmeans clustering methods, evaluation unit clustering was realized using MATLAB software, and the carrying capacity rating was evaluated. Because the K-means and PSO-Kmeans algorithms randomly select initial points, different initial points may lead to different clustering results. Therefore, ten operations were performed with the two methods, and 80% probability in PSO-Kmeans method is the same clustering result after multiple operations. However, only 50% of the probability under K-means is the same clustering result. The other clustering results are different, and the clustering results are unstable. The results of the evaluation units ranked by the entropy method and clustered by the PSO-Kmeans method are compared, as summarized in Table II. The clustering results under PSO-kmeans are shown in Figure 4. X6 and X12 units are coincident after dimension reduction processing.

In order to prove the generalization ability of PSO-Kmeans and the robustness of the results, Iris and Wine in the UCI data-set were selected for experiments. Iris has 150 labelled 4-dimensional samples; Wine has 178 labelled 13-dimensional samples. K-means and PSO-Kmeans were used for clustering, and the average accuracies of correct clustering are shown in Table III. It can be seen that PSO-Kmeans has good clustering ability for high-dimensional and low-dimensional data.

When the large data-sets of UCI are running well, in order to prove the stability of the evaluation results of the model, the virtual samples are expanded according to Equations [10]–[12] on the basis of the original samples, as shown in Table IV. The virtual samples are added to the original samples and put into the model to run 10 times randomly. The clustering results are shown in Figure 5. The probability of consistency with the evaluation results of the original samples is shown in Table V. It can be seen that, except for the large difference in X11 evaluation units, the evaluation results after adding the virtual samples are basically the same as the original evaluation results.

Table II

Results of the entropy and PSO-Kmeans methods

Evaluation unit	Entropy method	PSO-Kmeans
YanBian	High	High
XiChang	High	High
NingNan	High	Medium-high
HuiDong	Medium-high	Medium-high
MianNing	Medium-high	High
MiYi	Medium-high	High
XiDe	Medium	Medium
DeChang	Medium	Medium
HuiLi	Medium	Medium
YanYuan	low	Medium
YueXi	Low	Medium
DongQu	Low	Low

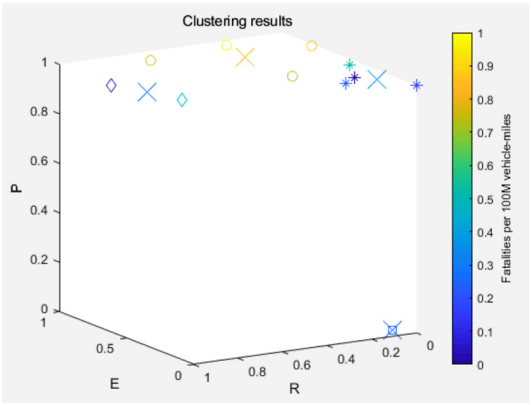

Figure 4—Clustering results under the PSO-Kmeans

Table III

Classification accuracy of the two algorithms

Data-set	K-means	PSO-kmeans
Iris	0.74	0.88
Wine	0.82	0.86

Table I

Evaluation unit and evaluation index

Evaluation unit	Resource support for mining	Mining support for the economy	Mining waste emission index	Degree of restoration of damaged areas
	R	E	P	O
Weights	**0.238868**	**0.170344**	**0.439427**	**0.151361**
DongQu (X1)	93.970161	0.096818	108.387237	0.297373
MiYi (X2)	140.05729	0.087796	12.951945	0.719569
YanBian (X3)	1026.576775	0.106991	2.548964	0.757423
XiChang (X4)	415.790468	0.112043	2.001617	1
YanYuan (X5)	221.057563	0.026387	0.147915	0.070261
DeChang (X6)	0	0	0	0.770115
HuiLi (X7)	328.556428	0.022085	0.822992	0.27494
HuiDong (X8)	1475.093053	0.030054	0.080008	0.508197
NingNan (X9)	1661.962941	0.068653	0.104193	0.1
XiDe (X10)	78.288835	0.04702	0.019142	0.555556
MianNing (X11)	16.910695	0.085449	0.12899	0.870486
YueXi (X12)	0	0	0	0.227273

Table IV

Virtual samples

Evaluation unit	R	E	P	O
X1'	1.972990	0.985958	4.034978	1.473301
X2'	2.146306	0.943477	3.112335	1.857073
X3'	3.011391	1.029348	2.406364	1.879338
X4'	2.618875	1.049385	2.301381	2.000000
X5'	2.344505	0.421393	1.170012	0.846714
X6'	0.000000	0.000000	0.000000	1.886556
X7'	2.516610	0.344104	1.915396	1.439238
X8'	3.168819	0.477896	0.903134	1.706032
X9'	3.220621	0.836663	1.017837	1.000000
X10'	1.893700	0.672282	0.281997	1.744727
X11'	1.228161	0.931705	1.110555	1.939762
X12'	0.000000	0.000000	0.000000	1.356547

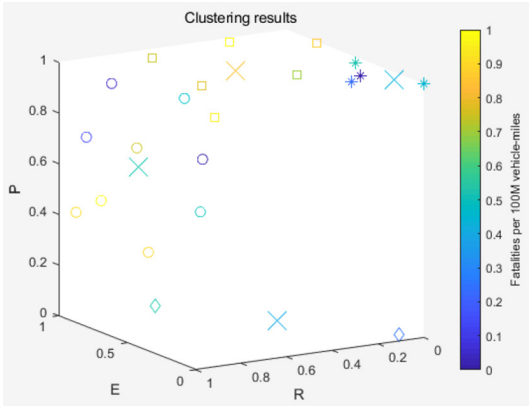

Figure 5—lustering results after adding virtual samples

Table V

Consensus probability of evaluation results under virtual samples

Evaluation unit	Evaluation grades	Consistency probability
DongQu (X1)	Low	100%
MiYi (X2)	High	70%
YanBian (X3)	High	100%
XiChang (X4)	High	100%
YanYuan (X5)	Medium	100%
DeChang (X6)	Medium	90%
HuiLi (X7)	Medium	100%
HuiDong (X8)	Medium-high	80%
NingNan (X9)	Medium-high	90%
XiDe (X10)	Medium	90%
MianNing (X11)	High	40%
YueXi (X12)	Medium	100%

Comparison of the different methods

Comparison of algorithms

Both the K-means and PSO-Kmeans algorithms rely on Equation [5] as the objective function, and the number of iterations is 50. After multiple calculations using the K-means algorithm, the clustering results are different, but the objective function values are convergent, as shown in Figure 6. After multiple operations, the PSO-Kmeans algorithm basically generates the same clustering result, and the value of the objective function also converges, as shown in Figure 7. The optimal clustering result is obtained when the distance within the class is minimized while the distance between the centres of the classes is maximized. That is, the difference between classes is larger, while the distance within classes is smaller. The total distance of the class centre and the total distance within the class were used to evaluate the validity of the two methods. After 10 random runs, the average values of the total distance to the centre of the class and the total distance within the class of the two methods are obtained, as summarized in Table VI. It can be observed that the total distance of the class centre under the PSO-Kmeans algorithm is larger than that under the K-means algorithm, and the total distance within the class is smaller than that under the K-means algorithm. Therefore, the clustering results of the PSO-Kmeans algorithm are better than those of the K-means algorithm, and after global and local optimization of the initial points with the PSO-Kmeans algorithm, the clustering results show almost no difference and are more stable than those of the K-means algorithm.

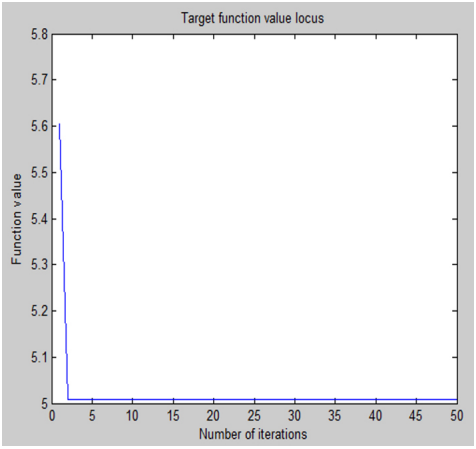

Figure 6—K-means objective function value trajectory

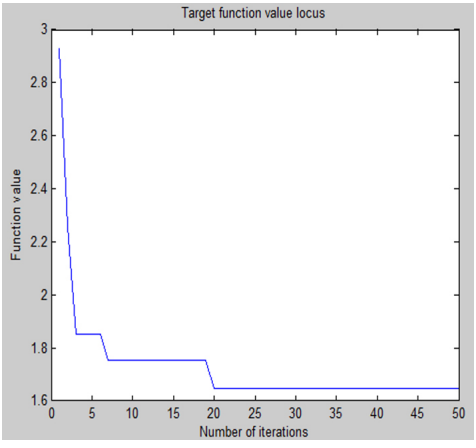

Figure 7—PSO-Kmeans objective function value trajectory

Table VI

Comparison of the performance of the two algorithms

Method	Total distance within class	Total distance of classification centre
K-means	5.564292	7.052792
PSO-Kmeans	1.428085	9.263421

Comparison of evaluation methods

Under the entropy method, the number of each grade can be set subjectively. The grade can also be determined by setting a threshold for the comprehensive evaluation value. However, at present there is no unified threshold standard, and there may be a problem in that the threshold is not applicable due to regional differences. Therefore, when the comprehensive evaluation value is taken as the evaluation standard (such as in the entropy method, TOPSIS), the number of samples for each grade can only be divided in a subjective way. Table II shows the evaluation results of 12 evaluation units using the two methods. With the entropy method, after sorting the comprehensive evaluation value, the number of each category is divided subjectively and equally. Compared with the PSO-Kmeans method, X9 changed from high to medium-high, and X12 and X5 from low to medium. As can be seen from Figure 9, X9 and X8 are the two regions with the most abundant resources, and the other three indicators are not significantly different. Using subjective division, the two areas are rated at different grades. Only taking them as an evaluation category can highlight the great differences between them and other regions under the common characteristics, and the evaluation will be more reasonable. As can be seen from Figure 11, the waste emission intensity in X1 is very high – thousands of times greater than in X5 and X12 while the differences in the other three indicators are very small. However, in the subjective division, X5, X12, and X1 are classified in the same grade. At the same time, it can be seen from Figure 4 that X1 has become very different from other regions. Therefore, it is more reasonable to treat X1 as a category by itself. PSO-Kmeans is data-driven and classifies high and low based on the principle of similarity to solve the subjective division of the number of samples for each grade.

Discussion of the evaluation results

Discussion under a single indicator

According to the evaluation results of the PSO-Kmeans algorithm, the mineral resources carrying capacity of the Panxi area is divided into four levels. The carrying capacity of the evaluation unit clustered by the PSO-Kmeans algorithm is used as the base map, and each evaluation index element is superimposed on the carrying capacity base map. Figure 8 reveals that the evaluation unit with a high regional economic support occurs in the region with high and medium-high carrying capacity levels. Figure 9 shows that the evaluation unit with a relatively short sustainable life of the regional mineral resources is the region with medium and low carrying capacities. Figure 10 demonstrates that the difference in the index of regional ecological restoration degree is not too large, and the better evaluation unit is the region with high and medium-high carrying capacity levels. Figure 11 shows that the mining waste emission index is high in the region with a low carrying capacity. Therefore, in the discussion under a single index, the evaluation result after clustering with the PSO-Kmeans algorithm is reasonable.

Discussion and suggestions for the results under comprehensive indicators

The evaluation method based on the PSO-Kmeans algorithm can better meet the needs of grade evaluation of the mineral resources carrying capacity of the Panxi region. After the evaluation grade has been objectively determined, the four indexes are superimposed. By combining the index data collected in the early stage and the superimposed graph, as shown in Figure 12, the following can be concluded.

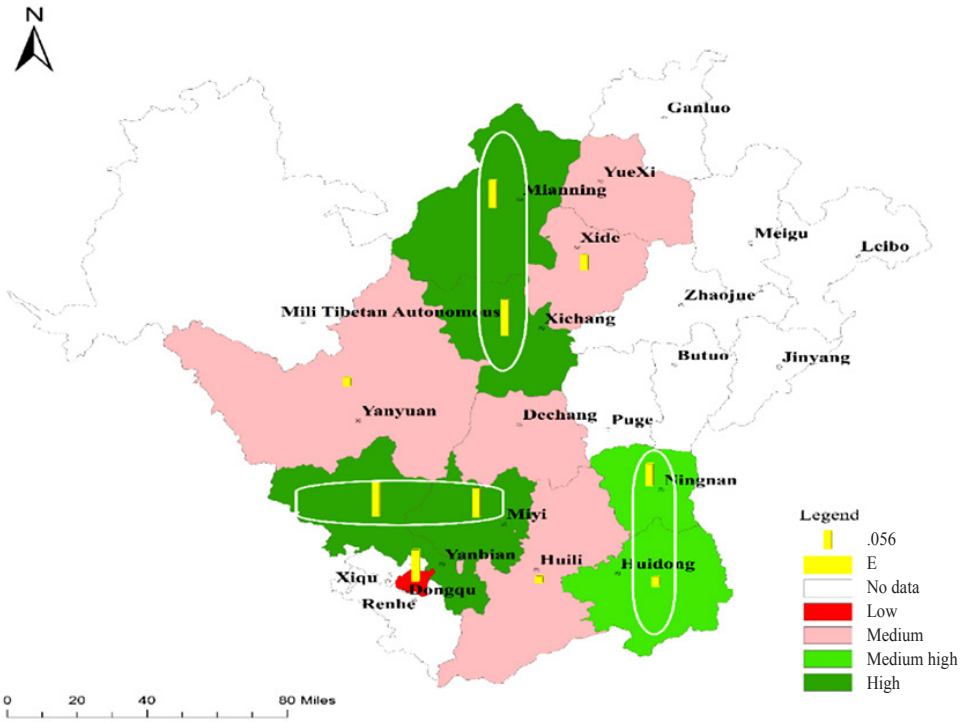

Figure 8—Carrying capacity map and mining support for the economy

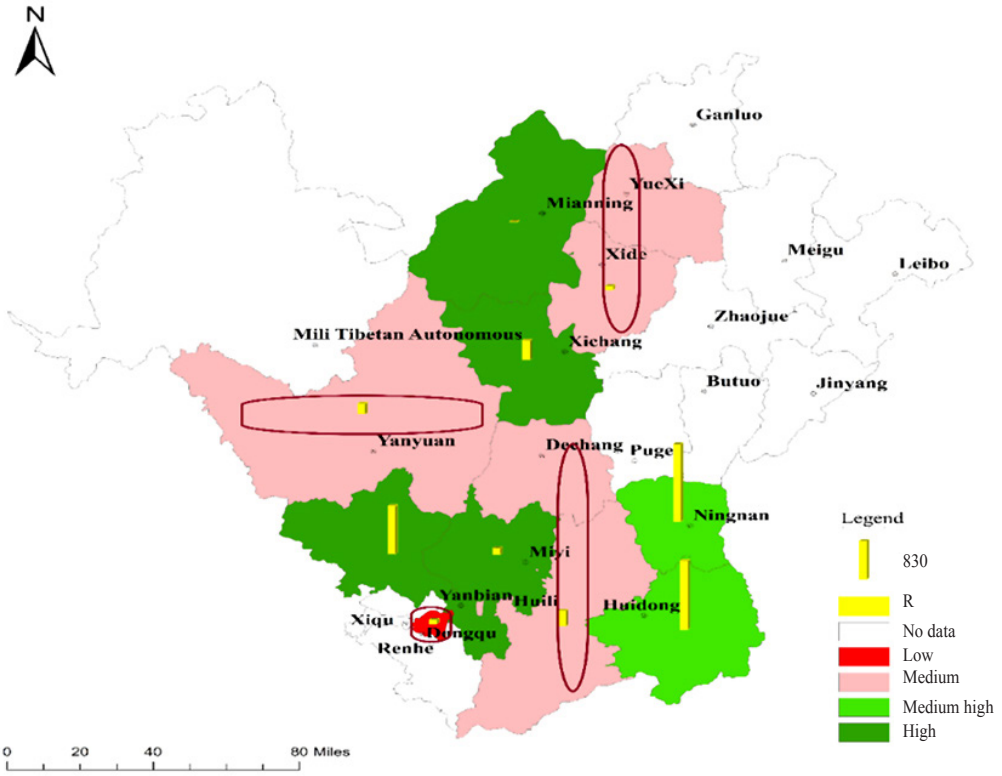

Figure 9—Carrying capacity map and resource support for mining

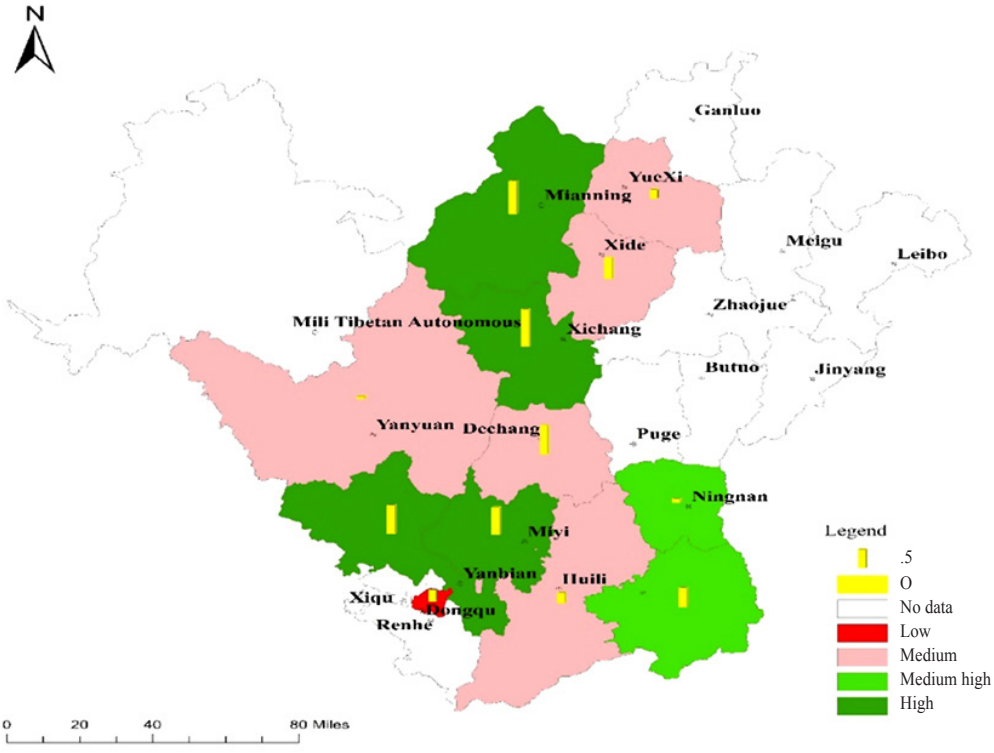

Figure 10—Carrying capacity map and degree of restoration of damaged areas

Xichang, Yanbian, and Miyi, with high carrying capacity levels, are rich in mineral resources with a long sustainable life. The high output of mineral products generates a high level of economic support and suitable conditions for ecological restoration. Although the sustainable life of Mianning's mineral resources is short, it has high degree of economic support and suitable ecological restoration. Therefore, in the short term, its carrying capacity is still high, but will decrease if resources are rapidly exhausted. Therefore, X11 also shows greater uncertainty after adding virtual samples.

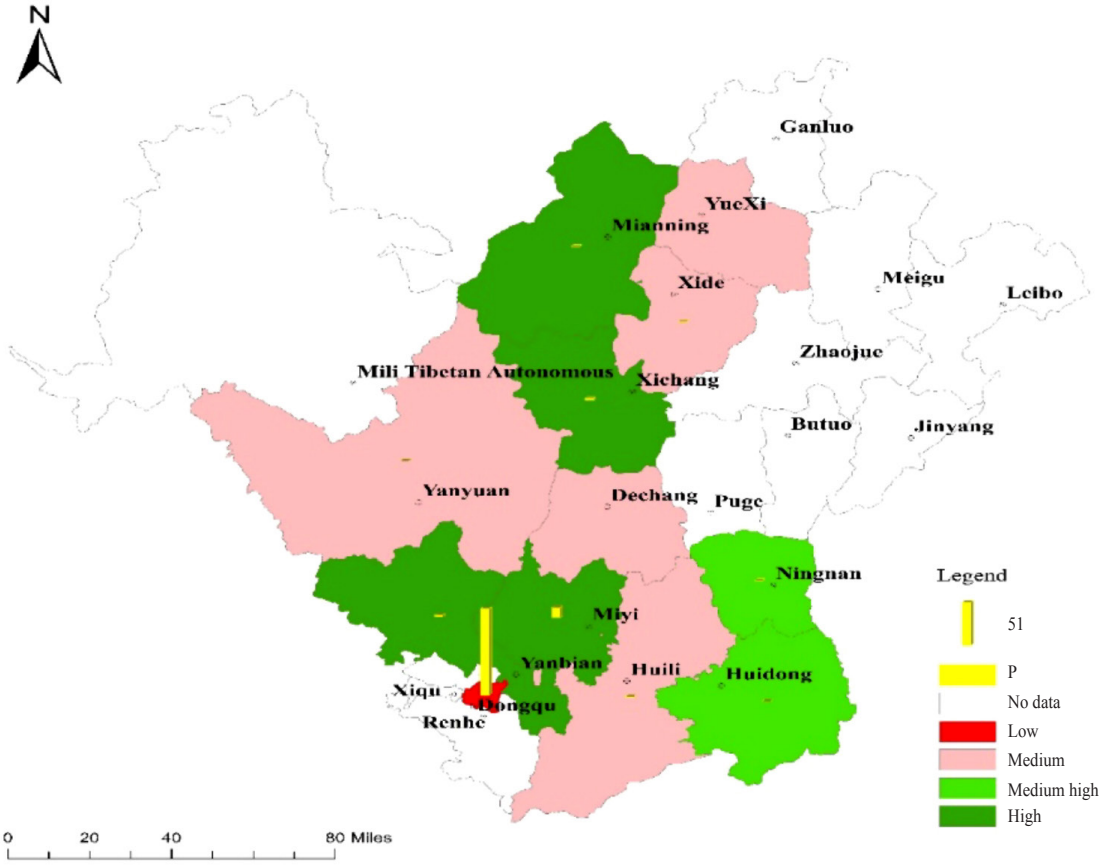

Figure 11—Carrying capacity map and mining waste emission index

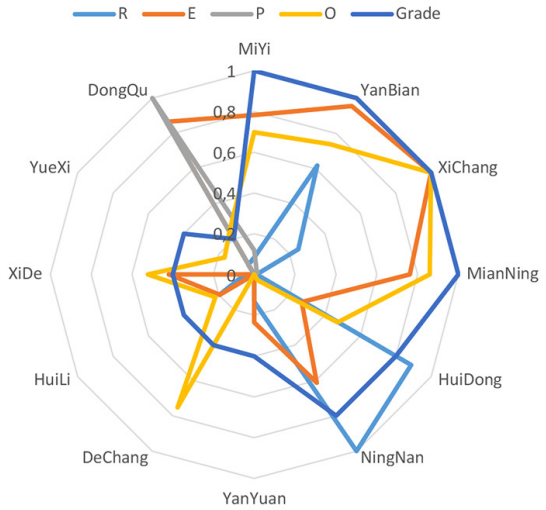

Figure 12—Evaluation of the unit indexes and grade comparison

The medium-high carrying capacity levels of Huidong and Ningnan are attained despite the low output of mineral products, and the region is highly dependent on the mineral economy, while its resources have a long sustainable life and the degree of ecological restoration is acceptable. The carrying capacity is relatively high in the short term but may be increased if mining output is moderately increased in the later period.

The medium carrying capacities of Yanyuan, Dechang, Huili, Xide, and Yue Xi are a result of very low mineral outputs, and there are no mining activities in certain areas. The mining economy is severely contracted, but ecological restoration is still being carried out. Therefore, the short-term carrying capacity is medium, but after ecological restoration reaches a certain level and mineral resources are developed and exploited, the carrying capacity will increase.

Dongqu, which has a low carrying capacity, has a high output of mineral products and a high degree of support for the economy, but its resources have a short sustainable life. Dongqu's high output and small area result in a high intensity of pollutant discharge per square kilometre of ore production in the area, and a low degree of ecological restoration. Therefore, in the short term, if the output is not controlled, the carrying capacity will decrease.

Conclusion

Mineral resources carrying capacity is an important indicator of the sustainable development potential of regions whose economies are based on mineral resources. To comprehensively evaluate the regional mineral resources carrying capacity and solve the problem of subjective division of the number of samples for each grade, a mineral resources carrying capacity evaluation model based on the PSO-Kmeans algorithm is proposed. This paper takes the Panxi region as an example and applies the PSO-Kmeans algorithm to carry out a grade evaluation of the mineral resources carrying capacities, which provides a basis for the relevant authorities to formulate sustainable utilization policies for mineral resources.

Evaluation of mineral resources carrying capacity based on the particle swarm optimization

This paper applies the improved data mining algorithm to the objective evaluation of the mineral resources carrying capacity. Because there are only 12 (city) counties in the area where iron ore mining and production are carried out, the number of possible evaluation units is small. However, iron ore is being mined in only 14 cities in the whole province. The evaluation model proposed in this paper is generated from the actual needs of the research area, and it is necessary to apply an objective data-mining algorithm in practice. Therefore, it is proposed to construct virtual samples and verify the algorithm through the virtual samples under the premise of the UCI data-sets verification. The next step is to evaluate the mineral resources carrying capacity of an entire province based on the unit of a city and the PSO-Kmeans algorithm model. The PSO-Kmeans algorithm evaluation model should also be applied to other resources and environmental carrying capacity fields.

Acknowledgements

This research is supported by the Opening Fund of the Geomathematics Key Laboratory of Sichuan Province (No. scsxdz2019yb06). Also thank these funds for their support: the Geomathematics Key Laboratory of Sichuan Province (NO. scsxdz2019zd02); Sichuan Mineral Resources Research Center(No. SCKCZY2019-ZD002); Sichuan Mineral Resources Research Center(No. SCKCZY2019-ZC002).

References

Bakhtavar, E. and Yousefi, S. 2019. Evaluation of shaft locations in underground mines: Fuzzy multiobjective optimization by ratio analysis with fuzzy cognitive map weights. *Journal of the Southern African Institute of Mining and Metallurgy*, vol. 119, no. 10. pp. 855–864.

Celestino, A.E.M. and Cruz, D.A.M. Groundwater quality assessment: An improved approach to K-means clustering, principal component analysis and spatial analysis: A case study. *Water*, vol. 10. pp. s437. doi:10.3390/w10040437

Civicioglu, P. and Besdok, E. 2013. A conceptual comparison of the Cuckoo-search, particle swarm optimization, differential evolution and artificial bee colony algorithms. *Artificial Intelligence Review*, vol. 39. pp. 315–346. doi: 10.1007/s10462-011-9276-0

Cui, C-Q., Wang, B., Zhao, Y-X., and Wang, Q. 2019. China's regional sustainability assessment on mineral resources: Results from an improved analytic hierarchy process-based normal cloud model. *Journal of Cleaner Production*, vol. 210. pp. 105–120. https://doi.org/10.1016/j.jclepro.2018.10.324

Ding, Z. 2013. A small sample clustering algorithm by generating random samples from Gaussian distribution. *Computer Knowledge and Technology*, vol. 9, no. 29. pp. 6609–6611.

Fana, Y. and Fang, C. 2020. Evolution process analysis of urban metabolic patterns and sustainability assessment in western China, a case study of Xining city. *Ecological Indicators*, vol. 109. pp. 105784. https://doi.org/10.1016/j.ecolind.2019.105784

Guo, Q. 2018. A comprehensive evaluation model of regional atmospheric environment carrying capacity: Model development and a case study in China. *Ecological Indicators*, vol. 91. pp. 259–267.

Hou, H-L. 2007. Research status and development of carrying capacity of mineral resources. *Proceedings of the 2007 Annual Conference of China Geological and Mineral Economics Association*.

Jia, R-Y. and Li, Z. 2016. The level of K-means clustering algorithm based on the minimun spanning tree. *Microelectronice & Computer*, vol. 33, no. 3. pp. 86–93.

Ismkhan, H. 2018. I-k-means An iterative clustering algorithm based on an enhanced version of the k-means. *Pattern Recognition*, vol. 79. pp. 402–413. https://doi.org/10.1016/j.patcog.2018.02.015

Javadi, S., Hashemy, S.M., Mohammdi, K., and Howard, K.W.F. 2017. Classification of aquifer vulnerability using K-means cluster analysis. *Journal of Hydrology*, vol. 549. pp. 27–37. https://dx.doi.org/10.1016/j.jhydrol.2017.03.060

Lei, X-F., Xie, K-Q., Lin, F., and Xia, Z- Y. 2008. An efficient clustering algorithm based on local optimality of K-means. *Journal of Software*. pp. 1683–1692.

Leote, P., Cajaiba, R.L., and Cabral, J.A. 2020. Are data-mining techniques useful for selecting ecological indicators in biodiverse regions? Bridges between market basket analysis and indicator value analysis from a case study in the neotropics. *Ecological Indicators*, vol. 109.p. 105833. https://doi.org/10.1016/j.ecolind.2019.105833

Li, M. and Lyu, Y. 2018. Evaluation of the bearing capacity of the coal resources in Taiyuan city. *China Mining Magazine*, vol. 27, no. 6. pp. 62–65.

Liu, L., Peng, X., and Wu, H. 2018. Fast identification of urban sprawl based on K-Means clustering with population density and local spatial entropy. *Sustainability*, vol. 10. p. 2683. doi:10.3390/su10082683

Niknam, T. and Amiri, B. 2010. An efficient hybrid approach based on PSO, ACO and k-means for cluster analysis. *Applied Soft Computing*, vol. 10. pp. 183–197. doi:10.1016/j.asoc.2009.07.001

Saisana, W.B.M., Paruolo, P., and Vandecasteele, I. 2017. Weights and importance in composite indicators: Closing the gap. *Ecological Indicator*s, vol. 80. pp. 12–22. https://dx.doi.org/10.1016/j.eecolind.2017.03.056

Salehnia, N., Ansari, H., and Kolsoumi, S. 2019. Climate data clustering effects on arid and semi-arid rainfed wheat yield: a comparison of artificial intelligence and K-means approaches. *International Journal of Biometeorology*, vol. 63. pp. 861–872.

Shi, Y.E. 1998. RCA modified particle swarm optimizer. *Evolutionary Computation. Prcoceedings of the 1998 IEEE World Conferemce on Computation Intelligence*. pp. 69–73. IEEE, New York.

Sun, Y-H., Li, Z-S., and He, P-L. 2008. K-means clustering algorithm based on local search mechanism. *Computer Engineering*, vol. 34,, no. 11. pp. 15–17.

Talebi, H., Mueller, U., and Tolosana-Delgado, R. 2019. Geostatistical simulation of geochemical compositions in the presence of multiple geological units: Application to mineral resource evaluation. *Mathematical Geosciences*, vol. 51. pp. 129–153. https://doi.org/10.1007/s11004-018-9763-9

Wang, Q., Wang, Y., and Niu, R. 2017. Integration of information theory, K-means cluster analysis and the logistic regression model for landslide susceptibility mapping in the Three Gorges Area, Chin. *Remote Sensing*, vol. 9. p. 938. doi: 10.3390/rs9090938

Wang, R., Cheng, J., Zhu, Y., and Xiong, W. 2016. Research on diversity of mineral resources carrying capacity in Chinese mining cities. *Resources Policy*, vol. 47. pp. 108–114.

Wang, Y. and Wang, D. 2010. Clustering study of fabric deformation comfort using bi-swarm PSO algorithm. *Journal of Textile Research*, vol. 31, no. 4. pp. 60–64.

Wang, Y-P. 1998. Population carrying capacity of mineral resources. *China Population Resources and Environment*, vol. 8, no. 3. pp. 19–22.

Wanga, D., Shi, Y., and Wan, K. 2020. Integrated evaluation of the carrying capacities of mineral resource-based cities considering synergy between subsystems. *Ecological Indicators*, vol. 108. https://doi.org/10.1016/j.ecolind.2019.105701

Wei, H. 2013. Improved hierarchical K-means clustering algorithm. *Computer Engineering and Applications*, vol. 49, no. 2. pp. 157–159.

Wei, J. 2006. Analysis on mineral resource carry capacity competitiveness and sustainable power in Hel Long Jang province. *China Mining Magazine*, vol. 15, no. 11. pp. 102–109.

Xie, G-D. and Zhou, H.L. 2005. Analysis of carrying capacity of natural resources in China. *China Population, Resources and Environment*, vol. 15, no. 5. pp. 93–97.

Xie, X-H. and Li, T-S. 2014. An optimized K -means clustering algorithm based on improved particle swarm optimization. *Computer Technology and Development*, vol. 24, no. 2. pp. 34–38.

Xiong, K-L, Peng, J-J., and Yabg, X-F. 2017. K-means clustering optimization based on kernel density estimation. *Computer Technology and Development*, vol. 27, no. 2. pp. 1–5.

Xu, D., Xu, Y., and Zhang, D. 2018. A survey on the initialization methods for the K-means algorithm. *Operations Research Transactions*, vol. 22, no. 2. pp. 31–40.

Xu, H. and Li, S-J. 2011. A clustering integrating particle swarm optimization and K-means algorithm. *Journal of Shanxi University (Natural Science Edition)*, vol. 34, no. 4. pp. 518–523.

Xua, H., Ma, C., Lian, J., Xu, K., and Chaima, E. 2018. Urban flooding risk assessment based on an integrated k-means cluster algorithm and improved entropy weight method in the region of Haikou, China. *Journal of Hydrology*, vol. 563. pp. 975–986.

Yang, J., Yu, X., Xie, Z-Q., and Zhang, J-P. 2011. A novel virtual sample generation method based on Gaussian distribution. *Knowledge-Based Systems*, vol. 24. pp. 740–748.

Yang, Y. 2016. Improved K-means dynamic clustering algorithm based on information entropy. *Journal of Chongqing University of Posts and Telecommunications (Natural Science Edition)*, vol. 2. pp. 254–59. doi:10.3979/j.issn.1673-825X.2016.02.018

Ye, Z-W., Yin, Y-J., Wang, <-W., and Zhao, W. 2015. A clustering approach based on cuckoo search algorithm. *Microelectronice & Computer*, vol. 32, no. 5. pp. 104–110.

Yu, S-S., Chu, S.W., and Wang, C-M. 2018. Two improved k-means algorithms. *Applied Soft Computing*, vol. 68. pp. 747–755. https://doi.org/10.1016/j.asoc.2017.08.032

Zhu, B. Chen, Z., and Yu, L. 2016. A novel mega-trend-diffusion for small sample. *CIESC Journal*, vol. 67, no. 3. pp. 820–826. ◆

Obituary

Dr Ferdi Camisani

July 1939 – November 2020

Ferdi Camisani was born outside Parma, Italy just a few weeks after the declaration of World War II

He was a student of the father of geostatistics, Georges Matheron, in Fontainebleau, France and together with Danie Krige, wrote some of the first papers on the application of geostatistics in South Africa.

During his long career in South Africa he worked with De Beers, Anglo American, the Atomic Energy Corporation, and Anglovaal.

Ferdi was a member of the Geostatistical Association of Southern Africa (GASA) and the Southern African Institute of Mining and Metallurgy (SAIMM). On his retirement from SAIMM activities in 2012 the President, Gordon Smith, acknowledged his contribution as follows:

- Attendance of the CMMI meeting in 1997 which established a set of standard reporting definitions which became known as the Denver Accord and which still remain today the backbone of international reporting standards.
- Chairpersonship, from its inception in 1996, of the Main Working Group which compiled the content for the first publication of the SAMREC Code in March 2000.
- Participation in the CMMI committee which was responsible for the adoption of the definitions in the Denver Accord by the United Nations Economic Commission for Europe (UN-ECE) in its International Framework Classification for Reserves and Resources – Solid Fuels and Mineral Commodities.
- Participation in October 2003 at the meeting in Reston VA that saw the formation of the Committee for Mineral Reserves International Reporting Standards (CRIRSCO).
- Continued attendance, as a CRIRSCO representative, until May 2012, at the many sessions under the auspice of the Sustainable Energy Division of the UNECE. Notable among these activities was his membership of the Bureau for the Expert Group on Resource Classification, working on a classification framework for solid minerals and the oil and gas industry.
- Continued representation of South Africa and the SAMREC Code on the CRIRSCO Committee from its inception in 2002 until 2012. This included meetings in Chile, China, Russia, and the UK where he gained the respect of the many people he came in contact with and in doing so enhanced the reputation of professionals in the SAIMM and in South Africa.
- Representation of the SAIMM over many years, which included presentation of papers, at the Application of Computer and Operations Research in the Minerals Industry (APCOM) conference held every four years.
- Lecturing at the University of Pretoria in Geostatistics, a field in which he was a recognized leader.

Ferdi was also recognized throughout the world by the many people he encountered as a true gentleman for whom nothing was too much trouble. He will be sadly missed and we all will be the poorer for his passing.

He is survived by his wife Lorraine and son Fernando.

J.R. Dixon

Optimization of chlorite and talc flotation using experimental design methodology: Case study of the MCG plant, Morocco

K. Boujounoui[1], A. Abidi[2], A. Baçaoui[1], K. El Amari[3], and A. Yaacoubi[1]

Affiliation:
[1] Faculty of Sciences Semlalia, department of chemistry, Marrakech Morocco.
[2] Mining Institute of Marrakech (IMM), Marrakech, Morocco.
[3] Georesources, Geo-environment and Civil Engineering Laboratory, Faculty of Sciences and Technologies Marrakech, Marrakech, Morocco.

Correspondence to:
K. Boujounoui

Email:
boujounoui.kh@gmail.com

Dates:
Received: 19 Apr. 2020
Revised: 15 Oct. 2020
Accepted: 20 Oct. 2020
Published: December 2020

How to cite:
Boujounoui, K., Abidi, A., Baçaoui, A., El Amari, K., and Yaacoubi, A. 2020
Optimization of chlorite and talc flotation using experimental design methodology: Case study of the MCG plant, Morocco. Journal of the Southern African Institute of Mining and Metallurgy, vol. 120, no. 12, pp. 693–700.

DOI ID:
http://dx.doi.org/10.17159/2411-9717/1186/2020

Synopsis

Response surface methodology (RSM), central composite design (CCD), and desirability functions were used for modelling and optimization of the operating factors in chlorite and talc (collectively termed 'mica') flotation. The influence of pulp pH, cyanide (NaCN) consumption, and particle size was studied with the aim of optimizing ssilicate flotation while minimizing recoveries of galena, chalcopyrite, and sphalerite.
Flotation tests were carried out on a representative sample of a complex sulphide ore from Draa Sfar mine (Morocco). The model predictions for the flotation of each of the minerals concerned were found to be in good agreement with experimental values, with R^2 values of 0.91, 0.98, 0.99, and 0.90 for mica, galena, chalcopyrite, and sphalerite recoveries, respectively. RSM combined with desirability functions and CCD was successfully applied for the modelling of mica flotation, considering simultaneously the four flotation responses to achieve the maximum recovery of mica and minimal loss of Pb, Cu, and Zn to the flotation concentrate.

Keywords
chlorite, talc, flotation, response surface methodology, central composite design, optimization.

Introduction

The Mining Company of Guemassa (MCG), located 30 km southwest of Marrakech in Morocco, applies a selective flotation process to produce 13.812 t of lead (galena) concentrate, 16.755 t of copper (chalcopyrite) concentrate, and 72.970 t of zinc (sphalerite) concentrate per annum (Managem Group, 2014). The ore processed consists of sphalerite, galena, chalcopyrite, pyrite, pyrrhotite, chlorite, talc, amphibole, calcite, dolomite, and ankerite (Hibti, 2001). The flotation circuit comprises three stages – galena recovery, followed by chalcopyrite, and finally sphalerite recovery, using common processes for sulphide flotation (Cao and Liu, 2006), but the presence of chlorite and talc, which have a natural floatability, lowers the grade of the lead concentrate. An additional 'mica' flotation circuit, upstream of the lead flotation circuit, is used from time to time to reduce the content of these silicate minerals in the feed to lead flotation.

The statistical design of experiments (DOE) (Box, Hunter, and Hunter, 1978; Akhanazarova and Kafarov 1982; Obeng, Morell, and Napier-Munn, 2005; Napier-Munn 2012; Ennaciri *et al.*, 2014), which has several advantages over the classical method of treating one variable at a time, is used for optimization and modelling process parameters in mineral processing. These statistical techniques have been used to study the flotation of minerals (Yalsin 1999; Rao and Mohanty 2002; Cilek and Yilmazer 2003; Martinez *et al.*, 2003; Martyn *et al.*, 2008; Mehrabani *et al.*, 2010; Vazifeh, Jorjani, and Bagherian, 2010; Boujounoui *et al.*, 2015, 2018) as well as in predicting performance in several plants using multivariable statistical modelling (Lind, Yalcin, and Butcher, 2003).

This study is a part of an overall project to improve the performance of the MCG flotation plant by optimizing the mica flotation, as well the recycling of process water. (Abidi *et al.*, 2014, 2016, 2019; Boujounoui *et al.*, 2015, 2017, 2018, 2019). Since the MGC plant is located in a semi-arid climate, improving the rate of process water recycling is still a serious target, despite the possible modification in the flotation conditions.

The aim of the present work is to apply DOE techniques for the optimization, at batch scale, of mica flotation ('natural flotation'). The study targeted the three most influential factors in flotation; *i.e.* the pulp pH, the consumption of cyanide (NaCN), and the particle size (d_{80}). The main effects and interactions of these factors on the flotation responses will be determined and modelled to find the optimum operating conditions, with the aim of selectively removing the mica minerals from galena, sphalerite, and chalcopyrite.

To achieve this goal, the response surface methodology (RSM) and the desirability functions were applied. RSM is a collection of statistical and mathematical techniques useful for the modelling and analysis of problems in which a response of interest is influenced by several variables and the objective is to optimize this response (Anderson and Whitcomb, 2000).

In this study the central composite design (CCD) was used extensively in building the second-order response surface models. CCD has been successfully used to design an experimental programme to provide data to model the effects of operating factors and cyclone geometry on the operational performance of a three-product cyclone (Obeng, Morrell, and Napier-Munn, 2005).

Experimental

Material and methods

Bench-scale flotation tests were carried out on a representative sample of the complex sulphide ore from MCG's Draa Sfar mine (Marrakech, Morocco). The ore used was the same as that used by Abidi *et al.* (2014) and Boujounoui *et al.* (2015, 2018, 2019). It was composed of sphalerite, galena, chalcopyrite, pyrrhotite, and gangue minerals consisting mainly of quartz, talc, chlorite, calcite, siderite, and ankerite.

A representative sample of 150 kg was taken from the feed belt of the primary ball mill at the flotation plant and crushed to 2 mm using laboratory roll crushers. The crushed sample was stored in vacuum-sealed bags to prevent oxidation of the sulphide minerals.

Prior to the flotation tests, samples of 500 g were milled in 250 ml of Marrakech drinking water using a Denver carbon-steel ball mill. The size fractions studied in this work were d_{80} = 60, 120, and 180 µm.

Flotation experiments

Flotation tests were carried out on 500 g samples of milled ore using tap water in a Denver flotation cell with a capacity of 1.5 liters. The initial solid concentration was approximately 27% by weight. The impeller rotation speed was fixed at 1000 r/min. NaOH: was used as a pH regulator, with NaCN: as a depressant for sphalerite, chalcopyrite, and, pyrrhotite, and methyl isobutyl carbinol (MIBC) as frother (40 g/t).

The flotation time was 9 minutes for each test and the concentrates were recovered by automatic scraping every 30 seconds. The level of the pulp was constantly adjusted by water addition. The concentrate and tails were filtered, dried, weighed, and analysed by atomic absorption spectroscopy for Cu, Pb, Zn, Fe, SiO_2, Al_2O_3, and MgO. Elemental recoveries to the concentrates were calculated according to the following equation:

$$R = 100\frac{C\,t_c}{A\,t_f} \quad [1]$$

where R (%) is the recovery, t_c (%) is the concentrate element grade, t_f (%) is the feed metal grade; C is the concentrate weight, and A is the feed weight.

Talc and chlorites ('mica minerals') recovery was calculated as:

$$R_{\text{'micas'}} = R_{SiO_2} + R_{MgO} + R_{Al_2O_3} \quad [2]$$

In this equation mica recovery could be overestimated due to the recovery of quartz by entrainment. However, this will not affect the target of the separation, *i.e.* removal of all the gangue.

Design of experiments

In order to determine the optimum operating conditions concerning mica flotation, and the corresponding metal losses (Pb, Cu, and Zn) in this step, the response surface methodology (MRE) (Baçaoui *et al.*, 2002; Ennaciri *et al.*, 2014; Boujounoui *et al.*, 2018) was applied. This method allows the search for the optimum settings of the factors to achieve a desired response. Central composite design (CCD) was used to assess the relationship between the three more influential factors (X_1, X_2, and X_3) in mica flotation (*i.e.* pH, NaCN, and particle size) and the studied responses – the recoveries of micas (Y1, $R_{(Micas)}$), galena (Y2, *RPb*), chalcopyrite (Y3, *RCu*), and sphalerite (Y4, RZn). It consists of the following parts:

(1) A full factorial or fractional factorial design
(2) An additional design, often a star design in which experimental points are at a distance from the centre
(3) A central point (Mehrabani *et al.*, 2010).

The number of experiments (N) for CCD is established according to the following relationship:

$$N = 2^k + 2*K + n \quad [3]$$

with N the number of tests, K the number of factors, and n the centre tests.

In this study, the three factors and five center tests correspond to 19 tests to be performed.

A second-order polynomial model was used, which contains only the terms (bi) and (bij) that will reflect the different effects (main and interactions) of factor on the four studied responses (Y1, Y2, Y3, and Y4).

The model can be written following Equation [4]:

$$Y = b_0 + b_1X_1 + b_2X_2 + b_3X_3 + b_{11}X_1^2 + b_{22}X_2^2 + b_{33}X_3^2 + b_{12}X_1X_2 + b_{13}X_1X_3 + b_{23}X_2X_3 \quad [4]$$

where
Y: studied response
X_i: investigated factor (i varies from 1 to 3)
b_0: a constant
b_i: main effect of the factor *ii*
b_{ij}: interaction coefficients between factors i and j

The CCD was processed by Nemrodw Software (Mathieu *et al.*, 2000), in which the experimental sequence was randomized in order to minimize the effects of the uncontrolled factors. The CCD and the corresponding experimental conditions and responses are given in Tables I and II.

Results and discussion

The results in Table II show that mica recovery vary between 37% and 78% and the metals losses between 26% and 67% for lead, 16% and 55% for copper, and 13% and 27% for zinc.

The estimation coefficients of the postulated model (Equation [4]) were determined by the least-squares method. The interpretation of the coefficients, main effects of factors (b_i), and interaction effects (b_{ij}) was done using statistical tests on the coefficients by using the estimated variance from replicates and Student's test ($t\alpha/2,d$) (Boujounoui *et al.*, 2015, 2018). Factors considered statistically significant are those with a significance level higher than 95% (p-value < 0.05). Positive coefficients (b_i

Table II

Experimental design and results of flotation tests

No. exp	X_1 pH	X_2 NaCN, mg/L	X_3 d_{80}, µm	Y1	Y2	Y3	Y4
1	7.5	0	60	59.6	57.29	55.29	24.07
2	12.5	0	60	51.2	67.03	32.64	19.29
3	7.5	350	60	47.05	35.76	17.73	16.47
4	12.5	350	60	47.38	66.18	21.58	17.57
5	7.5	0	180	37.09	26.42	33.7	18.38
6	12.5	0	180	38.16	57.78	41.8	27.32
7	7.5	350	180	50.2	37.11	22.28	13.41
8	12.5	350	180	45.32	51.33	18.86	16.4
9	7.5	175	120	63.24	35.37	23.3	23.64
10	12.5	175	120	48.79	52.67	21.41	18.44
11	10.0	0	120	58.84	43.22	43.36	27.07
12	10.0	350	120	75.16	45.9	25.25	20.33
13	10.0	175	60	78.44	54.88	26.81	23
14	10.0	175	180	66.41	36.12	20.77	19.21
15	10.0	175	120	45.06	41.65	16.51	14.09
16	10.0	175	120	61.65	35.27	18.53	17.66
17	10.0	175	120	51.14	37.32	16.43	13.58
18	10.0	175	120	56.8	43.94	17.32	14.78
19	10.0	175	120	47.42	46.56	19.36	16.87

Table I

Variables, factors, and experimental domains chosen for the CCD

Variable	Factor	Domains
X1	pH	7.5–12.5
X2	NaCN, mg/L	0–350
X3	d80, µm	60–180

or b_{ij}) indicate that the variables increase the studied response (Yi), and negative coefficients a decrease.

The considered mathematical models were validated using analysis of variance (ANOVA), F-test, and also checked by the correlation coefficient (R^2) (Haider and Pakshirajan, 2007). When the values of R^2 are close to unity, the model offers an appropriate explanation of the variability of experimental values with respect to the predicted values (Liu and Wang, 2007). An adjusted determination coefficient (R^2_{Adj}) was used as a measurement of the proportion of the total observed variability described by the model. After validation, the different models were used to graphically represent the response surfaces in the domain of interest (iso-response curves) to interpret the results (Boujounoui *et al.*, 2018).

Analysis of Y responses

Factor effects and coefficients estimation

The coefficients estimated from the results obtained are displayed in Table III.

For Y1: The analysis of the different effects shows that the particle size (b_3 = –4.649) has a significant effect on the mica flotation (with a significance level of 95% (p-value 0.05). Furthermore, the more significant interaction effect (with a significance level of 95% (p-value < 0.05) is NaCN/particle size (b_{23} = 4.580). From these results, the mica recovery can be described by the following model (Equation [5]):

$$\mathbf{Y1} = 55.290 - 4.649\ X_3 + 4.580\ X_2X_3 - 26.150\ X^2_2 + 17.135\ X^2_3 \quad [5]$$

Table III

Estimated coefficients for Y responses

Response	Coefficient	Coefficient estimation	F. Inflation	Significance (%)
Y1	b_0	55.290	-	<0.01***
	b_1	–2.633	1.00	11.3
	b_2	0.487	1.00	77.0
	b_3	–4.649	1.00	1.55*
	b_{11}	0.725	2.88	85.1
	b_{22}	–26.150	5.61	0.192**
	b_{33}	17.135	2.88	0.326**
	b_{12}	0.348	1.00	83.2
	b_{13}	0.532	1.00	75.1
	b_{23}	4.580	1.00	2.62*
Y2	b_0	44.076	-	<0.01***
	b_1	7.107	1.33	0.0202***
	b_2	1.651	1.33	8.1
	b_3	–10.435	1.33	<0.01***
	b_{11}	–0.075	1.52	95.4
	b_{22}	0.465	1.52	72.6
	b_{33}	1.405	1.52	31.4
	b_{12}	4.438	1.40	0.326**
	b_{13}	–3.318	1.40	1.15*
	b_{23}	7.323	1.40	0.0340***
Y3	b_0	17.845	-	< 0.01 ***
	b_1	–6.243	1.50	0.0365 ***
	b_2	–5.895	1.50	0.0471 ***
	b_3	–5.192	1.37	0.0527 ***
	b_{11}	-1.323	2.79	42.7
	b_{22}	12.764	2.79	0.0282 ***
	b_{33}	5.677	2.06	0.566 **
	b_{12}	–2.538	1.44	2.32 *
	b_{13}	7.346	1.44	0.0226 ***
	b_{23}	–2.628	1.44	2.03 *
Y4	b_0	14.830	-	< 0.01 ***
	b_1	1.031	1.00	22.6
	b_2	–3.195	1.00	0.379 **
	b_3	–0.568	1.00	44.3
	b_{11}	–10.861	5.50	0.557 **
	b_{22}	8.870	2.81	0.356 **
	b_{33}	6.275	2.81	1.57 *
	b_{12}	–0.009	1.00	98.8
	b_{13}	1.951	1.00	4.31 *
	b_{23}	–0.821	1.00	32.7

***: Statistically significant at the 99.9% level (p value < 0.001)
**: Statistically significant at the 99% level (p-value < 0.01)
*: Statistically significant at the 95% level (p-value < 0.05)

The mica recovery model presents a high determination coefficient $R^2 = 0.91$, explaining 91% of the variability in the response. The adjusted determination coefficient ($R^2_{Adj} = 0.80$) and F-test = 7.97 were also satisfactory and confirmed the significance of the model.

For Y2: The pH ($b_1 = 7.107$) and particle size (d_{80}) ($b_3 = -10.435$) have a significant direct effect (with a significance level of 99.9%, p-value < 0.001) on the galena recovery. The pH favours losses of galena (Pb); on the other hand, the particle size (d_{80}) reduces the losses of Pb at the mica flotation stage. As regards the interactions between factors, the more significant interaction effect is NaCN/particle size (d_{80}) ($b_{23} = 7.323$) followed by the pH/NaCN ($b_{12} = 4.438$), and finally the interaction pH/d_{80} ($b_{13} = -3.318$). The galena recovery (response Y2) can be described by the following model (Equation [6]):

$$\mathbf{Y2} = 44.076 + 7.107\ X_1 - 10.435\ X_3 + 4.438\ X_1X_2 - 3.318\ X_1X_3 + 7.323 X_2X_3 \quad [6]$$

The correlation between the theoretical and experimental responses, calculated according this model, is satisfactory ($R^2 = 0.98$, $R^2_{Adj} = 0.97$, and F-test = 50.28) (Sayyad *et al.*, 2007).

For Y3: All factors (X_1, X_2 and X_3) are involved in different interactions. The most significant interactions are pH/d_{80} ($b_{13} = 7.346$), pH/NaCN ($b_{12} = -2.5381$) and NaCN/d_{80} ($b_{23} = -2.628$). The mathematical model describing the response $R_{(Cu)}$ (Y3) as a function of the significant factors can be written as follows (Equation [7]):

$$\mathbf{Y3} = 17.845 - 6.243\ X_1 - 5.895\ X_2 - 5.192\ X_3 + 12.764\ X^2_2 + 5.677\ X^2_3 - 2.538\ X_1X_2 + 7.346\ X_1X_3 - 2.628\ X_2X_3. \quad [7]$$

The correlation between the theoretical and experimental responses, calculated by the model, according to $R^2 = 0.99$, $R^2_{Adj} = 0.97$, and F-test = 6.42, is satisfactory.

For Y4: The factor NaCN ($b_2 = -3.195$) has a significant effect on the sphalerite recovery (Zn), with a significance level of 99% (p-value < 0.01. Furthermore, the more significant interaction effect, with a significance level of 95% (p-value < 0.05), is pH/particle size ($b_{13} = 1.951$).

From these results, the sphalerite recovery can be described by the following model (Equation [8]):

$$\mathbf{Y4} = 14.830 - 3.195\ X_2 - 10.861 X_1{}^2 + 8.870\ X^2_2 + 6.275\ X^2_3 + 1.951\ X_1X_3 \quad [8]$$

The sphalerite recovery model presents a high determination coefficient $R^2 = 0.90$, explaining 90% of the variability in the response. The adjusted determination coefficient ($R^2_{Adj} = 0.76$) and F-test –4.48 were also satisfactory and confirmed the significance of the model.

Three dimensional (3D) responses surfaces and isoresponse curves

In order to visualize the relationship between the response and experimental levels of each variable, and the type of interactions between the variables, in order to deduce the operating conditions leading to optimal response (Tanyildizi, Ozer, and Elibol, 2005; Vazifeh, Jorjani, and Bagherian, 2010; Ebadnejad, Karimi, and Dehghani, 2013; Boujounoui *et al.*, 2018), three-dimensional (3D) response surface and isoresponse curves were used. The objective is to maximize the selectivity of mica flotation over metallic elements such as Pb, Cu, and Zn.

Figure 1 represents the variation in mica flotation according to the interaction NaCN (X_2) and particle size (d_{80}) (X_3), and shows that the effect of particle size on mica flotation depends on NaCN consumption. Indeed, the increase in cyanide consumption with a small particle size (d_{80} = 60 µm) allows a maximum recovery of mica (Y1 > 65%). On the other hand, at a particle size of 180 µm the response is Y1 < 65%.

Figures (2a) and (2a′) show that low galena recovery (Y2 < 36%) can be obtained when the consumption of NaCN (X_2) is maximal (220–350 g/t) and the pH value (X_1) a minimum (7.5–8). Increasing the pH to 12.5 with maximum cyanide consumption increases lead recovery (Y2 > 51%). This suggests that the alkaline pH favours lead flotation (Fornasiero and Ralston, 2006; Chandra and Gerson, 2009). On the other hand, cyanide has no action on the lead depression (Seke, 2005).

Figures 2b and 2b′ show that the minimum lead recovery is obtained for a d_{80} (X_3) between 150 and 180 µm and pH (X_1) between 7.5 and 9. The pH increase with decreasing particle size (d_{80}) gives a maximum lead recovery, because the basic pH and the fragility of galena favour its flotation even in the absence of the collector (Seke, 2005). Figures 2c and 2c′ also show that the lead recovery is minimal when the particle size (d_{80}0) (X_3) is between 150 and 180 µm and consumption of NaCN (X_2) is low.

Thus, to minimize the loss of Pb in the mica circuit, it is necessary to work at a d_{80} of 150–180 µm, a moderately alkaline pH value (7.5–9), and low consumption of cyanide.

Figures 3a and 3a′ show the 3D response surface curve for chalcopyrite (Cu) recovery (Y3) *versus* the interactions X_1X_3 (pH/d_{80}), X_1X_2 (pH/NaCN). It is obvious that a low chalcopyrite

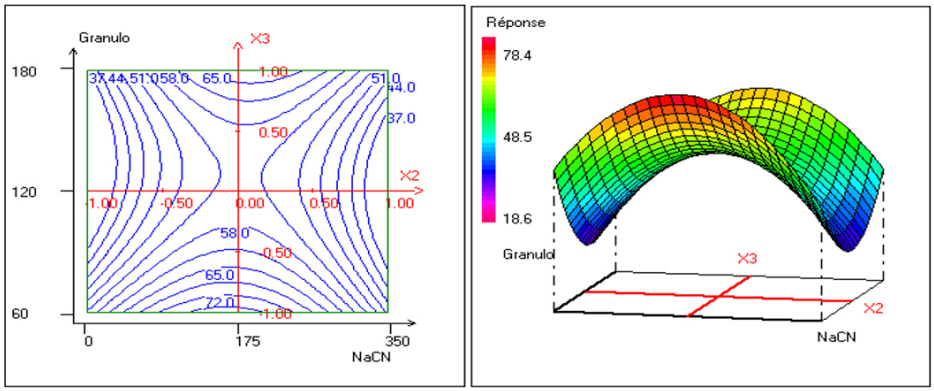

Figure 1—Mica recovery (Y1, %) *versus* the interaction between NaCN and particle size

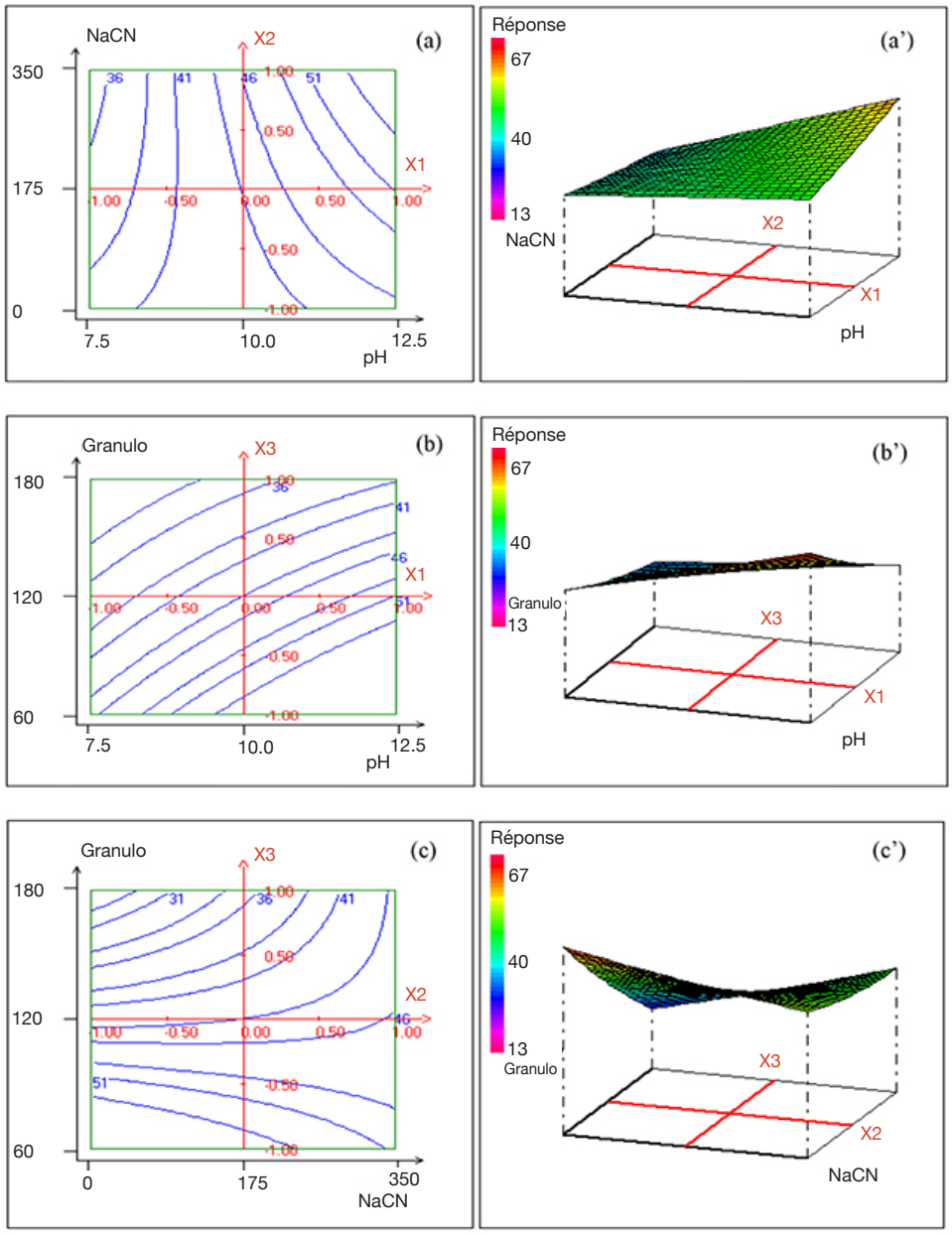

Figure 2—Lead recovery (Y2) *versus* the interactions between (a, a'') pH and NaCN, (b, b') pH and d_{80}, and (c, c') NaCN and particle size

recovery could be achieved with an increase in particle size (d_{80}) and pH. Figures 3b and 3b′ show that the low chalcopyrite recovery is obtained the higher levels of NaCN consumption (175–350 g/t) and pH between 11 and 12.5.

Generally, sodium cyanide is a depressant of chalcopyrite (Coetzer, du Preez, and Bredenhann, 2003; Seke, 2005; Lefèvre and Fédoroff, 2006; Ikumapayi, Johansson, and HanumanthaRao, *et al.* 2010, and this effect is more apparent at average concentrations.

Figure 4 shows the response surface curve of Zn recovery (Y4) as a function of interaction X_1X_3 (pH/ d_{80}). It is found that the effect of particle size (d_{80}) on sphalerite flotation depends on pH. Indeed, the minimal recovery of Zn (< 13%) is reached at the extreme ranges of pH (X_1) and particle size (X_3).

Multi-criteria optimization using desirability function

To reach the targeted mica flotation and selectivity with respect to lead, copper, and zinc in the mica circuit, (Y) responses were simultaneously optimized by using the desirability functions approach to determine an acceptable compromise zone (Derringer and Suich, 1980). This method first converts each estimated response Y_i into an individual scale-free desirability function d_i that varies over the range of zero outside of the desired limits (if $Y_i(x) \leq Y_i$; min.) to unity –the target (desired) value (if $Y_i(x) \geq Y_i$; max.) where Y_i; min. and Y_i; max. are the lower and upper acceptability bounds for response *i*, respectively (Boujounoui *et al.*, 2018). Once the function d_i (partial desirability of response Y_i) is defined for each response of interest, an overall objective function (D), representing the global desirability function, is calculated by determining the geometric mean of the individual desirabilities. Therefore, the function D over the experimental domain is calculated using Equation [9] as follows (Bruns, Scarminio, and de Barros Neto,. 2006):

$$D = (d1, d2, d3, d4)1/4 \quad [9]$$

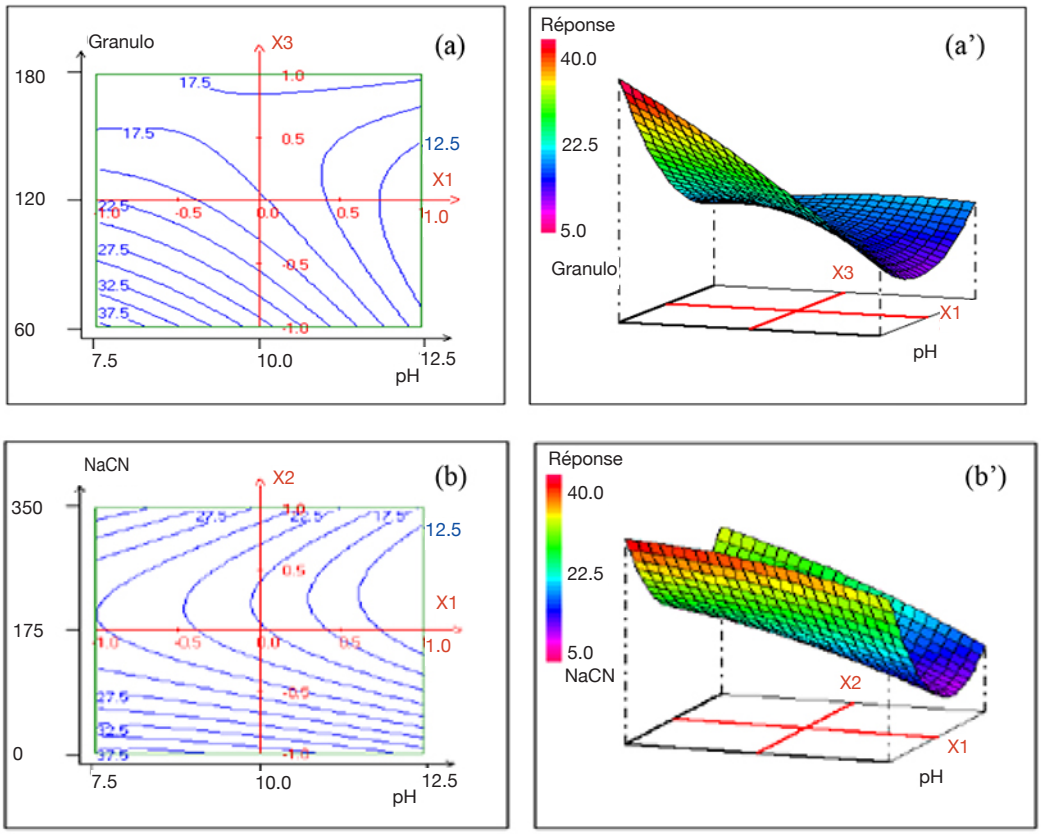

Figure 3—Copper recovery (Y3) *versus* the interactions between (a, a′) pH and particle size, (b, b′) pH and NaCN

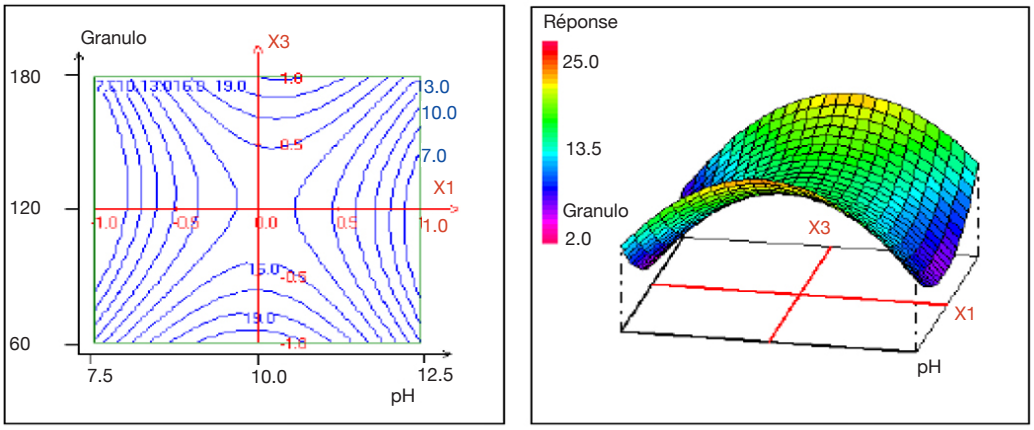

Figure 4—Zinc recovery (Y4) *versus* the interaction between pH and particle siz

The maximum of the function D gives the best global compromise in the studied domain and corresponds to optimal experimental conditions.

The low and target values assigned to each goal and the partial desirability associated to the four responses are shown in Table IV. The targeted value of mica recovery is 100%, and zero for galena, chalcopyrite, and sphalerite. The minimal acceptable value for mica recovery is 50%, and 25% is the maximal acceptable value for galena, chalcopyrite, and sphalerite recovery.

The global desirability function D was calculated using the Software NemrodW®, yielding a global degree of satisfaction for the four responses of 22%. The response surface corresponding to the global desirability function D is presented as contour and three-dimensional plots. It can be seen from Figure 5 that the acceptable compromise domain for better recovery of mica and low recoveries of galena chalcopyrite, and sphalerite was where pH values vary between 7.5 and 8.5, with average consumption of NaCN and a high particle size d_{80} of 160–180 µm.

The maximum recovery of mica (53%) and low recoveries of galena (28%), chalcopyrite (16%), and sphalerite (11%) were obtained with the optimal experimental conditions of pH 8, consumption of NaCN 180 g/t, and particle size d_{80} of 180 µm.

To validate these results and to check the proposed model, three additional flotation tests were carried out under the predicted optimal operating conditions (pH = 8; NaCN: 180 g/t; d_{80}: 180 µm; test duration: 9 minutes; impeller rotation speed:

Table IV

Lower limits and target value and the partial desirabilities associated with the four responses

Response	Lower limit %	Target value %	Weight	d_i %	Calc. values %	Exp. values %
Y1, (R_{Micas})	50	100	1	6.51	53.26	45.53
Y2, ($R_{(Pb)}$)	25	0	1	4.83	28.55	25.90
Y3, (R(Cu))	25	0	1	34.38	16.40	15.56
Y4, ($R_{(Zn)}$)	25	0	1	56.52	10.87	10.69

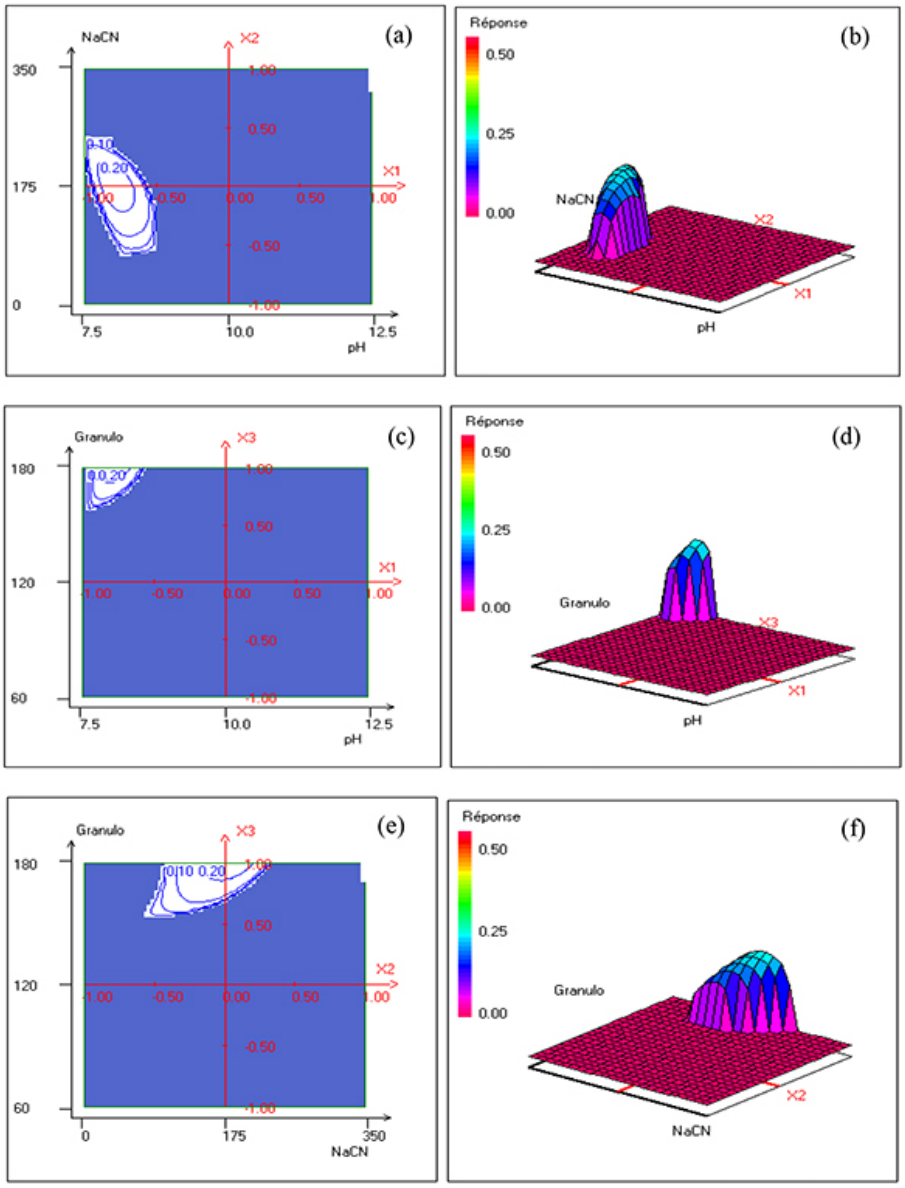

Figure 5—Desirability function *versus* (a, b) pH and NaCN,; (c, d) pH and particle size, and (e, f) NaCN and particle size

1000 r/min). The results, as well as the corresponding values calculated by the proposed model, are reported in Table IV. It can be seen that the deviation between the experimental and the predicted values is lower than 5%, indicating the good accuracy of the model.

Conclusions

Central composite design, response surface methodology, and multi-criteria optimization using desirability functions were used to optimize the flotation of chlorite and talc ('mica') and minimize the loss of valuable metals (Pb, Cu, Zn) when there is a need to float the micas prior to the current process at CMG. The modelling and optimizing study, which concerned particle size, pH, and the amount of NaCN, indicated the following:

- Better recovery of micas and low recoveries of galena, chalcopyrite, and sphalerite were obtained at a moderately alkaline pH, average consumption of NaCN, and a high particle size (d80)

- Optimal operating conditions in this stage were: pH 8, 180 g/t NaCN consumption, and particle size d_{80} of 180 µm. At these conditions, mica recovery was 53%, and valuable metals losses were Pb 28%, Cu 16 %, and Zn 11%.
- Flotation tests carried out with the optimal predicted operating conditions resulted in responses close to those calculated by the proposed model.

Recommendations

According to this study, the losses of Pb, Zn, and Cu in the mica circuit are high (especially for Pb), probably due to entrainment and not to true flotation.

Further studies should be undertaken to reduce these losses by (1) treating the mica concentrate to minimize Pb, Zn, and Cu losses in the final tailings, (2) focusing on the grinding-classification circuit in order to reduce the production of ultrafine particles, and (3) optimizing the hydrodynamic parameters within the flotation cells (agitation, air flow, and pulp density).

Acknowledgments

The authors thank the Mining Company of Guemassa for providing the sulphide ore sample and flotation reagents, and Reminex Society for the chemical analyses.

Compliance with ethical standards

The authors declare that they have no conflict of interest.

References

Akhanazarova, S. and Kafarov, V. 1982. Experiment Optimization in Chemistry and Chemical Engineering. Mir Publishers, Moscow.

Anderson, M.J. and Whitcomb, P.J. 2000. DOE simplified: Practical tools for effective experimentation. Productivity Inc. Portland, OR.

Abidi, A., Elamari, K., Bacaoui, A., and Yacoubi, A. 2014. Entrainment and true flotation of a natural complex ore sulphide. *Journal of Mining Sciences*, vol. 50. pp. 1061–1068.

Abidi, A. 2016. Flottation des minerais sulfurés complexes: Cas de Draa Lasfar (Maroc). Thesis, Université Caddi Ayyad, Faculté des Sciences Semlalia, Morocco.

Abidi, A., Boujounoui, K., El amari, K., Bacaoui, A., and Yacoubi, A. 2019. Contribution to improve water process recycling in the flotation plant of a complex Zn-Pb-Cu sulphide ore. *Journal of Mining Sciences*, vol. 55, no. 4. pp. 658–667.

Box, G.E.P., Hunter, W.G., and Hunter, J.S. 1978. Statistics for Experiments. Wiley, New York.

Baçaoui,A., Dahbi, A., Yaacoubi, A., Bennouna, C., Maldonado-HoädarF, Rivera-Utrilla, J., Carrasco-Marin, F., and Moreno-Castilla, C. 2002. Experimental design to optimize preparation of activated carbons for use in water treatment. *Environmental Science and Technology*, vol. 36, no. 3. pp. 844–3849.

Bruns, R.E., Scarminio, I.S., and de Barros Neto, B. 2006. Statistical design chemometrics. *Data Handling in Science and Technology*, vol. 25. Rutan, S. and Walczak, B. (eds). 1st edn. Elsevier.

Boujounoui, K., Abidi, A., Bacaoui, A., El Amari, K., and Yaacoubi, A. 2015. The influence of water quality on the flotation performance of complex sulphide ores: Case study at Hajar Mine. Morocco. *Journal of the Southern African Institute of Mining and Metallurgy*, vol. 115, no.12. pp. 1243–1251.

Boujounoui, K. 2017. Optimisation du potentiel de recyclage de l'eau de procédé dans les circuits de flottation des minerais sulfurés complexes: Cas de Draa Lasfar Sud (Maroc). Thesis, Université Caddi Ayyad, Faculté des Sciences Semlalia, Morocco.

Boujounoui, K., Abidi, A., Bacaoui, A., El Amari, K., and Yaacoubi, A. 2018. Flotation process water recycling investigation for the complex Draa Sfar sulphide ore, Morocco. *Mine Water and the Environment,* vol. 37, no. 1. pp. 75–87. https://doi.org/10.1007/s10230-017-0471-3

Boujounoui, K., Abidi, A., Bacaoui, A., El Amari, K., and Yaacoubi, A. 2019. Effect of water quality on the performance of the galena and blend flotation: case of Draa Sfar complex sulphide ore, Morocco. *Moroccan Journal of Chemistry*, vol. 7, no. 2. pp. 337–345.

Cilek, E.C. and Yilmazer, B.Z. 2003. Effect of hydrodynamic parameters on entrainment and flotation performance. *Minerals Engineering*, vol. 16. pp. 745–756.

Coetzer, G., du Preez, H.S., and Bredenhann, R. 2003. Influence of water resources and metal ions on galena flotation of Rosh Pinah ore. *Journal of the Southern African Institute of Mining and Metallurgy*, vol. 103. pp. 193–207.

Cao, M. and Liu, Q. 2006, Reexamining the functions of zinc sulfate as a selective depressant in differential sulfide flotation – the role of coagulation. *Journal of Colloid and Interface Science*, vol. 301, no. 2. pp. 523–531.

Chandra, A.P. and Gerson, A.R. 2009. 'A review of the fundamental studies of the copper activation mechanisms for selective flotation of the sulfide minerals, sphalerite and pyrite. *Advances in Colloid and Interface Science*, vol. 145. pp. 97–110.

Derringer, G. and Suich, R. 1980. Simultaneous optimization of several response variables. *Journal of Quality Technology*, vol. 12. pp. 214–219.

Ebadnejad, A., Karimi, G.R., and Dehghani, H. 2013. Application of response surface methodology for modeling of ball mills in copper sulphide ore grinding. *Powder Technology*, vol. 245. pp. 292–296.

Ennaciri, K., Baçaoui, A., Sergent, M., and Yaacoubi, A. 2014. Application of fractional factorial and Doehlert designs for optimizing the preparation of activated carbons from Argan shells. *Chemometrics and Intelligent Laboratory Systems*, vol. 139. pp. 48–57.

Fornasiero, D. and Ralston, J. 2006. Effect of surface oxide/hydroxide products on the collectorless flotation of copper-activated sphalerite. *International Journal of Mineral Processing*, vol. 78. pp. 231–237.

Haider, M.A. and Pakshirajan, K.K. 2007 Screening and optimization of media constituents for enhancing lipolytic by a soil microorganism using statically designed experiments. *Applied Biochemistry and Biotechnology*, vol. 141. pp. 377–390.

Hibti, M. 2001. Les amas sulfurés des Guemassa et des jebilets témoins del'hydrothermalisme précoce Dans le bassin mésetien. Thèse de Doctorat d'état, Faculté des Sciences Semlalia, Marrakech.

Hay, M.P. 2008. Optimising froth condition and recovery for a nickel ore. *Minerals Engineering*, vol. 21. pp. 861–872.

Ikumapayi, F., Johansson, B., and HanumanthaRao, K. 2010. Recycling of process water in sulfides processing and flotation selectivity. *Proceedings of the XXV International Mineral Processing Congress*, Brisbane, Australia, 6–10 September 2010. Australasian Institute of Mining and Metallurgy, Melbourne. pp. 4079–4088.

Lind, P., Yalcin, T., and Butcher, J. 2003. Computer simulation of the Bullmose coal preparation plant. *Coal Preparation*, vol. 23. pp. 129–145.

Lefèvre, G., and Fédoroff, M. 2006. Sorption of sulfate ions onto hematite studied by attenuated total reflection-infrared spectroscopy: kinetics and competition with other ions. *Physics and Chemistry of the Earth*, vol. 31. pp. 499–504.

Liu, G.C. and Wang, X.L. 2007. Optimization of critical medium components using response surface methodology for biomass and extra cellular polysaccharide production by Agaricus blazei. *Applied Biochemistry and Biotechnology*, vol. 74. pp. 78–83.

Mathieu, D., Nony, J., and Phan Tan Luu, R. 2000. Software NEMRODW. LPRAI, Marseille, France.

Martinez, A.L., Uribe, A.S., Carrillo, F.R.P., Coreno, J.A., and Ortiz, J.C. 2003. Study of celestite flotation efficiency using sodium dodecyl sulfonate collector: Factorial experiment and statistical analysis of data. *International Journal of Mineral Processing*, vol. 70. pp. 83–97.

Mehrabani, J.V., Noaparast, M., Mousavi, S.M., Dehghan, R., and Ghorbani, A. 2010. Process optimization and modelling of sphalerite flotation from a low-grade Zn-Pb ore using response surface methodology. *Separation and Purification Technology*, vol. 72. pp. 242–249.

Managem Group. 2014. Annual report, Casablanca, Morocco. http://www.managemgroup.com/en/investisseurs/managem/annual-reports

Napier-Munn, T.J. 2012. Statistical methods to compare batch flotation grade recovery curves and rate constants. *Minerals Engineering*, vol. 34. pp. 70–77.

Obeng, D.P., Morrell, S., and Napier-Munn, T.J. 2005, Application of central composite rotatable design to modelling the effect of some operating variables on the performance of the three-product cyclone. *International Journal of Mineral Processing*, vol. 76. pp. 181–192.

Rao, G.V., and Mohanty, S. 2002, Optimization of flotation parameters for enhancement of grade and recovery of phosphate from low-grade dolomitic rock phosphate ore from Jhamarkorta, India. *Minerals and Metallurgical Processing*, vol. 19. pp. 145–160.

Seke, M.D. 2005. Optimization of the selective flotation of galena and sphalerite at Rosh Pinah Mine. PhD thesis, University of Pretoria, South Africa.

Sayyad, S.A., Panda, B.P., Javad, S., and Ali, M. 2007. Optimization of nutrient parameters for lovastatin production by *Monascus purpureus* MTCC 369 under submerged fermentation using response surface methodology. *Applied Microbiology and Biotechnology*, vol. 73. pp. 1054–1058.

Tanyildizi, M.S., Ozer, D., and Elibol, M. 2005. Optimization of α-amylase production by bacillus sp. using response surface methodology. *Process Biochemistry*, vol. 40. pp. 2291–2296.

Vazifeh, Y., Jorjani, E., and Bagherian, A. 2010. Optimization of reagent dosages for copper flotation using statistical technique. *Transactions of Nonferrous Metals Society of China*, vol. 20. pp. 2371–2378.

Yalsin, T. 1999. Evaluation of Box-Wilson experimental design in flotation research. *Transactions of the Institution of Mining and Metallurgy*, vol. 108. pp. 109–112. ◆

A critical analysis of recent research into the prediction of flyrock and related issues resulting from surface blasting activities

J. van der Walt[1] and W. Spiteri[1]

Affiliation:
[1] Department of Mining Engineering, University of Pretoria, South Africa.

Correspondence to:
J. van der walt

Email:
Jennifer.vanderwalt@up.ac.za

Dates:
Received: 29 Jan. 2020
Revised: 30 Jun. 2020
Accepted: 9 Nov. 2020
Published: December 2020

How to cite:
van der Walt, J. and Spiteri, W. 2020
A critical analysis of recent research into the prediction of flyrock and related issues resulting from surface blasting activitiest.
Journal of the Southern African Institute of Mining and Metallurgy, vol. 120, no. 12, pp. 701–714.

DOI ID:
http://dx.doi.org/10.17159/2411-9717/1103/2020

ORCID
J. van der Walt
https://orcid.org/0000-0002-9542-3721

Synopsis

Since 2010, a number of researchers have investigated the development of new models to generate accurate predictions relating to the risks from flyrock. The purpose of this paper is to summarize and analyse these recent studies in order to determine the validity of the findings as a global solution. Recent publications have proposed a wide range of potential approaches and techniques to predict or investigate flyrock. Several authors have proposed viable solutions based on assumed causative parameters and their impact as inputs. However, the results were concluded to be site-specific and could not be applied to other environments. Since the actual impact of blast design parameters on the risk of flyrock remains debatable, based on the varying assumptions made in recent research, it is important to use an objective methodology for evaluating the impact of design parameters as well as environmental considerations. The testing methodologies used to measure the *actual* flyrock distance are not scientific and are highly dependent on the scrutiny of the researcher. In order to present results that are objective and uncriticizable, an accurate, quantitative and objective method of measuring the travel distance of flyrock is required.

Keywords
flyrock, flyrock prediction, flyrock measurement, blast safety, blast analysis, blast damage.

Introduction

Flyrock is the main cause of damage to equipment or infrastructure resulting from a blast and has fatally injured people in the vicinity of a blast (Bajpayee *et al.*, 2003). Injury to mine employees as well damage to surrounding property or infrastructure can result in high financial and reputational penalties for a mine. It is, therefore, imperative that the risk of flyrock is minimized. In order to reduce flyrock and minimize the severe consequences associated with excessive flyrock, it is important to understand the phenomena and how various blast parameter contribute to it.

The research relating to predicting the flight distances of flyrock prior to 2010, starting from a paper by Lundborg *et al.* (1975) has been reviewed in the 18th edition of the Blasters' Handbook (ISEE, 2011). This prior research culminated in the principle of scaled depth of burial (SDoB), which is currently considered the most effective model for estimating the flight distance of flyrock (ISEE, 2011). However, several studies have indicated that flyrock, and the effect of various blasting (causative) parameters on the risk of flyrock in different environments, is still not well understood. These studies recommended that the existing prediction models be reviewed and that the effect of the causative factors on the projection ranges of flyrock should be investigated further, in order to gain an understanding of how these parameters can affect the risk posed by flyrock.

Since 2010, a number of researchers have investigated flyrock and developed new prediction models in an effort to generate accurate predictions relating to the flyrock distance (*i.e.* the distance the flyrock is thrown from the blast). The purpose of this paper is to summarize and critically analyse these recent studies in order to determine the validity of the findings as a global solution, across all commodities and mining methods. All of these research studies were focused on surface mining operations since flyrock is largely associated with surface blasting activities.

The review of these studies served as a motivation for further work to develop a method to quantify the motion of flyrock, in order to develop a tool to accurately measure flyrock field data. This research is currently being pursued by the Mining Engineering Department at the University of Pretoria.

This paper aims to achieve three main objectives, namely:

1. To emphasise and support the statements made by previous researchers, *i.e.* that flyrock is a topic that is still not fully understood and that significant gaps in knowledge exist

2. To review the various methodologies, techniques, and technologies that have recently been used to develop flyrock prediction models
3. To investigate and critically analyse the methods of testing or evaluating the proposed prediction models (if the models was evaluated during the studies) and evaluate the conclusions based on the results obtained.

Literature review

Most of the recent work relevant to flyrock has been done since 2010. Research studies conducted before 2010 has been amalgamated in the Blasters' Handbook (ISEE, 2011) and will, therefore, not be reviewed in this paper. Several recent publications on flyrock have proposed models based on one of the following approaches.

1. Artificial Intelligence (AI) principles or techniques.
   (a) Artificial neural networks (ANNs).
   ANNs are developed in an attempt to imitate human thought processes. An ANN process consists of an input, weights, neurons (where the data is processed), and an output. ANNs are often the backbone of machine learning methodologies and can be combined with other systems such as fuzzy inference (Kukreja, *et al.*, 2016).
   (b) Adaptive neuro-fuzzy inference system (ANFIS).
   An ANFIS is based on the principles of ANN but incorporates the principles of fuzzy logic inference. Therefore, instead of just incorporating the input-output system flow of an ANN, ANFIS combines the ANN and the if-then rules of the fuzzy logic algorithms, allowing the system to model and interpret real-world scenarios (Prakash, 2014).
2. Rock engineering systems (RES).
   RES was first introduced by Hudson (1992). Faramarzi, Mansouri, and Farsangi (2014) describe this as an interaction matrix that represents the various relevant parameters and their relationships. The purpose is to reduce the uncertainty in the system by evaluating the interaction of these parameters in order to determine the degree of influence of each parameter on the overall system.
3. Empirical- and statistical analysis.
   Empirical and statistical analysis have been the foundation of most of the prediction approaches since the 1980s. Lundborg *et al.* (1975) published one of the first papers that considered an empirical approach in an attempt to predict the maximum throw resulting from a blast. However, due to the vast number of variables and uncertainties that influence flyrock, modelling based on empirical approaches have not been favoured in recent studies.
4. Forensic or ballistics approach.
   In terms of the basic principles of physics and natural laws that are accepted globally, flyrock should follow the principles that apply to projectile motion. Flyrock is fragments of rock propelled by a force from an external energy source. The energy exerted on these fragments is converted into kinetic energy, based on the law of conservation of energy.

These studies, categorized according to the authors' approaches, are summarized chronologically beow, in terms of the aim or focus of the researchers and the final outcome of the study.

Flyrock research based on AI principles

Numerous authors have presented concepts and techniques to predict or estimate flyrock or flyrock-related factors using AI principles. The main similarity between these proposed techniques is that the output of the system is highly dependent on the quality of the input parameters and the accuracy of estimation of these parameters. Note that the details pertaining to the algorithms used in these concepts or techniques are not discussed in detail. This section only serves as an overview of the work conducted in an attempt to predict flyrock.

1. Monjezi, Amini Khoshalan, and Yazdian Varjani (2010) used a a neuro-genetic approach to predict flyrock and back-break in open pit blasting operations: The motivation for this study was the poor predictions resulting from the existing empirical models at that time. The authors used a feed-forward ANN (with a 9-16-2 architecture) as the basis for their model and incorporated a genetic algorithm (GA) in an attempt to optimize the network parameters.
   The study concluded that the prediction results from the proposed model correlated with the measured flyrock distances. However, the methodology by which these 'actual' flyrock measurements were obtained and the accuracy thereof was not discussed. The neuro-genetic ANN model proved to be superior to the existing empirical and statistical models. Stemming length and powder factor were concluded to be the most influential parameters.
2. Monjezi *et al.* (2012) developed a model to predict flyrock using a feed-forward ANN with a 9-5-2-1 architecture. The outcomes were compared with thoss from existing empirical and statistical models, and the influential input parameters investigated. The motivation behind this study was the insufficient prediction capabilities of existing models. The input parameters were similar to those used in the aforementioned study. However, since the objective was to identify the influential parameters, some of the parameters were designed to be outputs of the system, along with flyrock.
   The study concluded by comparing the predicted flyrock with the measured flyrock. Again, the test methodology followed to obtain these 'actual' flyrock measurements or the accuracy thereof were not discussed. Similar to the 2010 publication, the ANN model was determined to be superior to the existing empirical and statistical models. Finally, the key influential parameters, based on this model, were identified as the powder factor, blast-hole diameter, stemming length, and charge mass per delay.
3. Raina, Murthy, and Soni (2013) investigated the influence of shape on the travel distance of flyrock. The motivation was that kinematic equations can be difficult to apply to flyrock in different environments

due to the uncertainty of air resistance based on the weight, size, and shape of a fragment. Air resistance or drag forms an essential component of motion analysis based on kinematic principles and cannot, therefore, be neglected.

The ANN model was made up of a 7-20-14-8-1 architecture, and was developed based on data collected from 75 test blasts. Seventy-five concrete blocks were blasted with a single hole and varying blast parameters in an attempt to identify the influence of these parameters. The input parameters were the initial velocity of the fragment, launch angle, sphericity, and the weight, length, width, and thickness of the fragment.

The initial velocity, launch angle, and weight of individual fragments were considered key parameters in this investigation. However, it was concluded that these are difficult to estimate in field conditions and further research and investigations were required. The authors noted that the effect of external factors such as the velocity of the air and specific weather conditions should also be investigated to determine their effect on the flyrock travel distance.

4. Ghasemi *et al.* (2014) applied artificial intelligence techniques for predicting flyrock distance. The aim was to develop and compare two predictive models based on AI concepts. The first model, based on ANN, was a feed-forward network with a 6-9-1 architecture. The second model, based on ANFIS, was described as consisting of 'triangular, trapezoidal membership functions' and was based on a Mamdani algorithm. Both models were presented with six input parameters, *i.e.* blast-hole length, burden, spacing, stemming length, powder factor, and charge mass per delay. The results showed that both models were able to yield accurate predictions when compared to the measured flyrock distances. This is, however, dependent on the accuracy and reliability of the measurements. Similar to the previous two publications, there is no discussion relating to the measurement methodology. The ANFIS method proved to be the better, but the ANN still produced accepted results and was concluded to be a 'good tool to minimize uncertainties' (Ghasemi *et al.*, 2014).
5. Marto *et al.* (2014) conducted a study on blast-induced flyrock prediction based on an imperialist competitive algorithm (ICA) and artificial neural network. The main objective was to predict flyrock by combining ANNs and ICA to produce a novel ICA-ANN prediction model. Seven input parameters were identified and determined to be influential to the system. These parameters are the blast-hole depth, burden-to-spacing ratio, stemming length, maximum charge mass per delay, powder factor, rock density, and the Schmidt hammer rebound number. The data from 113 blasts was recorded and the flyrock measured, but no discussion on the measurement methodology was presented. Predictions were first evaluated against the measured flyrock. The results from the developed ICA-ANN model were compared to that of other pre-developed ANN models and multiple regression analysis (MRA) results.

   The proposed ICA-ANN model did yield a tighter scatter of data-points, which implies that it presents an improved prediction capability compared to the other models. Marto *et al.* (2014) concluded their study by stressing that the models are dependent on the accuracy of the input parameters.
6. Trivedi, Singh, and Gupta (2016) used to predict flyrock using ANN and ANFIS approaches to predict flyrock. The same input parameters were used for both approaches, namely linear charge mass, burden, stemming length, specific charge, unconfined compressive strength, and rock quality.

   The proposed models were evaluated with data from 125 blasts. As in the previous publications, the predictions from the proposed models were evaluated against the measured flyrock. The authors conducted visual observations of the blast and measured the landing positions of the fragments with a hand-held GPS. High-speed cameras were used to record the blasts and estimate parameters such as initial velocities and launch angles. The authors concluded that the ANFIS approach produced better results than the ANN model.
7. Armaghani *et al.* (2016a) proposed a method to predict flyrock using an empirical approach. The motivation for conducting this study was that existing empirical models are not adequate due to the complex nature of flyrock. ANN and ANFIS models were also developed in an attempt to reduce the uncertainties and solve the complex nonlinear functions derived by an empirical approach.

   Two empirical formulae were presented that have been published. However, these empirical equations are often site-specific and cannot be used as a universal prediction model.

   The authors developed an empirical graph using the maximum charge per delay and powder factor as the two main influential parameters. This study also concluded that AI techniques, such as ANN and ANFIS, are superior for developing a prediction model.
8. Raina and Murthy (2016) presented a study based on the ANN method' with the aim of identifying the significance of different parameters in flyrock prediction. Blast data was collected from ten mines and analysed by means of ANN software, EasyNN-Plus©, in order to design, train, and validate a suitable ANN model. A feed-forward ANN model with a 20-16-6-4-1 architecture was suggested as an optimized network. The key input parameters for this model were identified as burden (B), spacing (S), P-wave (primary wave) velocity (cpi), the density of the rock (ρ_r), the effective in-hole density of the explosives (ρ_{ee}), and the charge length to hole depth ratio (l_q/l_d).

   The study concluded with a spider graph illustrating the relative importance and sensitivity of the various input parameters. This graph is reproduced in Figure 1.

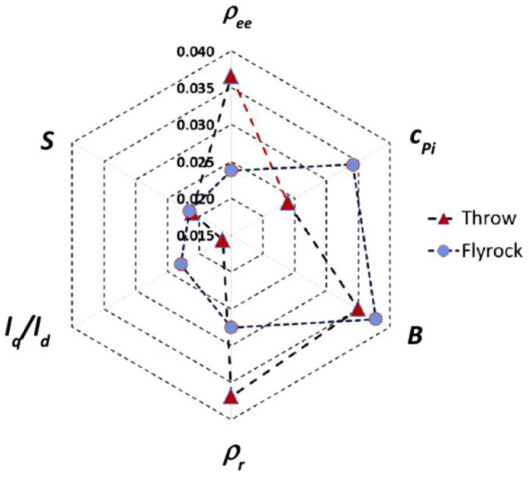

Figure 1—The relative importance and sensitivity of the variables for throw and flyrock (Raina and Murthy, 2016)

The main conclusion drawn from the above investigations is that implementing AI principles in prediction models yields improved results compared to existing empirical models. However, it is very important to note that all the aforementioned ANN or ANFIS models are highly dependent on the quality and accuracy of the input parameters.

The methodologies followed to measure the actual flyrock distance are not elaborated on in any of the publications. Since each proposed method was evaluated against these measurements, some of the results and conclusions come into question, owing to the uncertainty regarding the accuracy of these measurements.

Flyrock research based on rock engineering principles

Faramarzi, Mansouri, and Farsangi (2014) describe this as an interaction matrix that represents the various relevant parameters and their relationships. Hudson (2014) mentions that the effective parameters that drives specific circumstances are selected and the interactions between these parameters are considered in the matrix. The purpose is to reduce the uncertainty in the system by evaluating the interaction of these parameters and determining the degree of influence of each parameter on the overall system.

This degree of influence of each parameter is described by allocating weights, also known as coding, to the matrix. This can ultimately be used to derive a cause-and-effect graph from the system. Additional detail regarding RES is outside the scope of this project; however, this approach may hold some potential for minimizing the uncertainties relating to flyrock and flyrock prediction.

Only one publication (Faramarzi, Mansouri, and Farsangi, (2014) could be identified that implements this method to predict flyrock risk. The authors used data from 57 blasts and applied 13 input parameters – the burden, maximum instantaneous charge, powder factor, spacing-to-burden ratio, stemming-to-burden ratio, stiffness factor, time delay, blast-hole diameter, the velocity of detonation (VoD), blast-hole deviation, burden-to-hole diameter ratio, and RMR. Most of these parameters were measured on the bench with a measuring tape.

Flyrock travel distance was the only output of the system. The distances were measured after each blast and used to evaluate the performance of the proposed RES. Faramarzi, Mansouri, and Farsangi (2014) described the measuring methodology as properly cleaning the mine area prior to the blast, visually observing the flight path of the rock fragments, and measuring the landing positions with a hand-held GPS.

The authors concluded that the RES methodology is superior to other methods such as the multivariable regression analysis, and has better predictive capability. However, similar to most of the proposed predictive models, the RES model presented in this study was site-specific and cannot be used as a general solution.

Flyrock research based on empirical and statistical analysis

Empirical and statistical analysis have been the foundation of most of the prediction approaches since the 1980s. Lundborg (1975) published one of the first papers that considered an empirical approach in an attempt to predict the maximum throw resulting from a blast. However, due to the vast number of variables and uncertainties that influence flyrock, modelling based on empirical approaches has not been favoured in recent studies, although some researchers still conduct studies based on this approach.

Empirical and statistical approaches to develop flyrock prediction models have been proposed since the early 1980s. However, due to the significant progress in technology over the past two decades, only recent concepts and techniques proposed (publications from 2010) are summarized for the purpose of this review.

1. Ghasemi *et al.* (2012) described the development of an empirical model for predicting the effects of controllable blasting parameters on flyrock distance. The authors used data from 150 blasts and analysed this data by means of a dimensional approach. The large data-set presented the advantage of improving the overall accuracy of the system. However, all of the blasts were from a single mining operation and the results of this study can be considered to be very site-specific.

The data collected formed the input parameters to the dimensional analysis and included the burden (*B*), spacing (*S*), stemming length (*St*), blast-hole length (*H*) and diameter (*D*), powder factor (*P*), and mean charge mass per delay (*Q*). These input parameters were measured on the bench using a measuring tape.

The flyrock distances were also measured as evaluation criteria for the proposed model. The measurement data was acquired through visually observing the flyrock thrown from a blast and measuring the landing positions with a hand-held GPS. The fragments that were thrown the farthest distance from the blast were found to be 10 cm in diameter.

Ghasem, *et al.* (2012) proposed a model based on the assumptions that the influential parameters discussed above, resulting in a flyrock function:

Flyrock distance (F_d) = f(*B, S, St, H, D, P, Q*)

This function resulted in the following empirical formula:

$$F_d = 6946.547[B^{-0.796}.\ S^{0.783}.\ S_t{}^{1.994}.\ H^{1.649}.\ D^{1.766}.\left(\frac{P}{Q}\right)^{1.465}] \quad [1]$$

with

B = burden
S = Spacing
St = Stemming length
H = Blast-hole length
D = Blast-hole diameter
P = Powder factor
Q = Mean charge mass per delay

It is important that, again, this model is very site-specific. The validity of this equation was evaluated by means of Monte Carlo simulation. However, the authors noted that the validity of this prediction model depends on the range of the data and the quality of the samples and measurements taken.

Ghasemi *et al.* (2012) concluded by stating that, based on the sensitivity analysis, the stemming length, spacing, blast-hole length and diameter, and the powder factor showed a direct relationship to the flyrock distance, whereas, the burden and mean charge mass per delay showed an indirect relationship to flyrock distance. This was a counter-intuitive result since it would be logical to assume that burden and charge mass per delay would directly influence the distance travelled by rock fragments (Ghasemi *et al.*, 2012). This may indicate a flaw in the proposed system.

2. Armaghani *et al.* (2016b) conducted a study that combined multiple regression analysis (MRA) and Monte Carlo simulations of quarry blasting'. The main purpose was to develop a prediction model based on MRA and simulate flyrock using Monte Carlo (or probability) simulations.

The study utilized data from 62 blasts. The input parameters, consisting of the burden (*B*), spacing (*S*), stemming length (*ST*), blast-hole depth (*HD*), maximum charge mass per delay (*MC*), the powder factor (*PF*) and rock mass rating (RMR) were measured by means of a measuring tape. As in the study summarized previously, the flyrock was measured by cleaning the blast area prior to the blast, visually observing the flyrock thrown from the blast, and recording the landing positions with a hand-held GPS.

In order to run simulations of flyrock using Monte Carlo simulations, an empirical equation is required to describe the relationship between the input parameters and the output. Armaghan, *et al.* (2016b) therefore used software (SPSS, version 16) to generate this empirical equation, based on MRA. The resulting equation is:

$$F_d = 177.81 - (3.33 \times HD) - (2.55 \times S) - (3.49 \times B) - (13.93 \times ST) + (0.47 \times PF) + (1 \times MC) - (2.58 \times RMR) \quad [2]$$

with

F_d = Flyrock distance
B = Burden
S = Spacing
ST = Stemming length
HD = Blast-hole depth
MC = Maximum charge mass per delay
PF = Powder factor
RMR = Rock mass rating

The primary goal of the Monte Carlo simulations was to quantitatively determine the uncertainties and variabilities when exposed to certain risks. The secondary goal was to investigate the major drivers of this uncertainty and variability (Armaghani *et al.*, 2016b).

The results of this study favour the empirical equation based on MRA above previously published empirical models. The Monte Carlo simulations presented promising results, although the credibility of these results is highly dependent on the quality of the input parameters. The authors concluded that the powder factor was the most influential parameter. It is important to note that, similar to the previously proposed models, this model remains site-specific and is not a generalized solution.

3. Dehghani and Shafaghi (2017) attempted to address the inadequate predictive capability of existing empirical models by using a combination of differential evaluation (DE) and dimensional analysis (DA) algorithms. DA is defined as an engineering method that is used to create equations that will satisfy the analysis of complex multivariable systems. DE is defined as an optimization algorithm based on the evolution strategy of individuals in a population

The methodology involved collecting data from 300 blasts and measuring and recording both the input parameters and the resulting flyrock. The input parameters considered were the blast-hole diameter (*D*) and length (*L*), number of blast-holes (NB), spacing (*S*), burden (*B*), ANFO charge mass (*Q*), stemming length (*St*), powder factor (*PF*) and specific drilling (*SD*) (Dehghani and Shafaghi, 2017). Data was collected in the same manner as in the studies discussed previously.

The resulting equation obtained from DA is:

$$F_d = \exp(-16.569)\left(\frac{Q}{PF}\right)^{2.457}.\ D^{1.484}.L^{-2.315}.NB^{-2.453}.S^{-4.057}.\ B^{109.606}.St^{-117.001}.SD^{-3.523} \quad [3]$$

With

F_d = Flyrock distance
D = Blast-hole diameter

L = Blast-hole length
NB = Number of blast-holes
S = Spacing
B = Burden
Q = ANFO charge mass
St = Stemming length
PF = Powder factor
SD = Specific drilling

The relatioship obtained from DE is presented in Equation [4].

$$F_d = \exp(0.394)\left(\frac{Q}{PF}\right)^{0.06}. D^{0.59}.L^{0.26}.NB^{0.4}.S^{0.39}.B^{0.51}.St^{-0.32}.SD^{0.33} \quad [4]$$

With
F_d = Flyrock distance
D = Blast-hole diameter
L = Blast-hole length
NB = Number of blast-holes
S = Spacing
B = Burden
Q = ANFO charge mass
St = Stemming length
PF = Powder factor
SD = Specific drilling

Both of these equations are site-specific.

Dehghani and Shafaghi (2017) concluded that the DE equation yielded more accurate results than the DA equation. A sensitivity analysis showed that the powder factor and stemming length were the most influential parameters in both models. The authors recommended further research to investigate the principles of physics, incorporation of the pressure measured in the rock, trajectory in the air, and the influence of fragment size and shape on the travelling distance.

4. Hasanipanah (2017) used a regression tree technique to develop a model for prediction of blast-induced flyrock. The regression tree technique is broadly defined as a simple and understandable structure for decision-making. Data was collected from 65 blasts, with the important parameters being blast-hole length (*HD*), spacing (*S*), burden (*B*), stemming length (*ST*), maximum charge mass per delay (*MC*), and the powder factor (*PF*). The input parameters and the output (flyrock distance) were measured in a similar way to previous studies.

The developed regression tree model consisted of 52 nodes, with the powder factor as the root node. A multiple linear regression (MLR) model was also created, using SPSS (version 16) software, in order to conduct a brief comparative analysis between the performance of both models. The equation created during the development of the MLR model is:

$$F_d = (-90.62 \times HD) - (7.76 \times S) - (4.31 \times B) + (53.99 \times ST) + (0.62 \times PF) + (8.38 \times MC) + 5.23 \quad [5]$$

with
F_d = Flyrock distance
HD = Blast-hole diameter
S = Spacing
B = Burden
ST = Stemming length
PF = Powder factor
MC = Maximum charge mass per delay

Hasanipanah (2017) concluded that the regression tree model produced more accurate predictions compared to the MLR model, but both models were able to predict flyrock travelling distance. A sensitivity analysis of the models showed that the powder factor and the burden were the most influential parameters.

In each of the publication summarized, it is emphasised that the proposed models are site-specific and cannot be used as universal models. The important thing to notice is that the empirical equations presented differ significantly. This could be due to the site-specific input parameters used in each model; however, it does bring into question the validity of the proposed models.

Flyrock research based on ballistics principles

According to the fundamentals of physics, the same principles that describe projectile motion should be applicable to flyrock. Flyrock is fragments of rock propelled by a force from an external energy source. The energy exerted on these rock fragments is converted into kinetic energy, based on the law of Conservation of Energy. As stated in Newton's Second Law of Motion, the fragment maintains its motion unless it is subjected to an external force. Therefore, a system based on physics or a ballistics approach may possess the potential to accurately estimate flyrock distance.

Three consecutive articles were published from 2011 to 2015 by research teams led by Saša Stojadinović, driven by the need to develop a prediction model based on forensic analysis. Stojadinović, Pantović, and Žikić (2011) stressed that the scaled depth of burial (SDoB) approach of estimating flyrock behaviour is favoured across the mining industry, but it applies only to normal or expected flyrock. 'Wild' or unexpected flyrock due to bad blasting practices or unexpected geological factors was never considered and requires a forensic analysis.

These three articles are summarized chronologically.

1. Stojadinović, Pantović, and Žikić (2011 published the first article in the series, titled 'Prediction of flyrock trajectories for forensic applications using ballistic flight equations'. The objective was to develop a method of determining the maximum throw of flyrock in order to estimate safe distances.

Flyrock was considered to be a projectile (Figure 2), allowing the investigators to derive a numerical solution from ballistics flight principles (also known as projectile motion principles).

This numerical solution is presented for motion in the x- and y-directions and is given in Equations [6] and [7] respectively.

$$m\ddot{x} = -D_x = -C_1 v^2 cos\theta \quad [6]$$

$$m\ddot{y} = -mg - D_y = -mg - C_1 v^2 sin\theta \quad [7]$$

with
$\ddot{x}$ = acceleration in the x -direction (m/s²)
$\ddot{y}$ = acceleration in the y -direction (m/s²)
C_1 = a constant equal to the product of the density of air, the cross-sectional area of the projectile, and the drag coefficient ($\rho_{air}.A.C_D$)

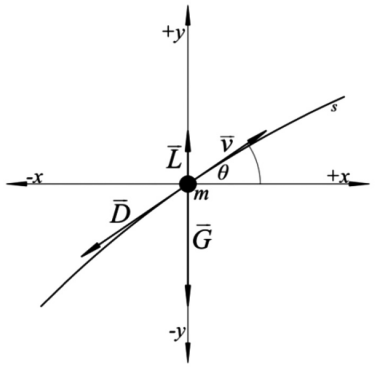

With:
L = Lift force vector
D = Drag force vector
v = velocity vector
G = Gravitational force vector
m = mass of the body or object
θ = Angle of trajectory
x = Horizontal direction of travel
y = Vertical direction of travel

Figure 2—Basic forces that act on flyrock fragments during its flight (Stojadinović, Pantović, and Žikić, 2011)

v = velocity of the projectile (m/s)
θ = angle between the velocity vector and the horizontal axis (degree or °)
m = mass of the projectile (kg)
g = gravitational force (N)

Data was collected from a mining operation using the blast design and bench conditions as input parameters. The flyrock (output) was measured by means of visual observation of the blast, measuring landing positions, and recording damage to surrounding structures and equipment (Stojadinović, Pantović, and Žikić 2011).

The assumptions applied to this analysis were:

- A launch angle of 45° reults in a maximum throw
- Launch velocity was calculated based on an equation presented by past publications.

According to the equations, the launch velocities are dependent on the size of the fragment, and ranged from 55 m/s for a 0.5m diameter fragment to 150 m/s for a 0.05 m diameter fragment.

Stojadinović, Pantović, and Žikić (2011) concluded that this forensic approach is better suited for post-incident analysis since the results are highly dependent on the accuracy of the input parameters, such as actual launch velocity and launch angle. In a final comment, the authors noted that aerodynamic drag has a crucial influence on the trajectory and overall motion of flyrock fragments. Therefore, further research is required for incorporating an accurate drag coefficient into the equations.

A key aspect of the conclusion of this article is a discussion of the relationship between the size of a fragment and the drag force exerted on it. Stojadinović, Pantović, and Žikić (2011) stressed that the acceleration of the fragment is dependent on the drag and the mass of the fragment, and the drag is dependent on the cross-sectional area of the fragment and its velocity squared. However,, the acceleration is also inversely dependent on the mass of the fragment, due to its inertia. Therefore, a smaller fragment with a smaller cross-sectional area and higher velocity will experience a larger drag force and, due to its smaller mass, will not be able to overcome these drag forces. This means that smaller fragments will not travel long distances (Stojadinović, Pantović, and Žikić 2011). Larger fragments, with more mass, have the potential to overcome the drag forces and travel further. However, lower travel velocities will also limit the travel distance. It can, therefore, be assumed that there is an ideal fragment size that can travel the maximum distance, which is the focus of most of the studies conducted.

2. In 2013, Stojadinović *et al.* published a sequel article describing a new model for determining flyrock drag coefficient. By comparing previous prediction models proposed throughout the years, the authors argued that implementing ballistics principles to predict flyrock is the most precise approach. However, the drag exerted on the rock fragments plays a significant role in the total travelling distance of the fragments. The main objective of this study was, therefore, to improve the ballistic approach by increasing the accuracy of the drag coefficient estimate.

From the previous article (2011), Stojadinović *et al.* (2013) deduced the following:

- The fragments that will travel the maximum distance range between 20 cm and 35 cm in diameter.
- Launch velocity is the most influential factor to be considered in a ballistics approach, and can be up to 150 m/s. Launch velocities of 350 m/s and 430 m/s have been recorded but, according to the final argument in the previous article, the maximum recorded launch velocity would not result in the maximum travel distance.
- The launch angle resulting in maximum throw ranges from 35° to 43°, taking the effect of drag into account.

Initially, it was planned to use a wind tunnel to evaluate the drag forces, but this idea was abandoned due to the complicated procedure involved (Stojadinović *et al.*, 2013). Therefore, the the blast was recorded with high-speed cameras (480 × 360 resolution). The known blast design parameters in the footage were used as control points and equipment in the field of view was used as scaling items (Stojadinović *et al.*, 2013).

The video footage was divided into individual frames and imported into CAD software in order to analyse the flyrock motion. The exact measuring technique is not discussed in the article. A key problem with this methodology was that the image quality was extremely poor, especially when magnified. The authors decided to measure the estimated centre points of the pixelated clouds thought to be the rock fragments. The initial purpose of this technique was to gather data on the launch velocity of the flyrock. However, the data could be used for the purpose of this study as well (Stojadinović *et al.*, 2013).

The drag coefficient was calculated by analysing the movement of the fragment at terminal velocity. The main

problems experienced by the research team were determining the size and trajectories of the individual fragments (Stojadinović *et al.*, 2013).

The equations presented in the 2011 paper were used to test the results, using the following initial conditions for a vertical shot:

- t_0 = 0 seconds
- v_0 = 200 m/s
- θ_0 = 90°.

A vertical shot was considered since it was the most likely situation in which to measure a fragment's motion at terminal velocity.

The final expectation was that the same, or a similar, drag coefficient would have been calculated for different rock fragments. However, this was not the case. The drag coefficient results did not yield a unique value. This could have been due to the influence of the shape of the fragment (Stojadinović *et al.*, 2013). Measurement error could also have contributed to the unexpected results, due to the poor quality of the images.

Stojadinović *et al.* (2013) concluded that since the drag coefficient is a very important input parameter to the ballistics equations, this drag coefficient should vary with changes in launch angle and fragment size.

3. The final article in this series was published in 2015. The motivation behind this study (Stojadinović *et al.*, 2015) was that most prediction models require an accurate launch velocity as a key input. All of the previously proposed models are highly dependent on the quality and accuracy of the input parameters. The main objective was, therefore, to develop an adaptive system application capable of predicting the launch velocities of flyrock.

Data was collected from a total of 36 blasts at three mining operations. The methodology followed for measuring and recording the input parameters as well as the output (flyrock) was the same as in Stojadinović *et al.*, 2013). The input parameters considered were divided into technical and natural parameters.

- Technical input parameters:
  - Blast-hole diameter, length, and inclination
  - Stemming length
  - Stemming factor
  - Specific stemming
  - Burden
  - Spacing
  - Volume of rock broken per blast-hole
  - Inter-hole delay;
  - Number of free faces
  - Charge mass per delay
  - Powder factor;
  - Explosives density
  - Velocity of detonation
  - Volume of gaseous products of detonation.
- Natural input parameters:
  - Rock density
  - Compressive and tensile strength
  - Presence of groundwater.

An ANN model with a 19-8-6-1 architecture was developed using a Peltarion synapse, described as a fuzzy algorithm for used optimization (Stojadinović *et al.*, 2015). The predictor that formed part of this system demonstrated the potential for predicting the initial velocity of flyrock fragments. However, Stojadinović *et al.* (2015) emphasised that the predictor in this system was only a concept and not fully developed. The authors concluded that this was due to the similar geology at the three mining sites, resulting in a lack of diversity in the data. They stated that this lack should be viewed as an opportunity for future research towards the ultimate goal of developing a universal prediction model.

Critical analysis of recent studies in the literature review

Several prediction models have been proposed in recent research studies based on various techniques. However, all these studies concluded that the respective models are primarily site-specific. Based on the the techniques used to develop the prediction models, the accuracy and reliability of the results are highly dependent on the quality and accuracy of the input parameters, as well as the postulated effect of these input parameters on the desired output (*i.e.* the weighting assigned to any input parameter in a model).

The following analysis is structured to address the three objectives of this paper. The first analysis emphasises the gap in knowledge and understanding of the flyrock phenomena by considering the most recent research in the field (*i.e.* objectives 1 and 2). Note that the aim of this first phase of analysis is not to evaluate the accuracy of the models. The second analysis is focused on evaluating the techniques used to assess the accuracy of the prediction results from each of the proposed models (objective 3).

Analysis and evaluation of the recent flyrock prediction methodologies

The first phase of this analysis is aimed at achieving the first two objectives stated at the beginning of this paper, and was conducted according to three distinct aspects, namely:

1. The approach or technique implemented to generate or develop a result
2. The input parameters considered in each study's model or solution
3. The factors or blast parameters that were assumed to be the most influential or primary causative parameter(s) of the proposed models.

The different techniques used to develop flyrock prediction models in recent research studies are summarized in Figure 3, which shows that AI techniques have been most favoured, followed by empirical and ballistics approaches.

However, it is important to note that not all of these models were created with the view of estimating flyrock distance as the primary output (Table I).

Two publications (highlighted in Table I) focused more on determining or estimating contiguous parameters, but was considered in this review since the research still related to flyrock and flyrock prediction. The related two models are not considered in the following analysis; however, some key information can still be deduced.

Empirical techniques

Empirical approaches have been proposed since the early

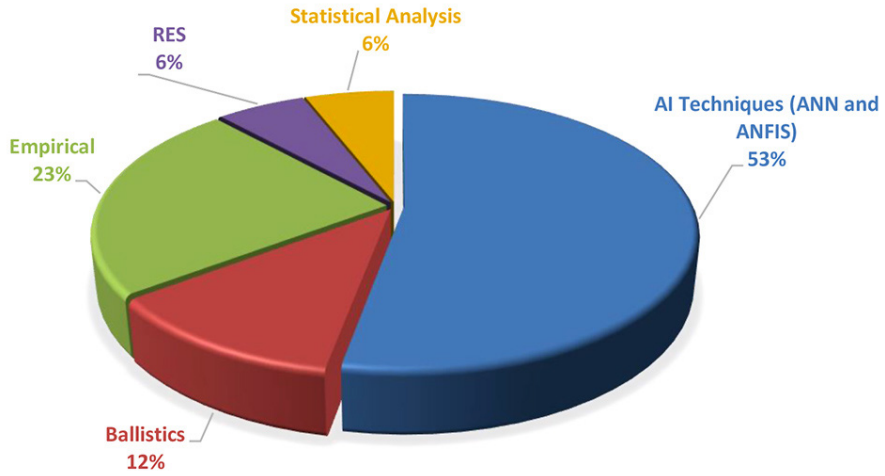

Figure 3—Techniques used in the recent flyrock prediction studies

Table I

Outputs or deliverables per publication

Publication	Primary deliverable	Secondary deliverable
Monjezi, Amini Khoshalan, and Yazdian Varjani A(2010)	Flyrock distance	Back-break
Stojadinović, Pantović, and Žikić (2011)	Flyrock distance	N/A
Ghasemi, Sari, and Ataei (2012)	Flyrock distance	N/A
Monjezi *et al.* (2012)	Flyrock distance	Influence of certain blast parameters
Stojadinović *et al.* (2013)	Flyrock drag coefficient	N/A
Raina, Murthy, and Soni (2013)	Flyrock distance	Influence of shape of flyrock fragment
Ghasemi *et al.* (2014)	Flyrock distance	N/A
Marto *et al.* (2014)	Flyrock distance	N/A
Faramarzi, Mansouri, and Farsangi (2014)	Flyrock distance	Flyrock risk
Trivedi, Singh, and Gupta (2015)	Flyrock distance	N/A
Stojadinović *et al.* (2015)	Flyrock launch velocity	N/A
Armaghani, *et al.* (2016a)	Flyrock distance	N/A
Raina and Murthy (2016)	Flyrock distance	Influence of certain blast parameters
Armaghani *et al.* (2016b)		
Flyrock distance (2016b)	N/A	
Dehghani and Shafaghi (2017)	Flyrock distance	N/A
Hasanipanah *et al.* (2017)	Flyrock distance	N/A

1980s, but recent empirical approaches have still proven to be inadequate. Empirical models tend to be very site-specific, taking into consideration variables specific to the site geology and blast design. These models cannot, therefore, be used as a generic approach to predicting flyrock.

AI techniques

ANN and other AI concepts have proven effective in minimizing the uncertainties related to flyrock. However, it is apparent that the architecture of these models has evolved significantly with time (Table II). These networks have become increasingly complex, *i.e.* taking more input parameters into account and processing them over more hidden layers. This indicates that there still are several uncertainties related to flyrock, as well as which blast parameters directly influence the risk of flyrock and to what degree.

Finally, the ANN prediction models are highly dependent on the input parameters and their estimated influence on the desired output (F_d). Considering the level of uncertainty regarding these input parameters and how much they contribute to flyrock behavious, some errors can be expected in these models. The testing methodology applied by researchers now becomes critical in order to determine what these error(s) are and the magnitude(s) thereof.

Table II

ANN architecture of proposed models

Publication (in chronological order)	ANN architecture
Monjezi, Amini Khoshalan, and Yazdian Varjani (2010)	9-16-2
Monjezi *et al.* (2012)	9-5-2-1
Raina,Murthy, and Soni (2013)	7-20-14-8-1
Ghasemi (2014)	6-9-1
Raina and Murthy (2016)	20-16-6-4-1

Ballistics principles:

The application of ballistics to flyrock prediction may not be an ideal solution due to the varying environments; however, it presents exciting new opportunities. An object, in this case a fragment of rock, moving through the air will behave according to Newton's three Laws of Motion. The established ballistics formulae are based on these laws. Ballistics should, therefore, be a viable and accurate method of analysing the motion of flyrock.

There are some pertinent considerations put forward in the studies incorporating ballistics concepts (Stojadinović, Pantović, and Žikić 2011; Stojadinović *et al.*, 2013, 2015), namely:

- The influence of drag or air resistance is significant but is often neglected.
- The effect of the shape of the fragment on the drag force experienced is unknown.
- The influence of external factors such as weather conditions has not been investigated.
- The fragments that will likely travel the furthest distance (*i.e.* small enough to experience a large launch velocity but big enough to overcome some of the drag force) range between 10 cm and 35 cm in diameter.
- The launch angle that will allow a fragment to travel a maximum distance is not 45°, as would be expected, but rather ranges between 35° and 43° when taking the drag force into account.

Parameters considered as causative inputs to the proposed models

The input parameters considered in the publications are noticeably variable (Figure 4), while some remain consistent when similar techniques are applied (see Figures 5–8). Some of the input parameters are considered in most of the publications, while others are unique to specific studies. Charge mass per delay, powder factor, burden, spacing, stemming, and blast-hole properties are the most popular input parameters.

Referring to Figure 5, it is evident that most of the ANN models incorporate similar causative factors, although some models do include unique inputs. The models developed from AI techniques incorporate more inputs than those in the other approaches. Since it is still uncertain which blast parameters contribute to flyrock and to what degree, it is always beneficial to consider as many parameters as possible. However, the influence (or weight) assigned to each of these parameters is not described in all of the proposed models and cannot, therefore, be analysed or commented on.

The inputs considered in the models based on empirical and statistical techniques are summarized in Figure 6. It is evident that, similar to the ANN models, various authors considered similar input parameters. This may be due to the use of similar background formulae or algorithms to build the models. However, the number of inputs is distinctly less that the number of inputs in the ANN models.

Three of the publications reviewed were based on ballistics principles, but only one focused on flyrock travel distance as its primary output. Therefore, only the input parameters considered in this single paper are summarized in Figure 7.

Similar to the ballistics approach, only one publication developed a model based on rock engineering principles. The input parameters for this model are summarized in Figure 8. Compared to the previous two graphs, the author considered more input parameters. It is also important to emphasise that this model also includes unique inputs such as the velocity of detonation (VoD).

From these graphical summaries of the various inputs considered in the recent proposed flyrock prediction models, it seems that there are some parameters that are accepted as being causative to flyrock. However, the variability between the prediction models using similar techniques, the additions of parameters unique to some models, and the assumed influence of each parameter on the desired output illustrate that the impact of various factors on flyrock behaviour is not an exact science. It will, therefore, be very difficult to apply a single model to multiple environments with the existing body of knowledge relating to flyrock.

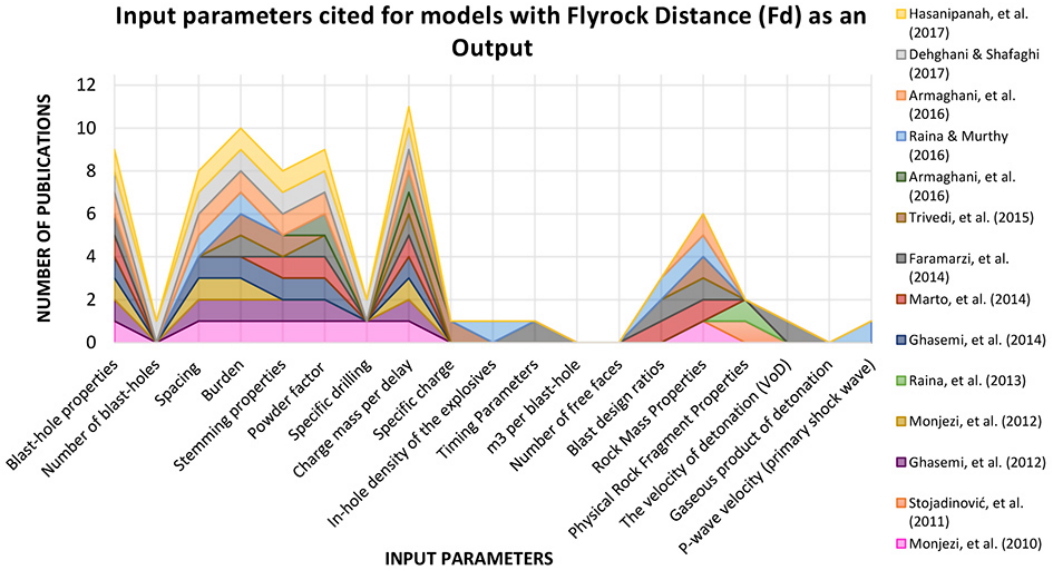

Figure 4—Input parameters considered in all models (regardless of the approach or technique used)

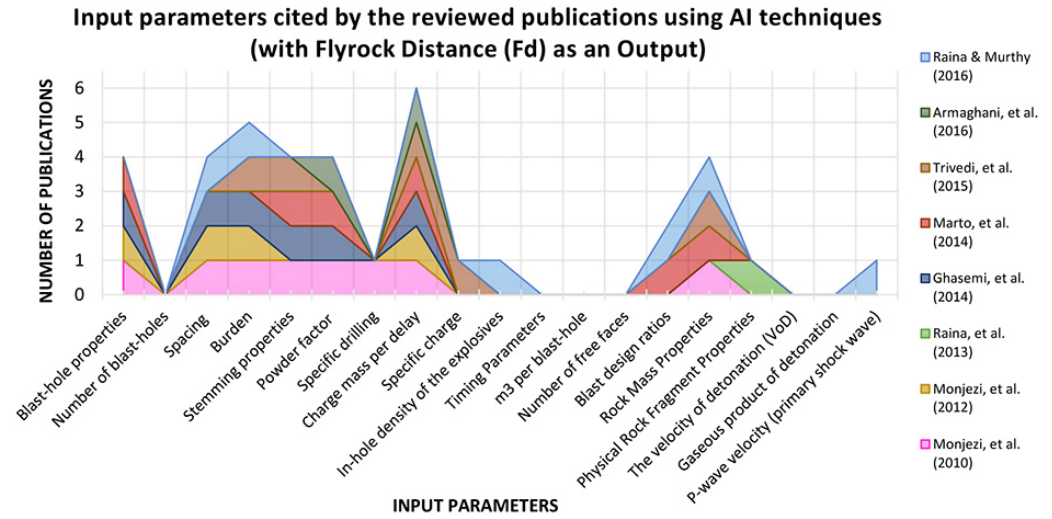

Figure 5—Input parameters considered in models where AI techniques were used

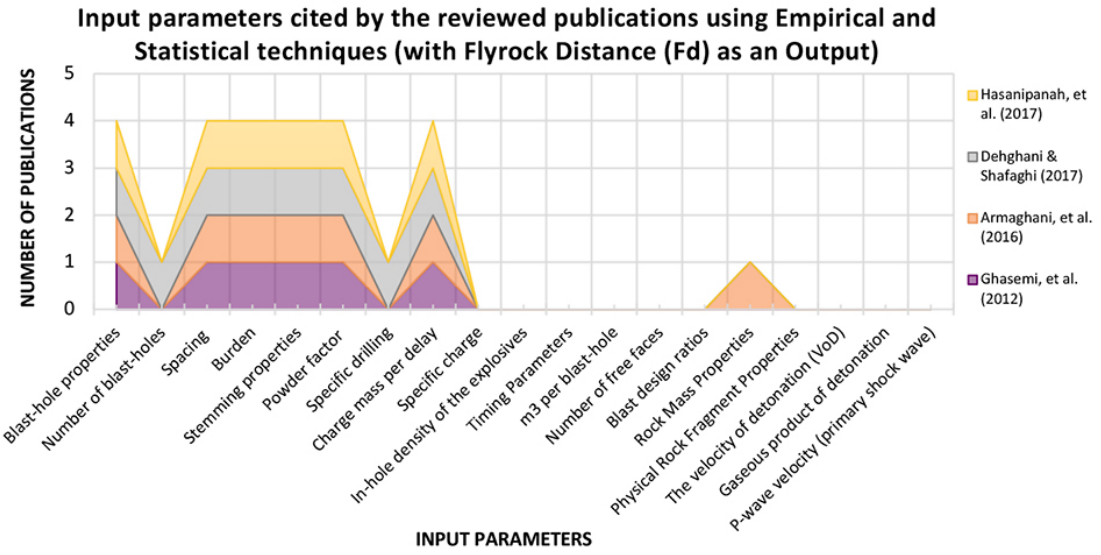

Figure 6—Input parameters considered in models where empirical and statistical techniques were used

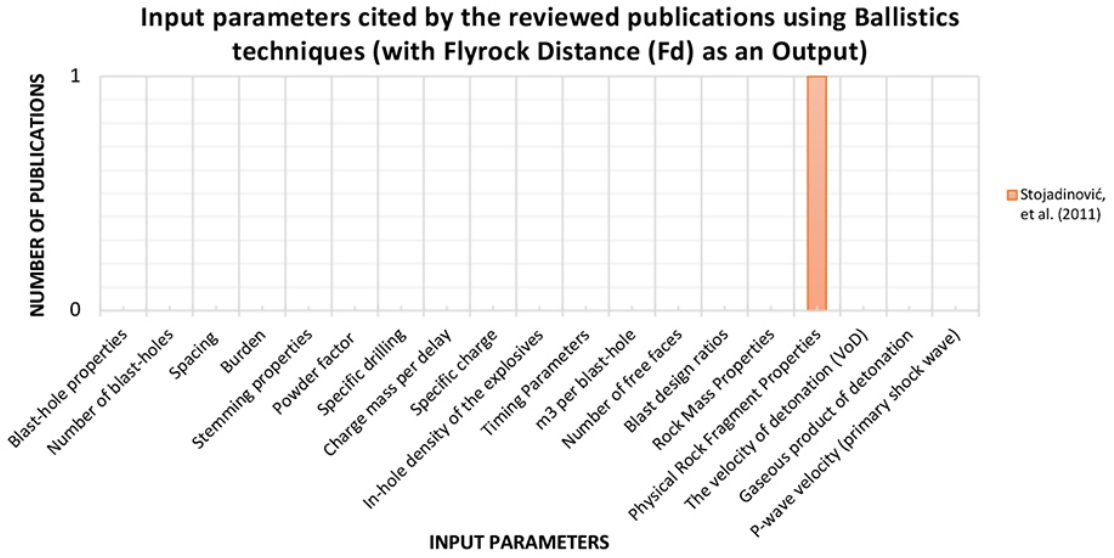

Figure 7—Input parameters considered in models where Ballistics techniques were used

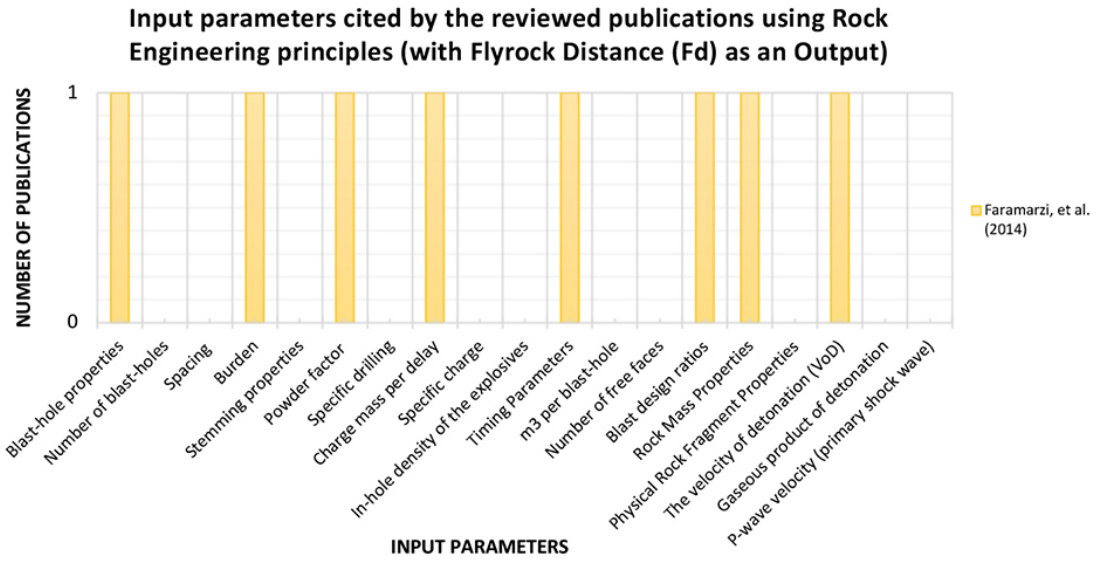

Figure 8—Input parameters considered in models where rock engineering principles were used

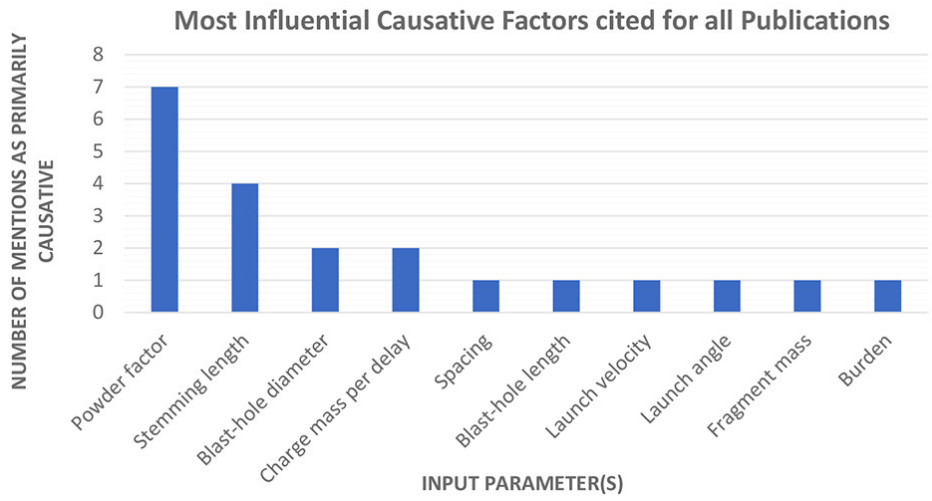

Figure 9—Most influential causative (or input) parameters

Key influential parameters

In most of these studies, a sensitivity analysis was conducted to identify the most influential or significant input parameter(s), based on the proposed model. These parameters are summarized in Figure 9. It is important to note that due to differences in the input parameters between the models, the sensitivity analyses and, therefore, the most influential parameters, may be indicated as outliers in Figure 9. This is only intended as an overview of which parameters are interpreted as essential by the authors of the papers.

Based on Figure 9, the powder factor and stemming length seem to be the key parameters relating to flyrock, which is what one would expect. However, the burden is not highlighted as a critical parameter, which is contradictory to the face burst mechanism of flyrock. This summary of the fundamental causative parameters and the disregarding of the importance of burden also support the argument that the effect of blast parameters on flyrock is not fully known or understood.

Considering the recent work conducted in flyrock prediction or investigating the effect of certain parameters on flyrock travel distance, it can be concluded that implementing ballistics principles to analyse flyrock motion is the best method to understand flyrock behaviour. However, a lot of uncertainty exists in terms of how external forces, such as drag, impact the travelling distance of flyrock. The effect of the shape of a fragment on the drag force, as well as the effect of various weather conditions, can be investigated through wind tunnel tests.

ANN and ANFIS approaches hold significant potential for further refining (*i.e.* minimizing the related uncertainties) of a flyrock prediction model. However, the impact and relevance of the input parameters must be estimated accurately in order to achieve accurate predictions.

Analysis of the testing methods used to evaluate the output results for each prediction model

It is essential that any model or prototype be thoroughly tested.

The test results are assessed by (as a minimum) comparing them to baseline data or 'actual' measurements. The purpose of this second phase of analysis is to critically analyse the testing methodologies used in the recent publications, which allowed the authors to draw conclusions regarding the efficiency and accuracy of the proposed models.

Unfortunately, most of the publications did not include a discussion on the testing methodologies used to acquire baseline or actual data. Only the testing methodologies discussed in the publications are analysed. The testing methodologies are summarized in Table III.

Visual observation of the blast and the resulting flyrock were the most popular methods used to collect 'actual' field data. The 'actual' flyrock distances (F_d) were measured by estimating the landing positions of some of the fragments through visual observation. These estimated landing positions were then measured using a hand-held GPS device. Even though this methodology may seem to be sufficient, it may not be the most scientific approach and the data acquired may be prone to error.

The subjectivity of the visual observation of flyrock trajectory may result in different researchers interpreting the landing positions differently. Visual observation can refer to video recordings of the blast or simple observation by eye. At increased distances form the blast, the error in visual estimation may increase significantly. To increase the accuracy of visual estimation some form of scale or control should be included within the observer's field of view. Two publications referred to the controls used in the respective test methodologies as the known blast design parameters visible, *i.e.* the burden and spacing. However, no discussions were included describing the correction factors considered (if any) relating to the different in visual planes, distances to the respective targets, influences of different lighting, *etc.*

An additional error should also be expected from the hand-held GPS device. These devices are not used by professional surveyors due to the error associated with the measurements, but are designed to give approximate coordinates or locations. Some of these hand-held GPS devices can include errors ranging from 5 m to 10 m in the x, y, and zdirections (Hussein, 2016).

Considering the cumulative errors from both the subjective estimation of the flyrock landing positions and the inherent error associated with hand-held GPS devices, the actual measurements against which the proposed models were evaluated may deviate significantly from the real positions.

In three publications, the researchers included high-speed photography in the testing methodologies. However, these publications did not aim to investigate flyrock distances, but rather the launch velocity of fragments and the drag coefficients. The use of high-speed photography cannot, therefore, be analysed in terms of evaluating the flyrock travel distances.

Conclusion

Several authors have proposed viable models for predicting and analysing flyrock based on assumed causative parameters as inputs and their impact on flyrock as weights assigned to each input. However, all of these papers concluded that the respective models were site-specific and could not be applied to other environments.

Table III

Testing methodologies used to evaluate the results obtained from the respective models

Publication	Testing methodology
Monjezi *et al.* (2010)	No discussion on testing methodology.
Stojadinović, Pantović, and Žikić (2011)	Flyrock was visually observed during the blast and the estimated landing positions were measured using a hand-held GPS and observation of damage to surrounding infrastructure or equipment (if possible).
Ghasemi, Sari, and Ataei (2012)	The bench and immediate blast area were cleaned of debris. Flyrock was visually observed during the blast and the estimated landing positions were measured using a hand-held GPS.
Monjezi *et al.* (2012)	No discussion on testing methodology.
Stojadinović *et al.* (2013) (output: flyrock drag coefficient)	High-speed cameras were used to record the blast. The blast design parameters were used as knowns within the footage to record estimated measurements of the landing positions of the flyrock. No discussion was included on the correction factors used.
Raina, Murthy, and Soni (2013)	No specific discussion on testing methodology. The input parameters for the models were determined from controlled test blasts using concrete blocks and single short holes.
Ghasemi *et al.* (2014)	No discussion on testing methodology.
Marto *et al.* (2014)	No discussion on testing methodology.
Faramarzi, Mansouri, and Farsangi (2014)	The bench and immediate blast area were cleaned of debris. Flyrock was visually observed during the blast and the estimated landing positions were measured using a hand-held GPS.
Trivedi, Singh, and Gupta (2015)	Flyrock was visually observed during the blast and the estimated landing positions were measured using a hand-held GPS. High-speed cameras were used to estimate the launch velocities and launch angles of some of the flyrock.
Stojadinović *et al.* (2015) (output: flyrock launch velocity)	High-speed cameras were used to record the blast. The blast design parameters were used as knowns within the footage to record estimated measurements of the landing positions of the flyrock. No discussion was included on the correction factors used.
Armaghani *et al.* (2016a)	No discussion on testing methodology.
Raina and Murthy (2016)	Blast data were collected from mines, however, there was no specific discussion on type of data or data acquisition methodology.
Armaghan, *et al.* (2016b)	The bench and immediate blast area were cleaned of debris. Flyrock was visually observed during the blast and the estimated landing positions were measured using a hand-held GPS.
Dehghani and Shafaghi (2017)	No discussion on testing methodology.
Hasanipanah *et al.* (2017)	Flyrock was visually observed during the blast and the estimated landing positions were measured using a hand-held GPS.

Since the actual impact of blast design parameters on the risk of flyrock is debatable, based on the variable assumptions made in these publications, it can be concluded that flyrock is still not well understood. The biggest gap in knowledge seem to be the uncertainties concerning which blast and environmental parameter contribute to flyrock, and to what degree. These uncertainties open an opportunity for developing new models for analysing the flyrock when it occurs, rather than predicting it beforehand.

The techniques used to measure the actual distance travelled by the rock fragments (flyrock) in these studies are subjective and highly dependent on the scrutiny of the researcher. Obtaining objective data is critical in any investigation. Since the results of the proposed models were evaluated by comparing the predicted and measured (or actual) data, some margin of error can be expected from the findings, based on the transferred error from the testing methodology.

In order to present results that are objective and uncriticizable; an accurate, quantitative, and objective method of measuring the actual travel distance of flyrock is required. The main recommendation from this study is that the potential for developing such a measuring tool, which will yield unbiased field data, be investigated. Such a tool can be used to evaluate the results from existing and future flyrock prediction models.

Acknowledgement

This work was carried out under the auspices of the AELMS Chair in Innovative Rock Breaking Technology and Visualising of New Results using Virtual Reality at the Mining Engineering Department of the University of Pretoria. The authors would like to specifically acknowledge AECI Mining Explosives (formerly known as African Explosives Limited or AEL) for their continued support throughout this study.

References

Armaghani, D.J., Tonnizam, E., Hajihassani, M., and Abad, S.V.A.N.K. 2016a. Evaluation and prediction of flyrock resulting from blasting operation using empirical and computational methods. *Engineering with Computers*, vol. 32, no. 1. pp. 109–121.

Armaghani, D.J., Mahdiyar, A., Hasanipanah, M., and Faradonbeh, R.S. 2016b. Risk assessment and prediction of flyrock distance by combined multiple regression analysis and Monte Carlo simulation of quarry blasting. *Rock Mechanics and Rock Engineering*, vol. 49, no. 9. pp. 3631–3641.

Bajpayee, T.S., Bhatt, S.K, Rehak, T.R., Mowrey, G.L., and Ingram, D.K. 2003. Fatal accidents due to flyrock and lack of blast area security and working practices in mining. *Journal of Mines, Metals and Fuels*, vol. 51, no. 11/12. pp. 344–350.

Dehghani, H. and Shafaghi, M. 2017. Prediction of blast-induced flyrock using differential evolution algorithm. *Engineering with Computers*, vol. 33, no. 1. pp. 149–158.

Faramarzi, F., Mansouri, H., and Farsangi, M.A. 2014. Development of rock engineering systems-based models for flyrock risk analysis and prediction of flyrock distance in surface blasting. *Rock Mechanics and Rock Engineering*, vol. 47, no. 4. pp. 1291–1306.

Ghasemi, E., Amini, H., Ataei, M., and Khalokakaei, R. 2014. Application of artificial intelligence techniques for predicting the flyrock distance caused by blasting operation. *Arabian Journal of Geosciences*, vol. 7, no. 1. pp. 193–202.

Ghasemi, E., Sari, M., and Ataei, M. 2012. Development of an empirical model for predicting the effects of controllable blasting parameters on flyrock distance in surface mines. *International Journal of Rock Mechanics and Mining Sciences*, vol. 52. pp. 163–170.

Hasanipanah, M., Faradonbeh, R.S., Armaghani, D.J., and Amnieh, H.B. 2017. Development of a precise model for prediction of blast-induced flyrock using regression tree technique. *Environmental Earth Sciences*, vol. 76. p. 27 (10).

Hudson, J.A. 1992. Rock Engineering Systems: Theory and Practice. Ellis Horwood, Chichester.

Hudson, J.A. 2014. A review of Rock Engineering Systems (RES) applications over the last 20 years. *Rock Characterisation, Modelling and Engineering Design Methods*. Feng, X., Hudson, J. A., and Tan, F., (eds). . Ellis Horwood, Chichester: pp. 419–424.

Hussein, Z.E. 2016. Improving the accuracy of handheld GPS receivers based on NMEA file . *Journal of Engineering*, vol. 22, no. 5. pp. 162–174.

ISEE, 2011. Flyrock. *Blasters' Handbook*. Stiehr, J.F. (ed.). International Society of Explosives Engineers, Cleveland, OH, Chapter 15: pp. 383–410.

Kukreja, H., Bharath, N., Siddesh, C.S., and Kuldeep, S. 2016. An introduction to artificial neural network. *International Journal of Advance Research and Innovative Ideas in Education*, vol. 1, no. 5. pp. 27–30.

Lundborg, N., Persson, P. A., Ladegaard-Pedersen, A., and Holmberg, R. 1975. Keeping the lid on flyrock in open-pit blasting. *Engineering and Mining Journal*, vol. 176. pp. 95–100.

Marto, A., Hajihassani, M., Armaghani, D.J., Mohamad, E.T., and Makhtar, A.M. 2014. A novel approach for blast-induced flyrock prediction based on imperialist competitive algorithm and artificial neural network. *The Scientific World Journal*, vol. 5. doi: 10.1155/2014/643715

Monjezi, M., Amini Khoshalan, H., and Yazdian Varjani, A. 2010. Prediction of flyrock and backbreak in open pit blasting operation: a neuro-genetic approach. *Arabian Journal of Geosciences*, vol. 5, no. 3. pp. 441–448.

Monjezi, M., Mehrdanesh, A., Malek, A., and Khandelwal, M. 2012. Evaluation of effect of blast design parameters on flyrock using artificial neural networks. *Neural Computing and Applications*, vol. 23, no. 2. pp. 349–356.

Prakash, A. 2014. ANFIS (Adaptive Neural Fuzzy Inference Systems). [interview] 14 September 2014.

Raina, A.K. and Murthy, V.M.S.R. 2016. Importance and sensitivity of variables defining throw and flyrock in surface blasting by artificial neural network method. *Current Science*, vol. 111, no. 9. pp. 1524–1531.

Raina, A.K., Murthy, V.M.S.R., and Soni, A.K. 2013. Relevance of shape of fragments on flyrock travel distance: An insight from concrete model experiments using ANN. *Electronic Journal of Geotechnical Engineering*, vol. 18. pp. 899–907.

SAS Institute Inc., 2019. Artificial intelligence: What is it and why it matters. https://www.sas.com/en_za/insights/analytics/what-is-artificial-intellegence.html[accessed 3 September 2019].

Stojadinović, S., Lilic, N., Obradović, I., Pantović, R., and Denić, M. 2015. Prediction of flyrock launch velocity using artificial neural networks. *Neural Computing and Applications*, vol. 27, no. 2. pp. 515–524.

Stojadinović, S., Lilic, N., Pantović, R., and Žikić, M. 2013. A new model for determining flyrock drag coefficient. *International Journal of Rock Mechanics and Mining Sciences*, vol. 62. pp. 68–73.

Stojadinović, S., Pantović, R., and Žikić, M. 2011. Prediction of flyrock trajectories for forensic applications using ballistic flight equations. *International Journal of Rock Mechanics and Mining Sciences*, vol. 48, no. 7. pp. 1086–1094.

Trivedi, R., Singh, T N., and Gupta, N. 2015. Prediction of blast-induced flyrock in opencast mines using ANN and ANFIS. *Geotechnical and Geological Engineering*, vol. 33. pp. 875–891. ◆

NATIONAL & INTERNATIONAL ACTIVITIES

2021

18–22 April 2021 — **IMPC2020**
XXX International Mineral Processing Congress
Cape Town, South Africa
Contact: Camielah Jardine
Tel: +27 11 834-1273/7
Fax: +27 11 838-5923/833-8156
E-mail: camielah@saimm.co.za
Website: http://www.saimm.co.za

6–9 June 2021 — **The 16th International Ferroalloys Congress (INFACON XVI)**
Clarion Hotel & Congress Trondheim
infacon2021@videre.ntnu.no

9–10 June 2021 — **Diamonds – Source To Use — 2021 Hybrid Conference**
'Innovation And Technology'
The Canvas, Riversands, Fourways, South Africa
Contact: Camielah Jardine
Tel: +27 11 834-1273/7
Fax: +27 11 838-5923/833-8156
E-mail: camielah@saimm.co.za
Website: http://www.saimm.co.za

28–30 June 2021 — **Renewable Solutions for an Energy Intensive Industry Hybrid Conference 2021**
Mintek, Randburg, South Africa
Contact: Camielah Jardine
Tel: +27 11 834-1273/7
Fax: +27 11 838-5923/833-8156
E-mail: camielah@saimm.co.za
Website: http://www.saimm.co.za

13–16 July 2021 — **Copper Cobalt Africa**
Incorporating
The 10th Southern African Base Metals Conference
Avani Victoria Falls Resort, Livingstone, Zambia
Contact: Camielah Jardine
Tel: +27 11 834-1273/7
Fax: +27 11 838-5923/833-8156
E-mail: camielah@saimm.co.za
Website: http://www.saimm.co.za

28–29 July 2021 — **5th Mineral Project Valuation Hybrid Colloquium**
The Canvas Riversands, Fourways, Johannesburg
Contact: Gugu Charlie
Tel: +27 11 834-1273/7
Fax: +27 11 838-5923/833-8156
E-mail: gugu@saimm.co.za
Website: http://www.saimm.co.za

16–17 August 2021 — **Worldgold Hybrid Conference 2021**
Misty Hills Conference Centre, Muldersdrift, Johannesburg, South Africa
Contact: Camielah Jardine
Tel: +27 11 834-1273/7
Fax: +27 11 838-5923/833-8156
E-mail: camielah@saimm.co.za
Website: http://www.saimm.co.za

29 August–2 September 2021 — **APCOM 2021 Minerals Industry Hybrid Conference**
'The next digital transformation in mining'
Misty Hills Conference Centre, Muldersdrift, Johannesburg, South Africa
Contact: Camielah Jardine
Tel: +27 11 834-1273/7
Fax: +27 11 838-5923/833-8156
E-mail: camielah@saimm.co.za
Website: http://www.saimm.co.za

21–22 September 2021 — **5th Young Professionals Hybrid Conference 2021**
'A Showcase of Emerging Research and Innovation in the Minerals Industry'
The Canvas, Riversands, Fourways, South Africa
Contact: Gugu Charlie
Tel: +27 11 834-1273/7
Fax: +27 11 838-5923/833-8156
E-mail: gugu@saimm.co.za
Website: http://www.saimm.co.za

27–30 September 2021 — **8th Sulphur and Sulphuric Acid Conference 2021**
The Vineyard Hotel, Newlands, Cape Town, South Africa
Contact: Camielah Jardine
Tel: +27 11 834-1273/7
Fax: +27 11 838-5923/833-8156
E-mail: camielah@saimm.co.za
Website: http://www.saimm.co.za

4–6 October 2021 — **PGM The 8th International Conference 2021**
Sun City, Rustenburg, South Africa
Contact: Camielah Jardine
Tel: +27 11 834-1273/7
Fax: +27 11 838-5923/833-8156
E-mail: camielah@saimm.co.za
Website: http://www.saimm.co.za

18–20 October 2021 — **Southern African Rare Earths International Conference 2021**
Swakopmund Hotel and Entertainment Centre, Swakopmund, Namibia
Contact: Camielah Jardine
Tel: +27 11 834-1273/7
Fax: +27 11 838-5923/833-8156
E-mail: camielah@saimm.co.za
Website: http://www.saimm.co.za

26–27 October 2021 — **SAMCODES Conference 2021**
The Canvas Riversands, Fourways, South Africa
Contact: Gugu Charlie
Tel: +27 11 834-1273/7
Fax: +27 11 838-5923/833-8156
E-mail: gugu@saimm.co.za
Website: http://www.saimm.co.za

8–10 November 2021 — **Global Tailings Standards and Opportuniries Hybrid Conference 2021**
'For the Mine of the Future'
Sun City, Rustenburg, South Africa
Contact: Gugu Charlie
Tel: +27 11 834-1273/7
Fax: +27 11 838-5923/833-8156
E-mail: gugu@saimm.co.za
Website: http://www.saimm.co.za

Owing to the current COVID-19 pandemic our 2020 conferences have been postponed until further notice. We will confirm new dates in due course.

Company affiliates

The following organizations have been admitted to the Institute as Company Affiliates

3M South Africa (Pty) Limited
AECOM SA (Pty) Ltd
AEL Mining Services Limited
African Pegmatite (Pty) Ltd
Air Liquide (PTY) Ltd
Alexander Proudfoot Africa (Pty) Ltd
AMEC Foster Wheeler
AMIRA International Africa (Pty) Ltd
ANDRITZ Delkor (Pty) Ltd
Anglo Operations Proprietary Limited
Anglogold Ashanti Ltd
Arcus Gibb (Pty) Ltd
ASPASA
Atlas Copco Holdings South Africa (Pty) Limited
Aurecon South Africa (Pty) Ltd
Aveng Engineering
Aveng Mining Shafts and Underground
Axiom Chemlab Supplies (Pty) Ltd
Axis House (Pty) Ltd
Bafokeng Rasimone Platinum Mine
Barloworld Equipment -Mining
BASF Holdings SA (Pty) Ltd
BCL Limited
Becker Mining (Pty) Ltd
BedRock Mining Support (Pty) Ltd
BHP Billiton Energy Coal SA Ltd
Blue Cube Systems (Pty) Ltd
Bluhm Burton Engineering (Pty) Ltd
Bond Equipment (Pty) Ltd
Bouygues Travaux Publics
Castle Lead Works
CDM Group
CGG Services SA
Coalmin Process Technologies CC
Concor Opencast Mining
Concor Technicrete
Council for Geoscience Library
CRONIMET Mining Processing SA (Pty) Ltd
CSIR Natural Resources and the Environment (NRE)
Data Mine SA
Digby Wells and Associates
DRA Mineral Projects (Pty) Ltd
DTP Mining - Bouygues Construction
Duraset
Elbroc Mining Products (Pty) Ltd
eThekwini Municipality
Ex Mente Technologies (Pty) Ltd
Expectra 2004 (Pty) Ltd
Exxaro Coal (Pty) Ltd
Exxaro Resources Limited
Filtaquip (Pty) Ltd
FLSmidth Minerals (Pty) Ltd
Fluor Daniel SA (Pty) Ltd
Franki Africa (Pty) Ltd-JHB
Fraser Alexander (Pty) Ltd
G H H Mining Machines (Pty) Ltd
Geobrugg Southern Africa (Pty) Ltd
Glencore
Hall Core Drilling (Pty) Ltd
Hatch (Pty) Ltd
Herrenknecht AG
HPE Hydro Power Equipment (Pty) Ltd
Immersive Technologies
IMS Engineering (Pty) Ltd
Ingwenya Mineral Processing (Pty) Ltd
Ivanhoe Mines SA
Joy Global Inc.(Africa)
Kudumane Manganese Resources
Leco Africa (Pty) Limited
Leica Geosystems (Pty) Ltd
Longyear South Africa (Pty) Ltd
Lull Storm Trading (Pty) Ltd
Maccaferri SA (Pty) Ltd
Magnetech (Pty) Ltd
Magotteaux (Pty) Ltd
Malvern Panalytical (Pty) Ltd
Maptek (Pty) Ltd
Maxam Dantex (Pty) Ltd
MBE Minerals SA (Pty) Ltd
MCC Contracts (Pty) Ltd
MD Mineral Technologies SA (Pty) Ltd
MDM Technical Africa (Pty) Ltd
Metalock Engineering RSA (Pty) Ltd
Metorex Limited
Metso Minerals (South Africa) Pty Ltd
Micromine Africa (Pty) Ltd
MineARC South Africa (Pty) Ltd
Minerals Council of South Africa
Minerals Operations Executive (Pty) Ltd
MineRP Holding (Pty) Ltd
Mining Projections Concepts
Mintek
MIP Process Technologies (Pty) Limited
MLB Investment CC
Modular Mining Systems Africa (Pty) Ltd
MSA Group (Pty) Ltd
Multotec (Pty) Ltd
Murray and Roberts Cementation
Nalco Africa (Pty) Ltd
Namakwa Sands(Pty) Ltd
Ncamiso Trading (Pty) Ltd
New Concept Mining (Pty) Limited
Northam Platinum Ltd - Zondereinde
Opermin Operational Excellence
OPTRON (Pty) Ltd
Paterson & Cooke Consulting Engineers (Pty) Ltd
Perkinelmer
Polysius A Division Of Thyssenkrupp Industrial Sol
Precious Metals Refiners
Ramika Projects (Pty) Ltd
Rams Mining Technologies
Rand Refinery Limited
Redpath Mining (South Africa) (Pty) Ltd
Rocbolt Technologies
Rosond (Pty) Ltd
Royal Bafokeng Platinum
Roytec Global (Pty) Ltd
RungePincockMinarco Limited
Rustenburg Platinum Mines Limited
Salene Mining (Pty) Ltd
Sandvik Mining and Construction Delmas (Pty) Ltd
Sandvik Mining and Construction RSA (Pty) Ltd
SANIRE
Schauenburg (Pty) Ltd
Sebilo Resources (Pty) Ltd
SENET (Pty) Ltd
Senmin International (Pty) Ltd
Smec South Africa
Sound Mining Solution (Pty) Ltd
SRK Consulting SA (Pty) Ltd
Time Mining and Processing (Pty) Ltd
Timrite Pty Ltd
Tomra (Pty) Ltd
Ukwazi Mining Solutions (Pty) Ltd
Umgeni Water
Webber Wentzel
Weir Minerals Africa
Welding Alloys South Africa
Worley

SAIMM HYBRID CONFERENCE

YOUNG PROFESSIONALS COUNCIL

5TH YOUNG PROFESSIONALS CONFERENCE

A SHOWCASE OF EMERGING RESEARCH AND INNOVATION IN THE MINERALS INDUSTRY

21-22 SEPTEMBER 2021

THE CANVAS, RIVERSANDS, FOURWAYS

2 CPD POINTS

Innovation and research into mining technology is necessary to position Africa as a world leader in minerals production and beneficiation. The Young Professionals Council is pleased to host a unique, two-day conference that will showcase a broad range of emerging research and innovation from young professionals in the metals and minerals industry. Presentations will focus on new technology, tools and techniques relevant to exploiting Africa's mineral resources safely, competitively and sustainably.

OBJECTIVES

- a broad range of topics covering the entire mining value-chain will give a quick sense of developments in the field of mining and metallurgy
- a large body of research at Masters, PhD and Post-doctoral level will give insights into emerging themes and advances in the minerals and metals knowledge-areas
- a focus on innovative practices, technological applications and case-studies from mining operations and research institutions will give the practicing professional an opportunity to learn about new tools and techniques relevant to their work
- a gathering of diverse professionals within the metals and minerals community will give delegates an opportunity to obtain exposure, build reputations, further their careers and network with peers and leaders in the African Minerals Industry

WHO SHOULD ATTEND

This conference should be of value to all professionals across the entire minerals industry value chain, including:

- All metallurgical fields
- Exploration
- Geology
- Geotechnical engineering
- Leadership/management/government/community
- Mining
- Occupational Hygiene and SHE practitioners
- ICT experts
- Mechanical, electrical/electronic engineers
- Mineralogy

EXHIBITION/SPONSORSHIP

Sponsorship opportunities are available. Companies wishing to sponsor or exhibit should contact the Conference Co-ordinator.

EVENT FORMAT

At this point in time, the event is planned as a hybrid conference. However, as we are still in lock down as a result of COVID-19, this will be constantly reviewed, and if it appears that the effects of the pandemic are still such as to pose a threat to the health and safety of delegates, this will be changed to a digital event.

Please advise on your submission if you will be presenting in person or virtually. Virtual presentations will be streamed live or pre-recorded.

Please continue to submit your abstracts and check www.saimm.co.za regularly for updates.

FOR FURTHER INFORMATION, CONTACT:

Gugu Charlie,
Conference Co-ordinator

E-mail: gugu@saimm.co.za
Tel: +27 11 834-1273/7
Web: www.saimm.co.za

As another successful and busy year comes to a close, we at

The Southern African Institute of Mining and Metallurgy

wish all of our members and those who supported us throughout this year, a heartfelt *Seasons greetings* to you and yours.

We point out to anyone who is interested in joining the SAIMM of the benefits of being a member:

SAIMM
THE SOUTHERN AFRICAN INSTITUTE OF MINING AND METALLURGY

- Receipt of a monthly professional Journal with informative technical content of a high standard which serves as a communication medium to keep members informed on matters relating to their professional interests.
- Attendance at conferences, symposia, colloquia, schools and discussion groups at competitive prices with discounted rates for members.
- Invitations to participate in technical excursions and social events which create further opportunities for inter-active professional association and networking.
- The SAIMM is registered with ECSA as a Voluntary Association and all SAIMM members qualify for discounted ECSA fees as a result of their SAIMM membership.
- Members obtain valuable ECSA Continued Professional Development (CPD) points when they attend our accredited events.

Visit
www.saimm.co.za
for more information on the SAIMM